ICE TANK TESTS OF A HIGHLY SKEWED PROPELLER AND A CONVENTIONAL ICE-CLASS PROPELLER IN FOUR QUADRANTS

SHAWN S. SEARLE

INFORMATION TO USERS

This manuscript has been reproduced from the microfilm master. UMI films the text directly from the original or copy submitted. Thus, some thesis and dissertation copies are in typewriter face, while others may be from any type of computer printer.

The quality of this reproduction is dependent upon the quality of the copy submitted. Broken or indistinct print, colored or poor quality illustrations and photographs, print bleedthrough, substandard margins, and improper alignment can adversely affect reproduction.

In the unlikely event that the author did not send UMI a complete manuscript and there are missing pages, these will be noted. Also, if unauthorized copyright material had to be removed, a note will indicate the deletion.

Oversize materials (e.g., maps, drawings, charts) are reproduced by sectioning the original, beginning at the upper left-hand corner and continuing from left to right in equal sections with small overlaps.

Photographs included in the original manuscript have been reproduced xerographically in this copy. Higher quality 6" x 9" black and white photographic prints are available for any photographs or illustrations appearing in this copy for an additional charge. Contact UMI directly to order.

Bell & Howell Information and Learning
300 North Zeeb Road, Ann Arbor, MI 48106-1346 USA

UMI®
800-521-0600

Ice Tank Tests of a Highly Skewed Propeller and a Conventional Ice-Class Propeller in Four Quadrants

By

©Shawn S. Searle, B. Eng.

A thesis submitted to the School of Graduate Studies
in Partial Fulfilment of the
Requirements for the Degree of
Master of Engineering

Faculty of Engineering and Applied Science
Memorial University of Newfoundland
May, 1999

St. John's Newfoundland Canada

Abstract

Recent work to update regulations for ice-class ships has resulted in, amongst other things, new methods for dimensioning ice-class propellers. These methods have focussed on the more traditional propeller geometry and arrangements so that unconventional designs, such as highly skewed propeller blades and azimuthing propellers, have been excluded and must be treated as special cases. Also, elements of the design methods are based on limited empirical sources and as such need testing, verification, and perhaps modification.

To address some of these issues, an experimental investigation was undertaken in the ice tank at the Institute for Marine Dynamics (IMD) using two different propeller models. A model of the propeller on the passenger ferry *MV Caribou* was tested specifically to investigate a highly skewed propeller under ice loading over a range of operating and ice conditions. The second propeller tested was a more conventional ice-class propeller from the *R-Class* icebreaker. The *R-Class* propeller model was tested over a wide range of operating conditions to give loading characteristics in all four quadrants. Such extreme loading might be experienced by fixed and controllable pitch propellers in off-design conditions, and by azimuthing propellers. The set of experiments involving the *R-Class* propeller were done over a range of ice strength conditions to examine nominal ice strength variation effects on the propeller loads.

Based on the experimental results it is concluded that a highly skewed propeller behaves in a similar manner to that of a conventional ice-class propeller. In addition, the tests conducted in all four quadrants of propeller operation concluded propellers do not experience the greatest loads in quadrant 1, which is currently used as the design criterion. Rather, the largest loads are experienced in quadrants 2 and 3 and modifications to current design proposals should consider this detail.

Acknowledgements

First and foremost, appreciation and thanks are bestowed upon Dr. Neil Bose and Dr. Brian Veitch for their guidance, support and advice. From the experimental stage through to the writing of this thesis, they have been there to support and keep me on the path to completion. For this, I am greatly indebted.

Acknowledgement is also extended, to Lloyd's Register of Shipping, particularly John Carlton and Andrew Smith, Marineering Ltd., KaMeWa, the Government of Newfoundland and Labrador and Memorial University of Newfoundland for their financial support during this undertaking.

Thanks are extended to the people at the National Research Council, Institute for Marine Dynamics, for assistance during the construction of the testing apparatus and while conducting the tests in the Ice Tank. For his assistance during the ice tank tests, Mark Wareham is gratefully acknowledged.

Special thanks and gratitude are extended to my parents, John and Annie Searle, for their moral support and encouragement during this program. Many friends and family are also thanked for their moral support and encouragement. Finally, last but not least, thanks are extended to my wife, Suzanne, for her support, encouragement and understanding during my studies.

Table of Contents

List of Figures

List of Tables

Nomenclature

Physical Constants and Measured Parameters during Experiments

g	Acceleration due to gravity
ρ_I	Mass density of ice
ρ_W	Mass density of water
ν	Coefficient for kinematic viscosity
μ	Coefficient for dynamic viscosity
E	Young's Modulus
S_C	Compressive Strength of Ice
S_F	Flexural Strength of Ice
S_τ	Shear Strength of Ice
h_I	Depth of cut into ice
f	Factor for friction

Propeller Geometry, Kinematics, and Loads

Q	Propeller Torque
T	Propeller Thrust
r	Relative radius
R	Propeller radius
r/R	ratio of relative radius to propeller radius
D	propeller diameter
n	rotational speed of the propeller
V_A	Axial velocity or advance velocity
EAR	Expanded area ratio
P/D	propeller pitch/diameter ratio
N	Number of blades
CL	Chord length

dL	Lift force component
dDg	Drag force component
dF_R	Resultant force
α	Angle of attack
ϕ	Geometric pitch angle
β_I	Hydrodynamic pitch angle
V_R	Resultant velocity
u	Induced velocity
γ_S	Suction side cutting angle
γ_P	Pressure side cutting angle
λ_d	Ratio of cut depth to propeller diameter
J	advance coefficient
K_T	Thrust coefficient
K_Q	Torque coefficient
K_S	Compressive Ice Strength Index
η_O	Open water efficiency

Scaling Terminology

λ	scaling factor
V_m	model speed
V_p	prototype speed
F_m	model force
F_p	prototype force
S_m	model strength
S_p	prototype strength

Chapter 1

Introduction

1.1 Objective & Scope of Work

Ships operating in the Arctic and sub-Arctic regions frequently encounter ice which increases the load on their propulsion systems. During operation in ice-strewn waters and during icebreaking, ice pieces tend to travel beneath the vessel hull and emerge at the propeller where they come into contact with the propeller blades. The extent of contact is dependent on various parameters including the propeller type, its depth of submergence, the physical characteristics of the propeller and the ice piece, as well as the operating condition of the vessel at the time of interaction. The load experienced by the propeller due to this contact can lead to propeller blades being damaged or broken.

In practice, regulations, such as the Finnish-Swedish Ice Class Rules and the Canadian Arctic Shipping Pollution Prevention Regulations (CASPPR), govern the design of propellers and propulsion systems. The formulas used are based on a prescribed ice torque, which is dependent on the ice class of the vessel. This ice torque, in combination with a cantilever beam analysis of blade bending is used for the design of propeller blades. These rules are inadequate as failures still occur and they do not accurately represent the current state of knowledge.

In November of 1996 a research project was initiated by the Ocean Engineering Research Centre, Memorial University of Newfoundland, the Institute for Marine Dynamics, NRC, Lloyd's Register of Shipping, Marineering Ltd., and KaMeWa to develop design and analysis methods for ice class propellers and their associated final drive shafting. A portion of this research project was devoted to a model testing program in the ice tank.

The focus of this model testing program was to improve the understanding of the theoretical/numerical modelling by providing experimental results to validate theoretical predictions. In addition, the model testing program was carried out to aid in filling in the gaps that exist in the current state of knowledge with respect to propeller-ice interaction. Two of these major areas include the loads experienced by highly skewed propellers operating in ice and the loads experienced by propellers in the four quadrants of propeller operation during interaction with ice. Prior to this

work, there were only a few experimental programs to investigate propellers of any type in ice and none that investigated propeller-ice interaction in all four quadrants.

The work reported here presents the results for the model testing program conducted in the ice basin at the Institute for Marine Dynamics, NRC. It is presented in four chapters. Chapter 1 provides a general description of the problem, a brief discussion of propeller geometry and a review of the relevant literature pertaining to propeller-ice interaction. In Chapter 2, a dimensional analysis is conducted to determine relevant variables involved in the problem, and the experimental set-up and test program are described in detail. The experimental results are presented and discussed in Chapter 3 and conclusions and recommendations are presented in Chapter 4.

1.2 Propeller Geometry

The screw propeller is the most common form of propulsion in the marine industry: it is a relatively simple device and is generally the most efficient (Harvald, 1983). An engine produces power, which is converted by the propeller into a thrust force that propels the vessel. The thrust and torque forces acting on a propeller blade are illustrated in Figure 1.

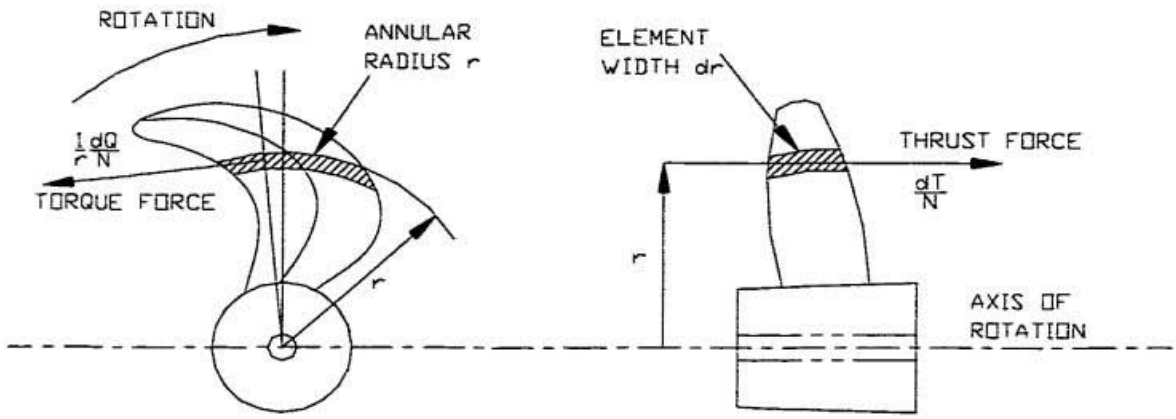

Figure 1: Thrust and Torque Forces acting on a Propeller Blade (after Harvald, 1983)

There have been various forms of screw propellers developed, but the main geometric features have remained the same. Propellers can be thought of as a continuous series of hydrofoil sections that are positioned radially and at varying angles relative to a reference. These hydrofoil sections are not flat but curved. Definition of the hydrofoil sectional shape in two dimensions is shown in Figure 2.

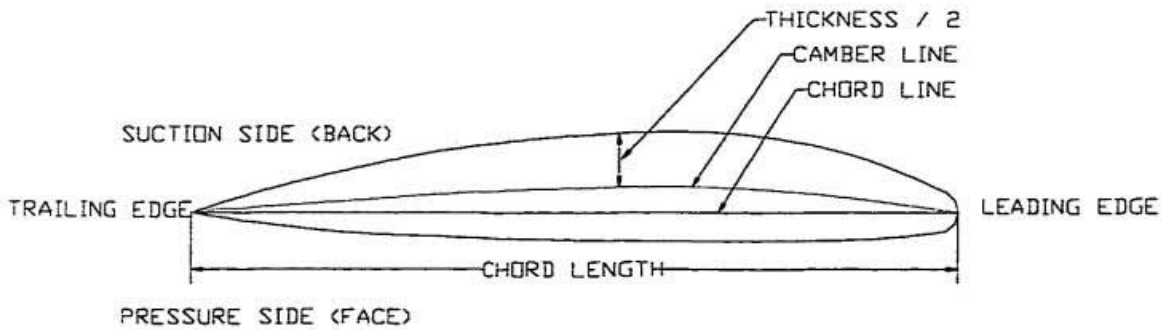

Figure 2: Hydrofoil Section

For a propeller that has its hydrofoil sections based on airfoil sections, the hydrofoil can be described using two dependent variables, camber and thickness, and one independent variable "*x*". The *x*-axis is defined as the straight line passing through the leading edge and the trailing edge of the hydrofoil. The independent variable *x* can be defined non-dimensionally as relative chord or "*x/CL*" where *x* is the position along the *x*-axis and *CL* is the chord length. The chord length of the hydrofoil in two dimensions is the same as the arc length of the chord of a propeller blade in three dimensions. For segmented sections, the baseline is the face and this is used for definition rather than the chordline.

Rake, skew, and pitch define the relative position and angle of the hydrofoils to one another along the blade. Rake defines the position of the hydrofoil forward or backward relative to a plane perpendicular to the shaft axis and skew defines the location of the hydrofoil perpendicular to the shaft axis as shown in Figure 3.

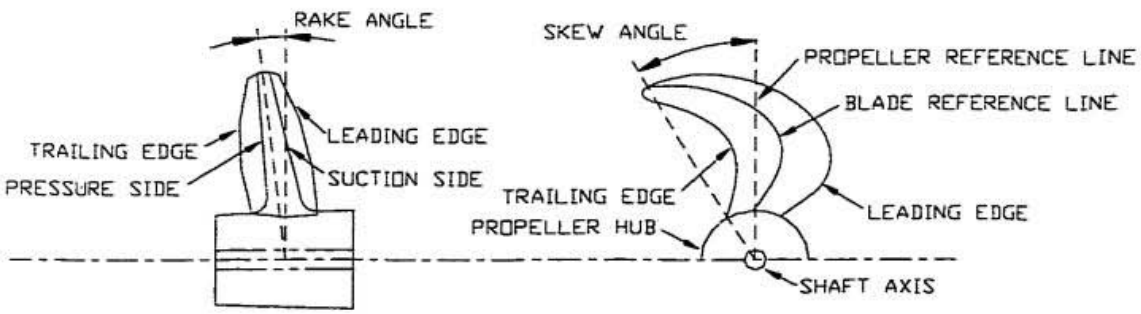

Figure 3: Definition of Rake & Skew

Figure 4 illustrates the velocities and forces on a blade section as it rotates in open water. The hydrodynamic pitch angle is the effective pitch angle, which takes into account the effects on the fluid velocity due to the presence of the propeller (induced velocity).

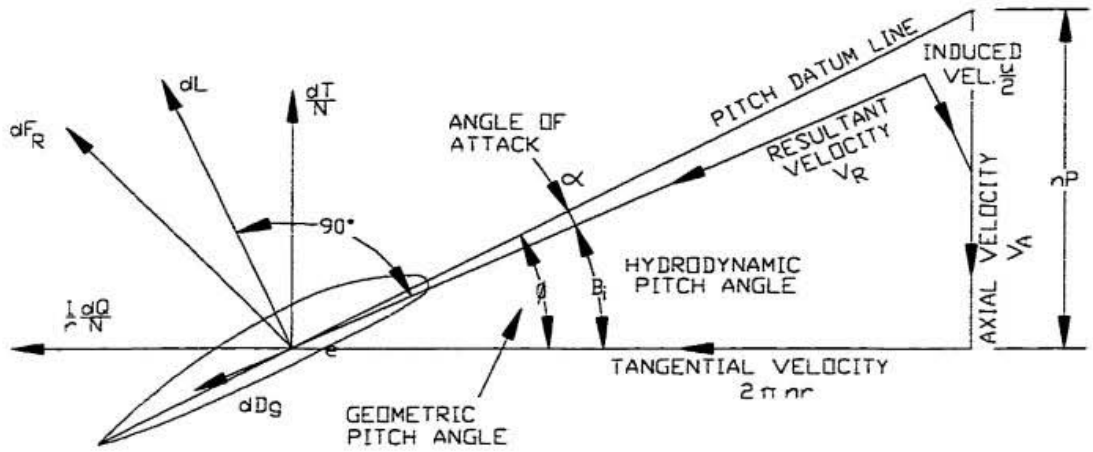

Figure 4: Velocities and Forces on a Propeller Section (from O'Brien, 1962)

A complete propeller blade is defined by a series of hydrofoil sections with values of pitch, rake and skew at various values of r/R. More detailed descriptions of propeller geometry and the forces acting on the blades are given by O'Brien (1962), Harvald (1983) and Carlton (1994).

1.3 Review of Work on Propeller-Ice Interaction

1.3.1 Previous Literature Reviews

Two extensive literature reviews have discussed the work performed in the field of propeller-ice interaction, Jussila and Soininen (1991) and Veitch (1992). These literature reviews present detailed discussions of the theoretical work performed by Jagodkin (1963), Ignatjev (1964, 1966), Belyashov and Shpakov (1983), Kotras et al. (1985), Wind (1983), Gabel et al. (1979), and Chernuka et al. (1989) as well as others.

In addition, discussions of experimental work at both full scale and model scale were presented. The model scale experiments include those of Enkvist and Johansson (1968), Edwards (1976), Okamoto et al. (1981a, 1981b, 1981c), Sasajima et al. (1981), Sasajima and Mustamaki (1984), Sasajima (1985), Bulat et al. (1985), Lindroos and Björkestam (1986), and Keinonen and Browne (1990). The full scale experiments include those conducted onboard the *Rauma I* (Jussila, 1983), the *Sotka* (Koskikivi and Kujala, 1985), the *M/V Robert LeMeur* (Duff et al., 1985, Laskow et al., 1986), the *M/S Gudingen* (Jussila and Koskinen, 1989a 1989b, the *Polar Star* (Antonides et al., 1981), the *CCGS Pierre Radison* (Edwards et al., 1981) and the *Karhu* (Kannari, 1988).

The literature review presented with this thesis will concentrate on the more recent work conducted in the field.

1.3.2 Review of Recent Work

Ice tank test programs have been conducted by Keinonen and Browne (1990), Browne et al. (1991a, 1991b), Newbury et al. (1993, 1994) and Tamura et al. (1997).

Keinonen and Browne (1990) investigated propeller-ice interaction in quadrant 1 or the forward operating condition. The test program included a systematic variation of design and operational parameters, which involved using a model Kaplan propeller tested as both an open and ducted propeller, variations in propeller pitch, ice thickness, ice strength, shaft speed, and forward speed. They concluded that the hydrodynamic loading on the marine propeller might be just as large as the ice contact loading. In addition, it was suggested that the method of superposition could be applied to the problem of propeller-ice interaction, meaning the contact load and non-contact load could be investigated independently. Further data analysis was conducted by Brown et al. (1991a, 1991b) and concluded that significant hydrodynamic non-contact propeller loads occur during ice milling and can affect the design and safety of marine propellers.

As part of a joint research project arrangement (JRPA #6) between the Ministry of Trade and Industry of the Republic of Finland and the Department of Transport of

Canada to determine the factors which affect propeller-ice interaction, Newbury et al. (1993, 1994) used ice tank tests to investigate the hydrodynamic non-contact load component during propeller-ice interaction. Like Keinonen and Browne (1990), tests were conducted with a Kaplan propeller model, which was also tested as an open propeller. As well, the test program was developed to test a range of conditions which included variations in forward speed, propeller rotational speed, size of ice block and ice strength. One of the blades was originally strain gauged in four places to measure blade bending, but three of the gauges failed during the test program. In addition they measured propeller shaft thrust and torque at a sampling rate of 500 Hz for the majority of the tests. The model experiments provided measurements for shaft thrust and torque and blade pressures during propeller operation in the blocked flow condition. The test program involved ice milling tests in both water and air to determine the hydrodynamic component of the load by subtracting one from the other. Based on their results, they concluded that there was a significant hydrodynamic component to the torque and thrust during milling and that the method of superposition put forth by Keinonen and Browne (1990) was justified

Prior to the work presented in this thesis, the most recent ice tank work on propeller-ice interaction was conducted by Tamura et al. (1997). The experimental study investigated ducted propellers and the loads experienced during interaction with ice. To investigate the phenomena, the total load on a blade was divided into four components and experiments were developed to investigate each component.

$$F_{total} = F_{ice} + F_{hydro} + F_{inertia1} + F_{inertia2} \quad [1]$$

where: F_{ice} is the load due to the breaking of an ice block

F_{hydro} is the hydrodynamic load due to the presence of ice

$F_{inertia1}$ is the load due to inertia of the total ice mass

$F_{inertia2}$ is the load due to inertia of the added mass of ice

An extensive test program was initiated which involved experiments in both air and water where the ice and propeller made contact, and a similar test where the ice and propeller were in close proximity but no contact was made. The test program was developed in an attempt to separate the different load components, so that each component could be investigated more easily and superposition could be used to determine the total load. The load components contained in the various tests are as shown in Table 1 below.

	F_{ice}	F_{hydro}	$F_{inertia1}$	$F_{inertia2}$
Ice Contact Test in Water	X	X	X	X
Ice Contact Test in Air	X		X	
Ice Blockage Test in Water		X		
Ice Strength Changing Test in Water	X	X	X	X
Ice Strength Changing Test in Air	X		X	

Table 1: Ice Load Components Contained in Various Tests (from Tamura et al., 1997)

The tests focused on operation in quadrant 1 and used a ducted propeller model. To measure pressure, bending moment and spindle torque, one of the propeller blades was instrumented with pressure and strain gauges. As well, shaft thrust and torque were measured using a dynamometer.

This work concluded that for thrust, the inertia force component was by far the largest load component and the ice failure force was small in comparison. As well, the hydrodynamic force increases thrust while the others decrease it over the range of parameters investigated. For torque it was found that the ice failure component was highly dependent on ice strength and the largest of the force components, with the hydrodynamic component second.

To provide insight into the mechanics of ice failure in propeller-ice tests, which had been the weak point in ice tank tests, a number of laboratory experiments were designed. The results from these experiments have been reported by Belyashov (1993), Veitch and Kivelä (1993), and Soininen et al. (1995).

Belyashov (1993) conducted tests in which fresh water ice specimens were cut by flat indenters simulating the leading edge of propeller blades. The experiments examined the contact on the pressure side of the blade and investigated cutting angles ranging from 20^0 to 100^0. The cutting tools were similar to the pressure side cutting tools illustrated in Figure 5. The cutting angle represents the local angle of attack of a blade

section with respect to the ice. The experiments were designed to investigate the mechanics of ice fracture inflicted by the indenters, as well as to investigate the contact zone between the propeller blade and the ice block. This work expanded on previous work (Belyashov and Shpakov, 1983) and presented a method for calculating ice loads encountered by propeller blades due to contact on the pressure side of the blade based on the experiments.

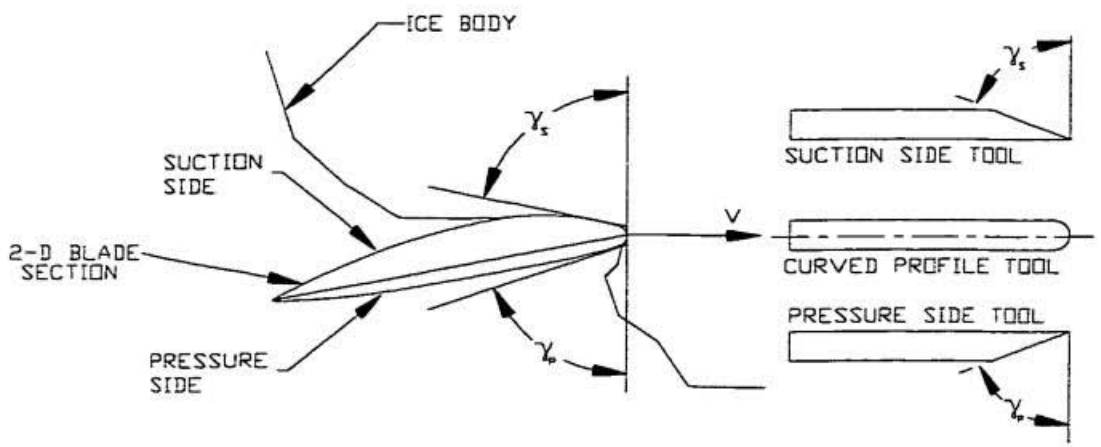

Figure 5: Blade cutting geometry represented by cutting tools (from Veitch, 1995)

Similar ice cutting experiments, using natural sea ice, were conducted by Veitch and Kivelä (1993) which extended the range of cutting angles past the pressure side geometry and into the suction side geometry. An illustration of the cutting tools used in their laboratory experiments is shown in Figure 5 above. From their work, it was concluded that contact occurs at the leading edge of the blade. In addition, they

concluded that the predominant ice failure mechanism for pressure side tests was spalling and for the suction side tests the failure mechanism was dependent on the cutting angle. For lower angles, ice failed by spalling, medium angles saw a combination of crushing and spalling, and higher angles saw a combination of crushing, spalling and splitting. As well, they presented an empirical relationship between contact pressure and cutting angle, which was later used as the basis for a model to predict blade forces due to ice contact (Veitch, 1995).

Similar, yet more elaborate experiments were conducted by Soininen et al. (1995) to investigate the pressure distribution on propeller blades under ice contact. Their experimental set-up consisted of a test rig supporting a large pendulum mechanism with an instrumented cutting tool attached. The cutting tool had a shape similar to the leading edge of a propeller blade on the car ferry *M/S Gudingen*. The diameter of the real propeller is 2m and the geometry was taken from the relative radius of $r/R = 0.8$. From their experiments, they concluded that the face (pressure side) of the blade hardly experienced any loads as flaking or spalling took place before any real contact developed on the face. The load tended to act on the back (suction side) of the blade. Both of these conclusions agreed with the results obtained by Veitch and Kivelä (1993).

The biggest concern with the experiments conducted by both Soininen et al. (1995) and Veitch and Kivelä (1993) involved the thickness of the ice layer that was cut off.

To illustrate the problem, Figure 6 is provided below. In both experimental programs, the cuts were done on the edge of the ice sheet causing an asymmetry in the boundary conditions as shown in Figure 6(a). This asymmetry caused the load to be concentrated on the suction side of the tool. It would have been beneficial to conduct additional tests with more symmetrical boundary conditions, as shown in Figure 6(b), to investigate how the pressure would have been distributed over the pressure and suction sides of the blade.

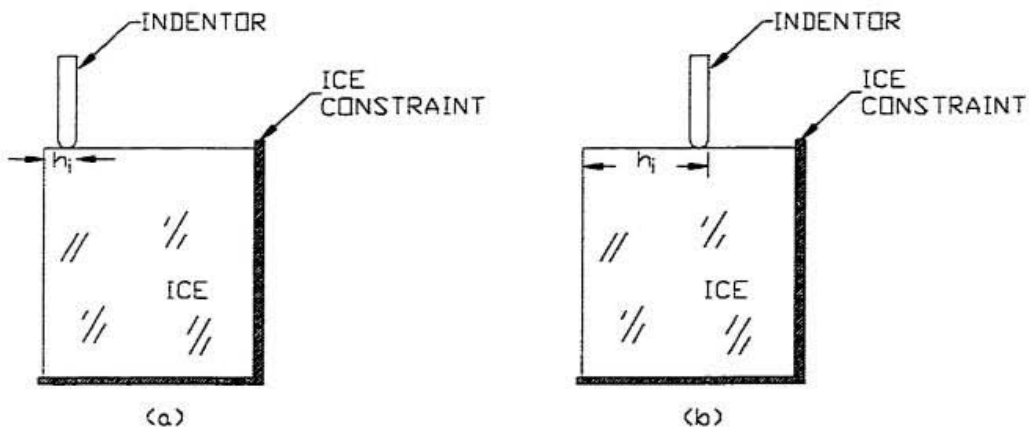

Figure 6: Boundary Conditions for Ice Cutting Tests

Based on the experimental work conducted by Veitch and Kivelä (1993), Veitch (1995) developed a propeller-ice contact model. To address the boundary condition problem discussed above; he conducted some computational work using boundary element methods to address the problem and extend the experimental results (Veitch, 1995). The computational work concluded that as the boundary conditions

approached symmetry, the load became symmetrical about the initial contact point. These results were combined with the experimental work to develop the propeller-ice contact model. The model simulates a propeller and a submerged ice block coming into contact and calculates the hydrodynamic and ice contact forces as well as the forces and motion response of the ice block. Veitch (1995) presented predictions and measurements for the *I/B Karhu* propeller. Prediction results for a collection of other propellers are presenting in Veitch (1999) and results from the simulation program have been used by Bose et al. (1998), Doucet et al. (1997), Veitch et al. (1997) and Veitch (1997).

Besides contact loads, propellers experience large hydrodynamic loads when the inflow is blocked by ice pieces. This is most common with a ducted propeller, where the ice piece can become lodged in the duct, but it can also occur with an open propeller, when the ice block becomes wedged between the propeller and the hull, skeg or other structure. Shih & Zheng (1992, 1993), Yamaguchi (1993), Bose (1996) and Liu (in Robbins et al., 1998) have investigated hydrodynamic effects of propeller blockage.

As part of the JRPA #6, Shih and Zheng (1992) used a potential flow panel method to predict the lift and drag on a two-dimensional hydrofoil passing close to a blockage in the absence of an inflow past the blockage. Their work was later extended (Shih & Zheng, 1993) to three dimensions to investigate propeller performance as an ice block

moved with the inflow into the propeller disk. Yamaguchi (1993), using unsteady lifting surface theory, made an attempt to predict propeller loading in an assumed wake from a blockage. He found that thrust and torque coefficients were higher in blocked flow than in uniform flow.

Bose (1996) developed a three dimensional unsteady panel method to predict the performance of ice class propellers in a blocked flow. The method was used to investigate two conditions: a simplified inflow field to approximate a wake behind an ice blockage and the same inflow field with panels upstream to represent an ice blockage. The results from the panel method were compared with those obtained from tests involving a model propeller in a similar blocked flow (Luznik et al., 1995). From the comparison, it was noted that the panel method showed a good correlation to the experimental work at higher values of advance coefficient, but tended to under predict at lower values. When the gap between the propeller and the ice block was investigated, the program correlated very well with the experimental results at larger gaps but tended to over predict the thrust coefficient and under predict the torque coefficients at smaller gaps. The author suggested that the model could be improved by restricting the fluid velocities through the gap using a number of possible methods as outlined in his conclusions. Overall, the program represents a very good attempt at theoretically modelling the hydrodynamic effects on propellers due to an ice blockage. More recently, Liu rewrote this panel method code using his code OSFBEM (Liu, 1996). He used his panel method to investigate blocked flow only

(Robbins et al., 1998) and later included a method to predict the ice contact component (Doucet et al., 1998).

Blade cavitation is also a concern for propellers operating in icy waters. As stated previously, blockages can generate fast flows between the propeller blades and the ice block, which creates low-pressure areas that result in the development of cavitation. Walker et al. (1994a, 1994b, 1994c, and 1996) have examined hydrodynamic loads and cavitation due to propeller blockage in cavitation tunnels. From this work it was concluded that, even under atmospheric pressure, cavitation occurs during ice blockage. Cavitation erosion under these conditions was investigated by Doucet (1995).

Methods to design ice class propellers have been presented by Soininen et al. (1997), Katzmann and Andriushin (1997) and Bose et al. (1998). The method put forth by Soininen et al. (1997) derives from the JRPA #6 work and encompasses experimental, theoretical and full-scale data to formulate their method for the design of ice class propellers. The design methods presented Katzmann and Andriushin (1997) are based mostly on full-scale experiences and a statistical evaluation of these experiences. Their published work discusses model experimental work but does not provide any data from the model test program to compare with similar work. Bose et al. (1998) present design methods based on a limit state analysis. The method accounts for extreme hydrodynamic mean loads, oscillating hydrodynamic loads due to wake

effects, residual and centrifugal loads and unsteady loads due to ice (both hydrodynamic non-contact and contact). In addition they provide a method to examine the exceptional load case, which would involve the load experienced by a propeller contacting ice while the propeller was stopped. The authors present a detailed method for initial design and suggest that final designs should entail a more detailed stress analysis of the blade using finite element modelling, to identify the position of maximum stresses where the design equation can be applied.

These methods have focussed on traditional propeller geometry and arrangements so that unconventional designs for ice-class propellers, such as highly skewed propeller blades, have been excluded and must be treated as special cases. Further, the methods have focussed on the design operating conditions and have not put much emphasis on off-design conditions where propellers receive the highest loads and in turn the most damage. Also, elements of the design methods are based on limited empirical sources and as such need testing, verification, and perhaps modification. To address these issues, a model testing program in model ice aimed at coming to a better understanding of loading on highly skewed ice-class propellers and on propellers operating in off-design conditions was undertaken. The results from that experimental test program are the focus of this thesis.

Chapter 2

Experimental Program

2.1 Objectives

The primary objectives of this chapter are to show the processes behind the development of a test program to investigate propeller-ice interaction. The first section discusses a dimensional analysis to determine the relevant variables to consider with such a test program. The remainder of the chapter presents the physical requirements to examine propeller-ice interaction and the method by which the problem was tackled.

2.2 Design of Experiments

2.2.1 Determination of Relevant Variables

High loads occur on screw propellers during navigation in ice due to the interaction between the propeller and submerged ice pieces that are in the propeller race. Investigations have shown that these loads are dependent on the size and strength of the ice pieces, geometric characteristics of the propeller, and relative motion between ice and propeller.

When testing model propellers it is necessary to fulfil a number of conditions to ensure similarity between the full scale and the model scale results. These conditions include:

- Geometric Similarity
- Kinematic Similarity
- Dynamic Similarity

Due to the presence of ice in the test program, an additional condition must be met to ensure similarity. This condition is defined here as mechanical similarity. For mechanical similarity, it is required that the ice properties scale between full-scale and model scale.

For these experiments, the variables required to maintain similarity are discussed below and a summary of the variables is given in Table 2 where L = Length, T = Time and M = Mass.

For geometric similarity, the model propellers are constructed as smaller copies of their full-scale counterparts. The geometric variables included in the analysis are the propeller diameter and the depth of cut into the ice sheet. The depth of cut is included to represent the extent of interaction between the ice and propeller.

To comply with kinematic similarity, the ratio of speed of advance and the propeller revolution rate must be the same for model and full scale. For this reason both variables are included in the dimensional analysis.

In addition, variables representing the fluid have to be included. These variables consist of the dynamic viscosity and the density of the fluid. An additional variable that could be included is temperature. Although small temperature changes occur during the testing period (1-2 °C) which can effect the density and viscosity, the changes were considered minimal and ignored in the analysis.

For mechanical similarity, ice properties are required. The variables included in the analysis are Young's modulus, compressive strength, flexural strength, shear strength and the density of the ice.

In addition, gravitational acceleration and a frictional factor are included in the dimensional analysis.

Variable	*Symbol*	*Units*
Propeller Diameter	D	L
Depth of Cut	h_I	L
Rotational Speed of the Propeller Shaft	n	1/T
Speed of Advance	V_a	L/T
Gravitational Acceleration	g	L/T^2
Dynamic Viscosity	μ	M/(LT)
Mass Density of Water	ρ_w	M/L^3
Mass Density of Ice	ρ_I	M/L^3
Young's Modulus of Ice	E	$M/(LT^2)$
Compressive Strength of Ice	S_C	$M/(LT^2)$
Shear Strength of Ice	S_τ	$M/(LT^2)$
Flexural Strength of Ice	S_F	$M/(LT^2)$
friction factor	f	---
Propeller Thrust	T	ML/T^2
Propeller Torque	Q	ML^2/T^2

Table 2: Summary of Relevant Propeller-Ice Interaction Variables

2.2.2 Dimensional Analysis

The dimensions of physical quantities can be manipulated algebraically and the results can be interpreted to provide a great deal of information about the physical processes involved in the situations examined. This study is defined as the "method of

dimensions" or dimensional analysis. It is useful in that it allows the engineer or scientist to explore all possible avenues in attempting to define the problem at hand and form a guide as to what results can be expected from a set of tests (Sharp et al., 1992).

Propeller thrust and torque are the dependent variables under consideration, thus two functional equations are developed from the relevant variables listed in Table 2. The functionals describing the loads on the propeller in terms of relevant ice properties and blade geometry are given as:

$$T = \Phi(D, h_I, n, V, g, \mu, E, S_c, S_t, S_F, f, \rho_I, \rho_w) \qquad [2]$$

$$Q = \Phi(D, h_I, n, V, g, \mu, E, S_c, S_t, S_F, f, \rho_I, \rho_w) \qquad [3]$$

To develop the non-dimensional equations for each of the dependent variables, the method of synthesis developed by Barr, (1969) was used. This method allows the experimenter to guide the analysis towards a convenient solution while controlling the frequency at which the dependent variables appear in the final terms. Linear terms are first developed, then the non-dimensional terms are developed from these linear terms.

Solving first for propeller thrust as the dependent variable, a total of 23 linear proportionalites exist to describe the problem and are summarised in Table 3.

$\left(\frac{T}{V^2\rho}\right)^{\frac{1}{2}}$	$\frac{S_c}{\rho g}$	$\frac{g}{n^2}$	$\left(\frac{T}{S_t}\right)^{\frac{1}{2}}$
$\left(\frac{T}{n^2\rho}\right)^{\frac{1}{4}}$	$\left(\frac{S_c}{\rho n^2}\right)^{\frac{1}{2}}$	$\frac{E}{\rho g}$	$\frac{S_t}{\rho g}$
$\left(\frac{T}{g\rho}\right)^{\frac{1}{3}}$	$\frac{V}{n}$	$\left(\frac{\mu^2}{g\rho^2}\right)^{\frac{1}{3}}$	$\left(\frac{S_t}{\rho n^2}\right)^{\frac{1}{2}}$
$\left(\frac{T}{E}\right)^{\frac{1}{2}}$	$\frac{V^2}{g}$	$\frac{\mu}{\rho V}$	D
$\frac{S_f}{\rho g}$	$\left(\frac{S_f}{\rho n^2}\right)^{\frac{1}{2}}$	$\left(\frac{T}{S_f}\right)^{\frac{1}{2}}$	h_t
$\left(\frac{T}{S_c}\right)^{\frac{1}{2}}$	$\left(\frac{E}{\rho n^2}\right)^{\frac{1}{2}}$	$\left(\frac{\mu}{\rho n}\right)^{\frac{1}{2}}$	

Table 3: Possible Linear Proportionalites for Thrust

Originally there are 9 variables (excluding density, friction and variables with units of length). Therefore, to develop a correct dimensionally homogeneous equation, it is necessary to choose 8 of the 23 derived linear proportionalites. In addition, these 8 variables must be chosen such that they include all of the original variables.

Based on this, the following linear functional is developed.

$$\Phi\left(\left(\frac{T}{\rho_w n}\right)^{\frac{1}{4}}, \left(\frac{S_C}{\rho_f n^2}\right)^{\frac{1}{2}}, \left(\frac{E}{\rho_f n^2}\right)^{\frac{1}{2}}, \left(\frac{S_t}{\rho_f n^2}\right)^{\frac{1}{2}}, \left(\frac{S_f}{\rho_f n^2}\right)^{\frac{1}{2}}, \frac{V^2}{g}, \frac{\mu}{\rho_w V}, \frac{V}{n}, D, h_t\right) \quad [4]$$

Taking equation [4], dividing through by D and compounding some of the additional terms, the following non-dimensional equation can be developed for the thrust on a propeller interacting with ice.

$$\frac{T}{\rho_w n^2 D^4} = \Phi\left(\frac{V^2}{gD}, \frac{\mu}{\rho_w VD}, \frac{V}{nD}, \frac{h_t}{D}, \frac{S_C}{\rho_f n^2 D^2}, \frac{E}{S_C}, \frac{S_t}{S_C}, \frac{S_f}{S_C}\right) \quad [5]$$

Conducting a similar procedure for the propeller torque parameter a non-dimensional equation can be developed for the torque on a propeller interacting with ice.

$$\frac{Q}{\rho_w n^2 D^5} = \Phi\left(\frac{V^2}{gD}, \frac{\mu}{\rho_w VD}, \frac{V}{nD}, \frac{h_t}{D}, \frac{S_C}{\rho_f n^2 D^2}, \frac{E}{S_C}, \frac{S_t}{S_C}, \frac{S_f}{S_C}\right) \quad [6]$$

As shown in equations [5] and [6], the same non-dimensional parameters exist for both the thrust and torque.

Taking the square root of V^2/gD produces a form of the Froude Number.

$$Fn = \frac{V}{\sqrt{gD}} \qquad [7]$$

Inverting $\mu/\rho_W VD$ and substituting ν for μ/ρ_W, a form of Reynolds Number is obtained.

$$Rn = \frac{VD}{\nu} \qquad [8]$$

The advance coefficient is defined as V/nD.

$$J = \frac{V}{nD} \qquad [9]$$

The degree of contact between the propeller and the ice can be defined as the ratio between the depth of cut and the propeller diameter

$$\lambda_d = \frac{h_I}{D} \qquad [10]$$

The non-dimensional parameter derived for propeller thrust is defined as the thrust coefficient,

$$K_T = \frac{T}{\rho_w n^2 D^4} \qquad [11]$$

and the non-dimensional parameter derived for propeller torque is defined as the torque coefficient.

$$K_Q = \frac{Q}{\rho_w n^2 D^5} \qquad [12]$$

The following four parameters associate the ice properties (compressive strength, shear strength, flexural strength and Young's modulus) with the propeller characteristics.

$$\frac{S_C}{\rho_I n^2 D^2}, \frac{S_t}{S_C}, \frac{S_f}{S_C}, \frac{E}{S_C} \qquad [13]$$

Compressive ice strength is of particular importance for propeller-ice tests. For this reason a non-dimensional parameter is defined for compressive strength.

$$K_S = \frac{S_C}{\rho_I n^2 D^2} \qquad [14]$$

As stated previously, when testing model propellers it is necessary to fulfil a number of conditions to ensure similarity between the full scale and the model scale results.

Geometric similarity is realised by using a correctly scaled model of the propeller. A model with the largest diameter practically possible should be constructed to minimise scaling errors. In this experimental program, two propeller models were used: a 250mm diameter highly skewed propeller and a 200mm diameter conventional ice class propeller.

Kinematic similarity can be achieved by keeping the advance coefficient constant for model and full scale. The advance coefficient ensures that the ratio between the speed of advance and the rotational speed of the model is the same as for the full-scale propeller.

For dynamic similarity, both the Reynolds Number and Froude Number must be satisfied, but it is not possible to satisfy both of these conditions simultaneously at model scale.

Froude number is important when gravitational effects are a concern. In this experimental program, the propeller was cutting ice close to the surface, thus there was some free surface effect. However, the free surface was minimal due to the fact

that the ice sheet acted as a barrier, thus scaling by Froude Number was not necessary.

To scale by Reynolds number is unrealistic for model propeller testing in the ice tank, as the required advance speed would be beyond the capabilities of the test equipment. Reynolds number is important when viscous forces are a concern, therefore to avoid problems with Reynolds number it is important to ensure that the flow around the propeller remains turbulent ($R_n \geq 2 \times 10^5$ according to ITTC, 1978). Reynolds number for each propeller was checked using equation [15],

$$R_n = \frac{C_{0.75R}\sqrt{V_A^2 + (0.75\pi nD)^2}}{\nu} \qquad [15]$$

where $C_{0.75R}$ is the blade chord at 0.75R, R is the propeller radius, D is the propeller diameter, n is the rate of revolution, V_A is the speed of advance of the propeller, and ν is the coefficient of kinematic viscosity.

As free surface effects were considered unimportant, the shaft RPM was chosen as high as practical, given the constraint of the carriage speed, to provide the highest possible Reynolds number for a given propeller diameter. Keeping the flow turbulent during the test period did not present a problem, as Reynolds Number ranged from

approximately 3.2 x 10^5 to 4 x 10^5 over the range of speeds investigated. In this case it was possible to get reasonable $Rn_{0.7}$ while still satisfying $Fn_P = Fn_M$.

Due to the presence of ice in the test program, an additional condition had to be met to ensure similarity. This condition is defined here as mechanical similarity. For mechanical similarity, it was required that the ice properties scale between full scale and model scale. This condition raises problems when it comes to model propeller testing in ice and is discussed in the following section.

2.2.3 Scaling Concerns

Ice model tests are carried out when the situation under investigation is too complicated to be tackled theoretically. Since the 1950's, ice tank model testing has been dominated by ship-ice interaction where bending failure of ice has been the main concern. Recently other forms of tests have been conducted and this widening spectrum of ice model testing has detected deficiencies in the modelling techniques (Riska et al., 1994).

One such deficiency occurs when modelling propellers and ice. For propeller-ice interaction, failure mechanisms other than flexural take place and are a concern. For ship hull model testing in ice, the common practice is to scale velocity in accordance with Froude number. Scaling in this manner establishes the following relationships.

$$\frac{V_M}{V_P} = \left(\frac{L_M}{L_P}\right)^{\frac{1}{2}} = \lambda^{\frac{1}{2}} \qquad [16]$$

$$\frac{F_M}{F_P} = \left(\frac{L_M}{L_P}\right)^{3} = \lambda^{3} \qquad [17]$$

$$\frac{S_M}{S_P} = \left(\frac{L_M}{L_P}\right) = \lambda \qquad [18]$$

Based on experimental results, the strength relationship developed applies for flexural strength but a problem occurs when investigating compressive strength. During model tests, propeller torque measurements are typically over-predicted compared to full-scale torque, which can be attributed to several things including improper scaling of the compressive strength of ice (Riska et al., 1994).

Currently, there are problems in obtaining complete similarity between full scale and model scale when modelling propeller-ice interaction. This problem is due to the fact that it is currently impossible to properly model all the mechanical properties of real ice with model ice. There has been recent work done to compensate for this problem, as mentioned, but additional work in this area would be beneficial.

This test program was not set up to model ice strength but rather vary it and see its effects on the propeller loads. However, a method of extrapolating full-scale results from the model results is described in Section 3.3.3.2, which is based on the experimental results and the preceding dimensional analysis.

2.3 Model Propeller Boat

The test program was carried out in the ice model basin at the Institute for Marine Dynamics (IMD). A detailed description of the ice tank facilities is presented by Jones (1987). The propeller boat shown in Figure 7 was used for the test program. A propeller boat is arranged to allow the propeller to move in front of the boat in a homogeneous velocity field, which is nearly undisturbed by the flow of the boat. For these experiments the propeller boat was mounted on the frame of the ice tank carriage, which moved vertically so that the propeller could be positioned at different depths. The propeller boat had been constructed for a previous experimental program (Keinonen and Browne, 1990) and was modified for this test program. The modifications included an extension to the propeller shaft tube of an additional 350mm to provide a longer interaction time between the propeller and ice without the effects of the propeller boat hull. As well, a deflection plate was added to the bow of the propeller boat to reduce the direct loads on the hull and help reduce ice sheet wastage. A 3kW 3000 rpm electric motor, with a peak torque rating of 84 N·m, was installed on the top of the boat, which drove a 3:1 ratio bevel gearbox, rated at 108 N·m at a 2400 rpm input speed. The output shaft from the gearbox was rigidly

connected to the dynamometer, which was used to measure the shaft thrust and torque loads and the output shaft of the dynamometer was connected to the inboard end of the propeller shaft by a small stub shaft. Two bearings, one at either end of the propeller shaft tube, supported the propeller shaft. A schematic of the propulsion shafting system is shown in Figure 8.

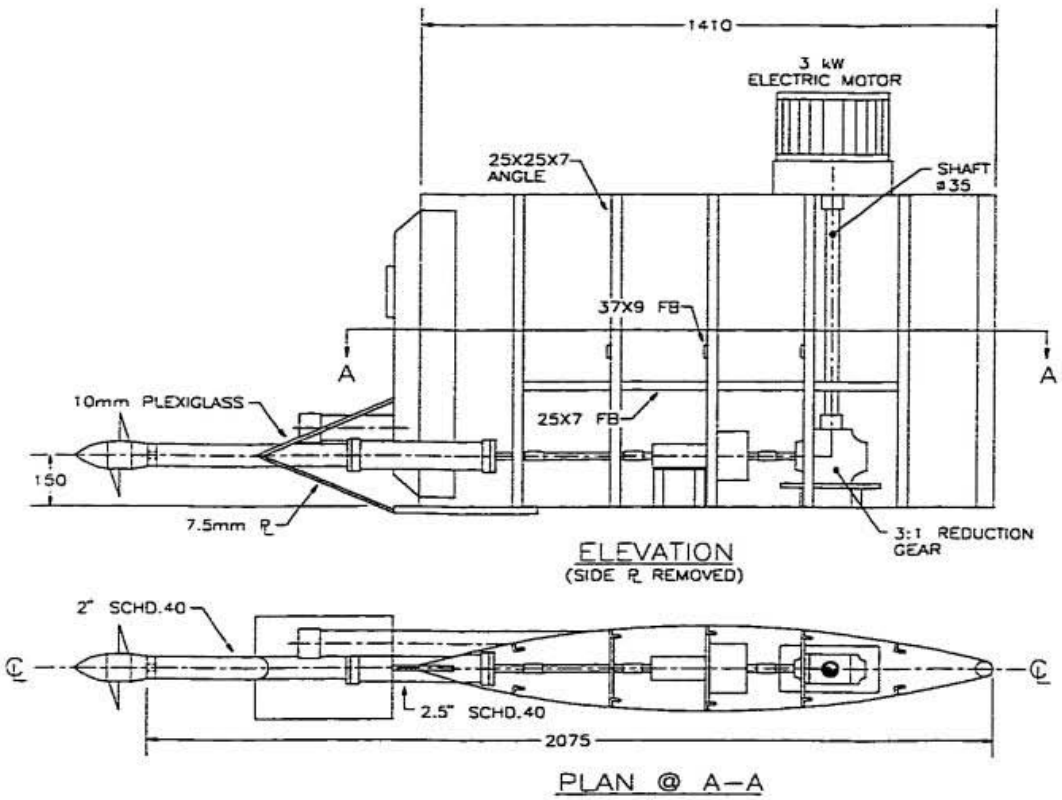

Figure 7: Schematic of Propeller Boat

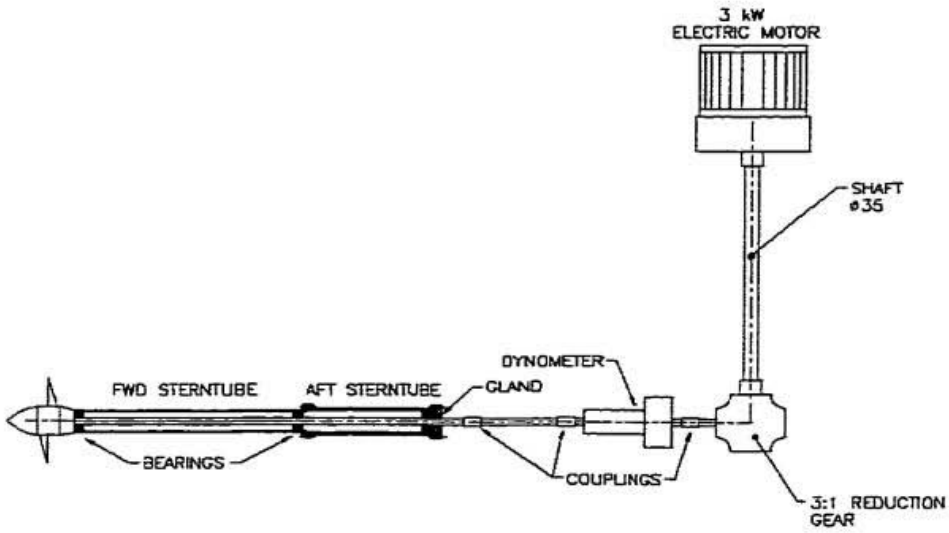

Figure 8: Propulsion System Schematic

2.4 Model Propellers

2.4.1 *Caribou* Propeller

The propeller used was a 250mm diameter model of the highly-skewed controllable-pitch propeller fitted to the *M/V Caribou*. The propeller is classed as a Lloyd's 1A Super. The test propeller was provided by KaMeWa and had the characteristics presented in Table 4. A photograph of the model is provided in Figure 9. The *M/V Caribou* is an *ice-class* Ro-Ro ferry that operates between Newfoundland and Nova Scotia year round. The *M/V Caribou* and her sister ship, the *M/V Joseph and Clara Smallwood*, can each accommodate over 300 automobiles and up to 1200 passengers. They are Canada's largest ferries and among the biggest of their class in the world.

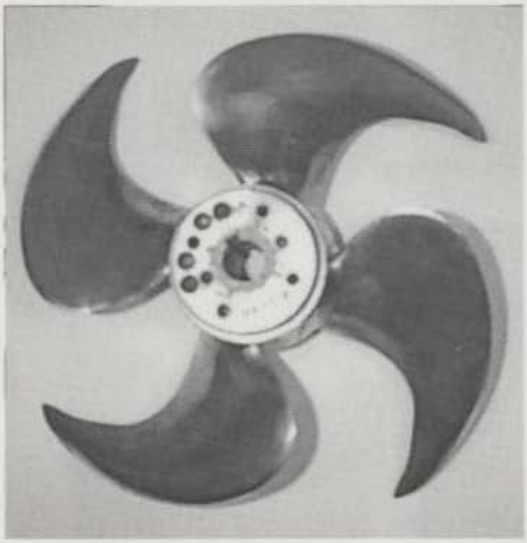

Figure 9: *Caribou* Propeller

Number of Blades	4
Diameter	0.250 m
Design Pitch/Diameter	1.320
EAR	0.511
Skew angle	50°

Table 4: *Caribou* Propeller Particulars

2.4.2 *R-Class* Propeller

The propeller used was a 200mm diameter model of the fixed pitch propeller fitted to the Canadian *R-Class* ice-breakers. This propeller model was used for previous experimental programs investigating the propeller ice interaction problem (Walker 1996, Doucet, 1996). The *R-Class* propeller characteristics are given in Table 5 and a photograph of the propeller is provided in Figure 10.

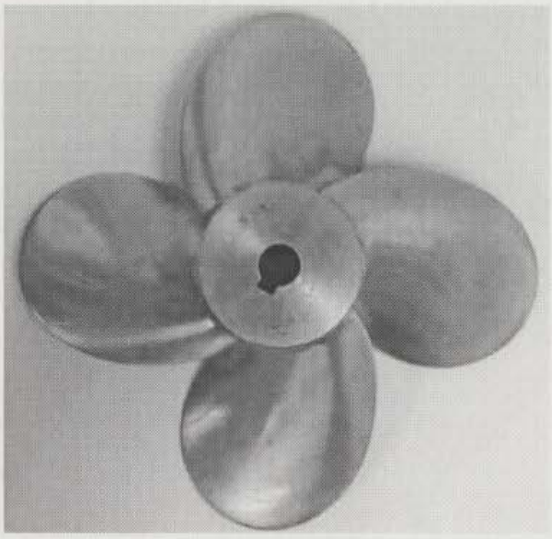

Figure 10: *R-Class* Propeller

Number of Blades	4
Diameter	0.20 m
Design Pitch/Diameter	0.779
EAR	0.670

Table 5: *R-Class* Propeller Particulars

2.5 IMD Ice Tank Facility

The following section gives a brief description of the major components of the IMD Ice Tank Facility. A more detailed description of the facilities and its capabilities has been presented by Jones (1987). The overall dimensions of the ice tank are summarised in Table 6 and a schematic of the ice tank and components are shown in Figure 11 for clarity.

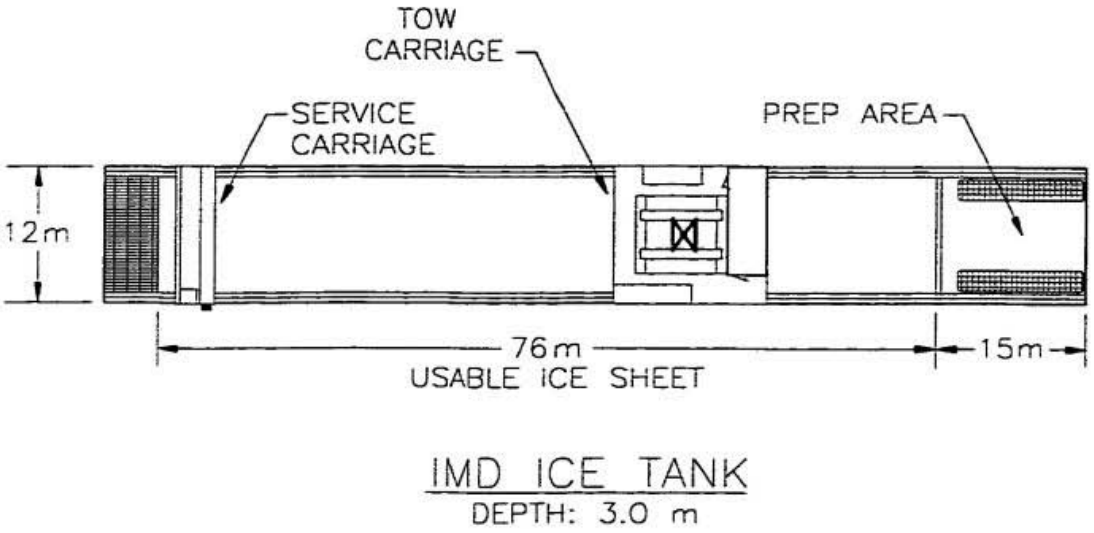

Figure 11: Ice Tank Layout

Length	**76 m**
Width	**12 m**
Depth	**3 m**

Table 6: Overall Tank Dimensions

To ensure that the ice properties remained uniform for the test program, the usable ice sheet was decreased to 60m in length by 6m wide. An additional 15m long set-up area was located at one end of the ice tank, separated by a thermal barrier door to allow for equipment set-up while an ice sheet is growing.

The ice tank towing carriage is an 80 tonne steel structure with dimensions of 15m in length, 14.2 m wide and 3.96m high with an operating speed ranging from 0.02 to 4.0

m/s. The test frame has the capabilities to move transversely and vertically to make efficient use of the ice sheet.

In addition, a separate hydraulically driven service carriage with speeds of up to 0.5 m/s in either direction can be used for ice control and measurement work.

2.6 Model Ice

For the experimental program, EG/AD/S model ice was used. It is a diluted aqueous solution of ethylene glycol (EG), aliphatic detergent (AD), and sugar (S). The model ice was developed by the National Research Council of Canada (NRC) and is described in detail by Timco (1986).

Two distinct ice sheets were used in the test program: one for the *Caribou* propeller, which had a thickness of approximately 90mm and a target flexural ice strength of 100kPa and one for the *R-Class* propeller, which had a thickness of approximately 60mm and a target flexural strength of 60kPa. A thicker ice sheet was used for the *Caribou* propeller test program to provide for the range of ice cut depths tested. Figure 12 defines cut depth into the underside of a level, stationary ice sheet. To investigate ice strength effects during the test program, repeat tests were conducted at different intervals of the day as the strength of the model ice decreased gradually over the coarse of the test period.

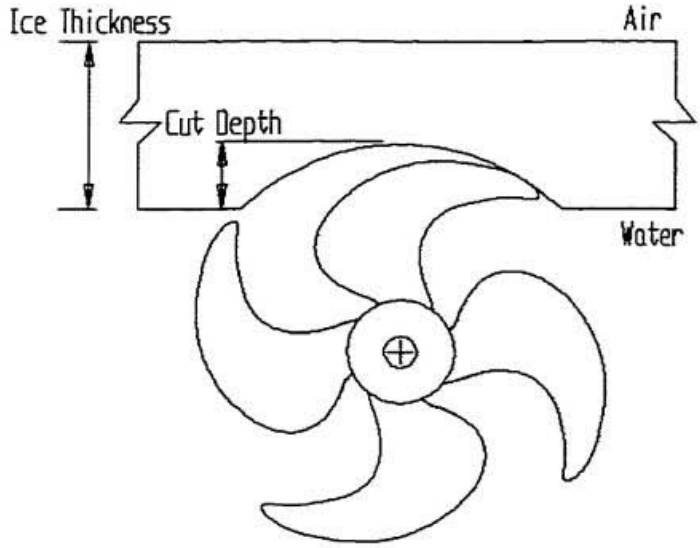

Figure 12: Definition of Cut Depth

2.7 Instrumentation

The experimental data measured during the test program were collected using two different data acquisition systems on board the ice tank carriage.

The primary measurements collected during the experimental program were shaft thrust, shaft torque, carriage speed, and shaft speed. To measure these variables the sensors were connected to a telemetry signal conditioner unit (TSCU) which provided excitation for the thrust and torque sensors and filtered the signal. Excitation was not required for the motor tachometer and carriage speed signals. Through an analog I/O cable, the TSCU was connected to an I/O Daqbook / 200 Data Acquisition System

where the signals were converted from analog to digital and then fed through a parallel port cable to an Industrial PC Telemetry server (200MHz Pentium Processor). From the Industrial PC, the signals were transferred to an Alpha workstation where the data could be analysed. A high sampling rate of 5000Hz was used because of the high rotational speed and the need to get many data points over a blade/ice contact period. The sampled data was filtered at 1000Hz.

The dynamometer used to measure shaft thrust and shaft torque was manufactured by Sensor Developments Inc. The dynamometer's load measuring capacities were specified to be 890 N of thrust and 113 N·m of torque, with 100% overload capacity and a maximum rpm of 1200.

The data acquisition system was calibrated in-situ, with the exception of the dynamometer. The dynamometer was calibrated using the manufacturer's calibrations and validated with pre-determined thrust and torque loads.

All of the test runs were recorded on videotape by an above ice video camera. Early attempts to use underwater video camera were frustrated by poor visibility caused by submerged pieces of ice. As well, ice pieces for each run were collected, measured and photographed to ensure accurate cut depths.

To record the vertical position of the propeller, a potentiometer was connected via a NEFF Instruments Signal Processing System. Through an interface cable, the potentiometer was connected to a NEFF System 620 Series 300 Signal Conditioner system, which provided excitation for the sensor. The sensor output was filtered and digitised by a NEFF System 620 Series 100 amplifier/filter/multiplexer and then displayed in the ice tank control room to assist the operator in setting the vertical position of the propeller. The sampling frequency was set at 50Hz and filtered at 10Hz to eliminate high frequency noise.

2.8 Test Program

2.8.1 Set-Up Procedures

Before the start of the test program and with the carriage stationary, the shaft bearings were run in by turning the shaft over slowly.

As well, the frictional torque in the shaft bearings was measured throughout the test program by conducting regularly scheduled friction tests. Each friction test involved replacing the propeller with a dummy hub, submerging the apparatus and running through a range of different shaft speeds with the test shaft speed as the mean. The friction tests were then used to account for friction in the torque results when analysing the data.

Another set-up procedure required cutting a path in the ice sheet for each run. The path was cut to control the amount of ice used in each run and to prevent wastage of ice. It was noticed in the early stages of the test program that the ice sheet would lift as the propeller boat came into contact with it. This would in turn cause the sheet to lift up from the propeller and vary the depth of cut, affecting the thrust and torque readings. To counteract this problem, the ice sheet along the test path was pre-cut so the ice blocks would break away from the main ice sheet as it came into contact with the boat. This procedure worked well and was used for the entire test program.

2.8.2 *Caribou* Propeller: Test Program

For the *Caribou* propeller test program, the test matrix was designed to investigate the ice milling loading condition and to cover the contact and non-contact components of the propeller ice interaction. A full range of loading conditions were investigated, which accounted for variations in advance coefficient and cut depth. The test program was subdivided into five sets of experiments to investigate cut depth and advance coefficient and each test series is described. It was initially intended to investigate the effects of ice strength but as the model propeller was damaged during the test program it was not possible to adequately investigate the ice strength effects with the *Caribou* propeller. The damage experienced by the model and a comparison with the full-scale propeller is presented in section 3.2.5.

Series 1 investigated the effect of cut depth while operating at a constant advance coefficient (J=0.30) and nominally constant ice strength. A number of test runs were conducted for cut depths ranging from a minimum depth of 11mm to a maximum of 60mm. The cut depth was controlled by the vertical position of the test frame and load data was collected over the ice milling period. The cut depth setting was checked by taking samples of the cut ice. The test matrix for Series 2 is summarised in Table 7.

Variable	*Range of Test Values*
J	0.3
h_I (mm)	11, 15, 19, 31, 36, 40, 45, 46, 47, 53, 53, 60
S_C (kPa)	180

Table 7: Test Matrix for Series 1

Series 2 considered the effects of advance coefficient on thrust and torque. Three different runs, each at a different depth of cut, were made in the series. For each run, the advance coefficient was varied from J = 0.1 to 0.8 in steps of 0.1. These tests were done in rapid succession so that ice strength variations were minimal. In addition, running in rapid succession helped reduce variation in results due to deviations in depth of cut. The test matrix for Series 2 is summarised in Table 8.

Variable	*Range of Test Values*
J	0.1 to 0.8, steps of 0.1
h_I (mm)	30, 46, 70
S_C (kPa)	170, 168, 130

Table 8: Test Matrix for Series 2

Series 3 was the same as Series 1 with the exception of a change in advance coefficient. For this series of tests, advance coefficient was kept constant at J = 0.50 while the depth of cut was changed from approximately 14mm to 67mm. A total of 8 runs were conducted including a repeat run to examine the repeatability of the test program. Table 9 presents the test matrix for this series.

Variable	*Range of Test Values*
J	0.5
h_I (mm)	14, 22, 34, 40, 48, 49, 50, 67
S_C (kPa)	160

Table 9: Test Matrix for Series 3

Series 4, like Series 2, investigated the effects on thrust and torque due to variations in advance coefficient. Three runs at different depth of cut values were made with the advance coefficient ranging from J = 0.1 to 0.8 in steps of 0.1. Series 4 was conducted in order to check the repeatability of the test program and investigate changes in thrust and torque due to variations in ice strength by comparing the results of series 4 with those of series 2. The test matrix for series 4 is illustrated in Table 10.

Variable	*Range of Test Values*
J	0.1 to 0.8, steps of 0.1
h_I (mm)	25, 48
S_C (kPa)	147, 145

Table 10: Test Matrix for Series 4

Series 5 of the test program was similar to series 1 and 3 except the advance coefficient was held constant at J = 0.70. The depth of cut varied from approximately 19mm to 72mm and a total of 7 runs were conducted to investigate the effects of cut depth on propeller thrust and torque. The test matrix is provided in Table 11.

Variable	*Range of Test Values*
J	0.7
h_I (mm)	19, 27, 46, 48, 54, 56, 72
S_C (kPa)	138

Table 11: Test Matrix for Series 5

In addition to experiments investigating propeller-ice interaction, open water experiments were conducted with the *Caribou* propeller. The open water tests were conducted in the Ice Tank. A total of 15 runs were completed with advance coefficients ranging from J = 0 to J = 1.4 at steps of 0.1 while measuring carriage speed, propeller rate of rotation, propeller thrust and propeller torque. Shaft friction torque was measured at the start and the end of the test program by replacing the propeller with a dummy hub and running the shaft over a range of rotational speeds

with the test rps as the mean. Test runs were conducted at every other specified speed starting from the lowest speed and moving to the highest speed and then continued from the highest speed to the lowest speed filling in the gaps. At the beginning of each run, with the carriage stopped and the shaft rotating at the specified rps, thrust and torque measurements were made to record the bollard pull values. These values were used as a check for each run as there should have been minimal change in the bollard readings during the test program. To correct for the effects of friction on the propeller torque, the shaft friction torque measurements were plotted versus rps and a mean line drawn through them. The mean line at the test rps determined the friction associated with each test run. The propeller torque was calculated by subtracting the test friction from the mean test value of shaft torque. To present the data, the non-dimensional propeller coefficients advance coefficient, thrust coefficient, torque coefficient were used.

2.8.3 *R-Class* Propeller: Test Program

For the *R-Class* propeller test program, the test matrix was designed to investigate the ice milling loading condition and to cover the contact and non-contact components of the propeller ice interaction. No variation in depth cut was made for the *R-Class* propeller tests, but tests were done over four quadrants of operation and an investigation of ice strength effects was possible. Measurements were made of shaft torque and thrust, shaft speed and advance speed. As with the *Caribou* propeller tests, a range of model ice strengths and ice mechanical properties were measured

throughout the test program. To define the four quadrants of propeller operation, a sketch is shown in Figure 13.

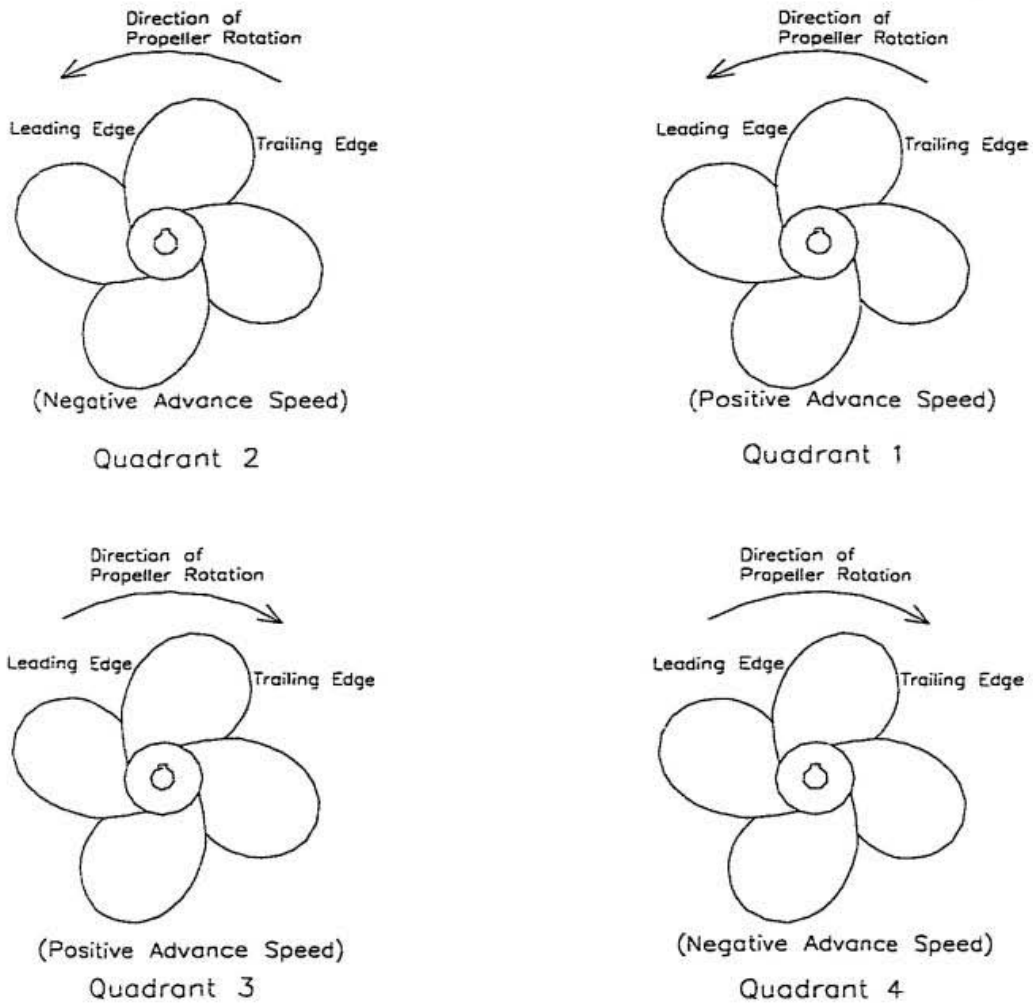

Figure 13: Four Quadrants of Propeller Operation

Quadrant 1 is defined as the propeller in the forward operating condition where the advance speed is positive and the shaft is rotating in a positive direction. Quadrant 2

is defined as a negative advance speed with a positive shaft speed. Quadrant 3 is defined, as the operating condition where the advance speed is positive while the shaft speed is negative. Quadrant 4 is defined as the reversing condition where both the advance speed and the shaft speed are negative.

To reduce inaccuracies in results due to variations in cut depth and ice strength, the test runs for each quadrant were conducted in rapid succession and contained eight points for the lower values of advance coefficient and four points for the higher end. Tests were completed in successive order for each quadrant, and repeats were carried out to observe the effects of ice strength. After each run, an ice sample was taken to confirm the cut depth and the propeller boat was repositioned using the potentiometer for the next run.

As quadrant 1 is the most frequent operating condition, it was the most analysed in the test program. During the test period, a total of six runs were completed for quadrant 1 (runs 1, 2, 3, 9, 10, and 15). Runs 1, 2, and 3 were conducted at the beginning of the test day, runs 9 and 10 took place later in the test period and run 15 was conducted at the end of the test day as an extra run to observe ice strength effects. The test matrix for runs in quadrant 1 is shown in Table 12.

Run Number	*J*	S_C *(kPa)*	h_I *(mm)*
Run 1	0.1 to 0.8 step 0.1	93	24
Run 2	0.8 to 1.0 step 0.1	91	24
Run 3	0.05 to 0.75 step 0.1	89	24
Run 9	0.1 to 0.8 step 0.1	66	25
Run 10	0.8 to 1.0 step 0.1	66	25
Run 15	0.1 to 1.0 step 0.2	58	24

Table 12: Test Matrix for Quadrant 1

For quadrant 2, two independent runs (run 4 and run 13) were performed to investigate the propeller operating from J = -0.05 to J = -0.4 in steps of -0.05. For the test program the propeller boat was mounted to the ice tank carriage so that the test could only be conducted in one direction. To simulate the negative advance speed required for quadrant 2 testing, the propeller was oriented in a manner opposite to that of traditional propeller boat tests. The test matrix for quadrant 2 is provided in Table 13.

Run Number	*J*	S_C *(kPa)*	h_I *(mm)*
Run 4	-0.05 to -0.4 step –0.05	84	24
Run 13	-0.05 to -0.4 step –0.05	60	25

Table 13: Test Matrix for Quadrant 2

Similarly, two independent runs (run 5 and run 14) were conducted for quadrant 3. This part of the test program was developed to investigate the thrust and torque

experienced due to the propeller operating with a positive advance speed but a negative shaft rotation, which is an operating condition that occurs during emergency situations (crash stopping), or during ramming cycles. The advance coefficient range was J = -0.05 to -0.4 in steps of -0.05, as for the quadrant 2 tests. The test matrix is shown in Table 14.

Run Number	***J***	S_C ***(kPa)***	h_I ***(mm)***
Run 5	-0.05 to -0.4 step –0.05	80	25
Run 14	-0.05 to -0.4 step –0.05	59	26

Table 14: Test Matrix for Quadrant 3

The advance coefficient range for quadrants 2 and 3 were kept lower than that for quadrants 1 and 4 to avoid extreme conditions in which the model might be damaged.

For quadrant 4 (reversing condition), the advance coefficient was investigated from J = 0.1 to 1.1. A total of 5 test runs were conducted in quadrant 4 (Runs 6, 7, 8, 13 and 14) to investigate the propeller loads while operating in reverse. As with other tests, effects of ice strength were observed by repeating runs 6 and 8 (runs 13 and 14).

Run Number	*J*	S_C *(kPa)*	h_I *(mm)*
Run 6	0.1 to 0.8 step 0.1	73	26
Run 7	0.8 to 1.0 step 0.1	71	26
Run 8	0.05 to 0.75 step 0.1	70	26
Run 13	0.1 to 0.8 step 0.1	65	24
Run 14	0.8 to 1.0 step 0.1	64	24

Table 15: Test Matrix for Quadrant 4

Previous work with the *R-Class* propeller included open water hydrodynamic tests (Luznik, 1994). The results from that work have been included here to observe how propeller thrust and torque are affected by the presence of ice.

Chapter 3

Experimental Results & Discussion

3.1 Objectives

The objectives of this chapter are to display and present a discussion of the results from the experimental program. The chapter is subdivided into two main components: the results from the *Caribou* propeller test program and the results from the *R-Class* propeller test program. Each of the variables investigated is presented and discussed in the relevant subsections.

3.2 Results: *Caribou* Propeller Test Program

For the *Caribou* propeller test program, the test matrix was designed to investigate the ice milling loading condition. A full range of loading conditions were investigated,

which accounted for variations in advance speed and cut depth. In addition, an open water test program was conducted to determine the performance characteristics of the model propeller in an unrestricted uniform flow.

3.2.1 Open Water Test Results

To present the data, the non-dimensional propeller coefficients: advance coefficient, thrust coefficient, torque coefficient and open water efficiency were determined using equations 19 through 22 respectively,

$$J = \frac{V_A}{nD} \qquad [19]$$

$$K_T = \frac{T}{\rho_w n^2 D^4} \qquad [20]$$

$$K_Q = \frac{Q}{\rho_w n^2 D^5} \qquad [21]$$

$$\eta_o = \frac{JK_T}{2\pi K_Q} \qquad [22]$$

where V_A is the speed of advance of the propeller, which is equal to the carriage speed as there is no wake effect, n is the shaft rotational speed, D is the propeller diameter and ρ_W is the water density, which is 1.0025 kg/m^3 for tests in the ice tank.

The propeller open water performance results are presented in Figure 14. Through both the thrust and torque coefficients, 3rd order polynomials have been fitted and show a good correlation. The results are similar to those of a B-Series propeller with a P/D of 1.3. The bollard pull values of K_T and K_Q are 0.8 and 0.06 compared to 0.53 and 0.095 for the B-Series and the maximum efficiency is 0.8 compared to 0.76 for the B-Series propeller. Compared to other highly skewed propellers the open water efficiency and bollard pull values are reasonable (Harvald, 1983).

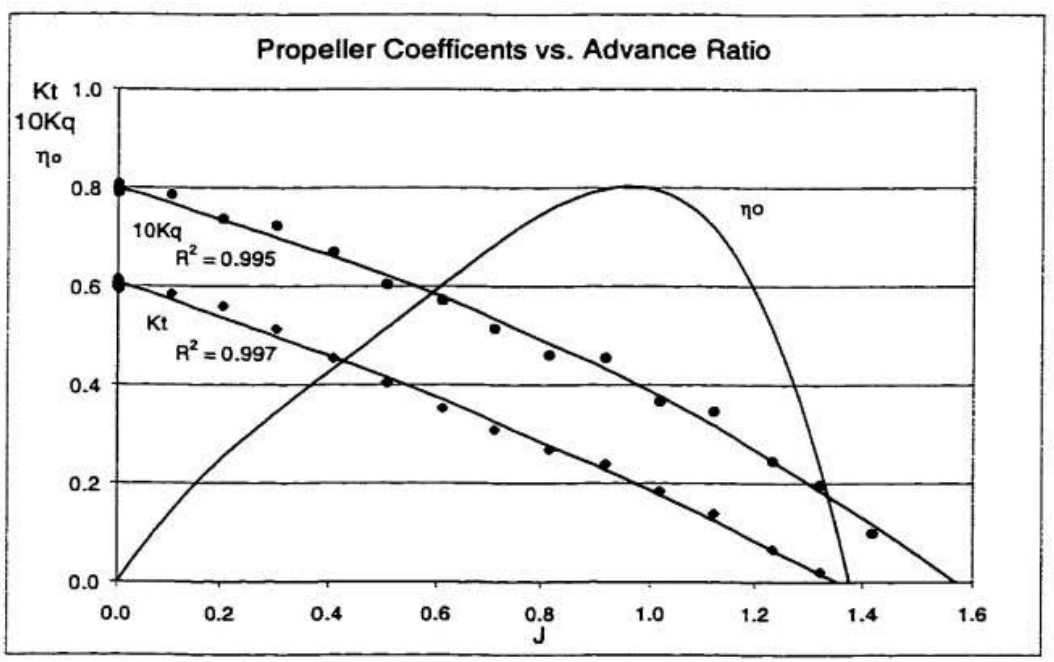

Figure 14: Open Water Performance Curves for *Caribou* Propeller

3.2.2 Distribution of Load during Contact Period

At a sampling rate of 5000 Hz, milling test times of between 2 and 3 seconds gave 10000 to 15000 collected data points, which gave a clear picture of the load variation during a milling event. The time series for the milling event during run S3_T5_005 is shown in Figure 15, where thirty consecutive blade passes through the ice can be detected from the shaft torque time history. Run S3_T5_005 consisted of a test that involved an advance coefficient of J = 0.5 and a cut depth of approximately 48mm from the tip of the propeller blade ($\lambda_d \equiv 0.19$). In addition to the time history, the probability density histograms of the thrust and torque loads for this run are given in Figures 16 and 17. For each test run, the maximum and minimum values were determined and 50 evenly spaced cell ranges were constructed between the extreme data points. This procedure was conducted for each test run and time histories and histograms for additional test runs are provided in Appendix A for review.

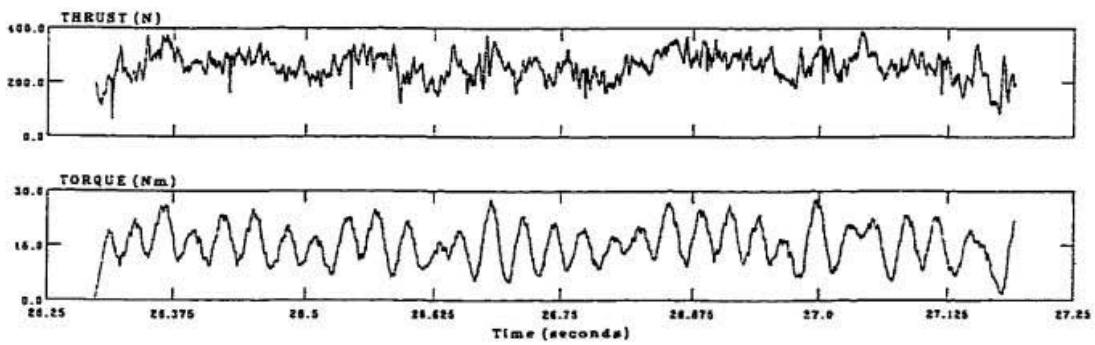

Figure 15: Time Series for Run S3_T5_005

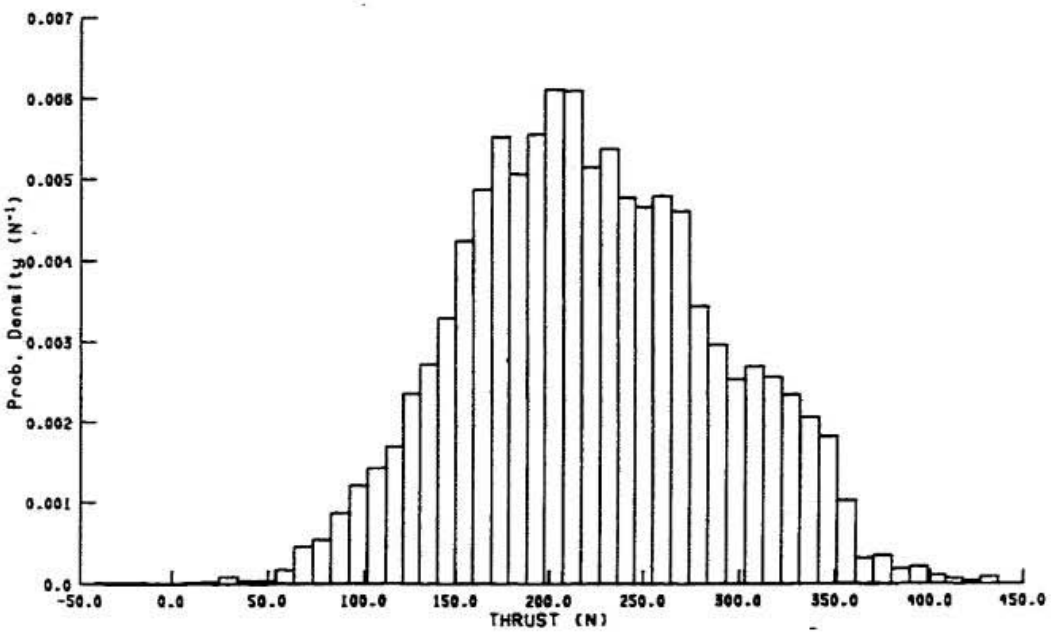

Figure 16: Thrust Density Distribution for run S3_T5_005

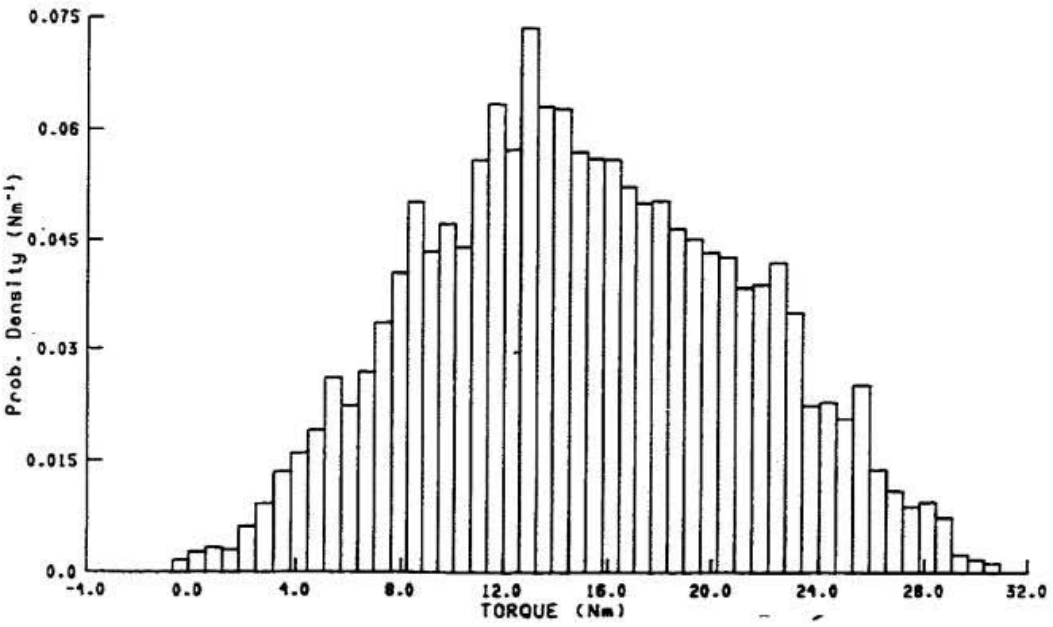

Figure 17: Torque Density Distribution for run S3_T5_005

From Figure 16 it can be seen that during the contact period, the shaft thrust distribution is close to normally distributed. The same type of distribution was found to occur for the majority of the runs while the range of distribution was dependent on the magnitude of the loads measured: the larger the loads, the larger the range. For low values of torque, the distribution behaved in a similar manner to the thrust. For runs, like that shown in Figure 17, where the torque loads were relatively high, the torque distribution tended to have a larger range. For runs that had lower values of torque, the loads tended to be more concentrated and the range was less wide.

3.2.3 Variations in Cut Depth

To investigate the effects on propeller thrust and torque due to variations in cut depth, series 1, 3 and 5 of the test program were conducted. Advance coefficient was held constant at J = 0.3, 0.5 and 0.7 respectively while the depth of cut was changed. The cut depth was set using the vertical potentiometer and verified by measuring ice samples taken from the test run. Examples of these ice pieces is shown in Figures 18 and 19.

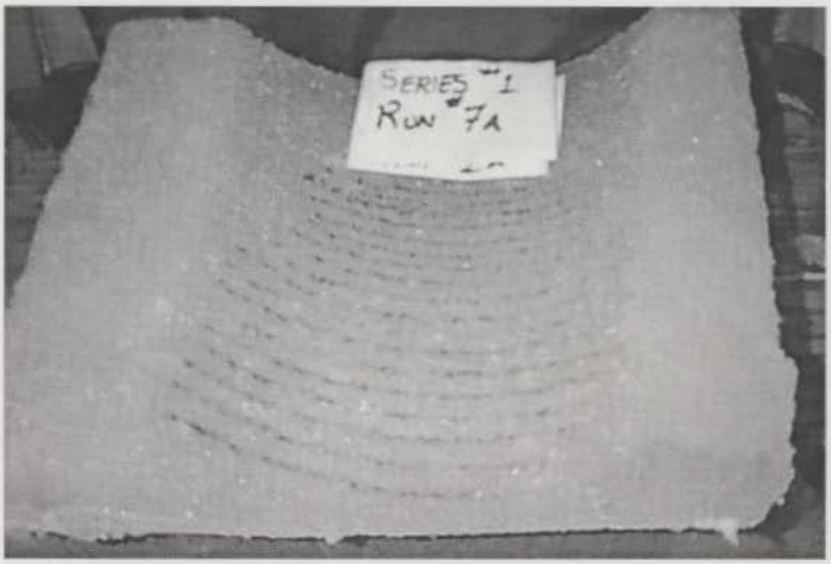

Figure 18: Ice Sample #1

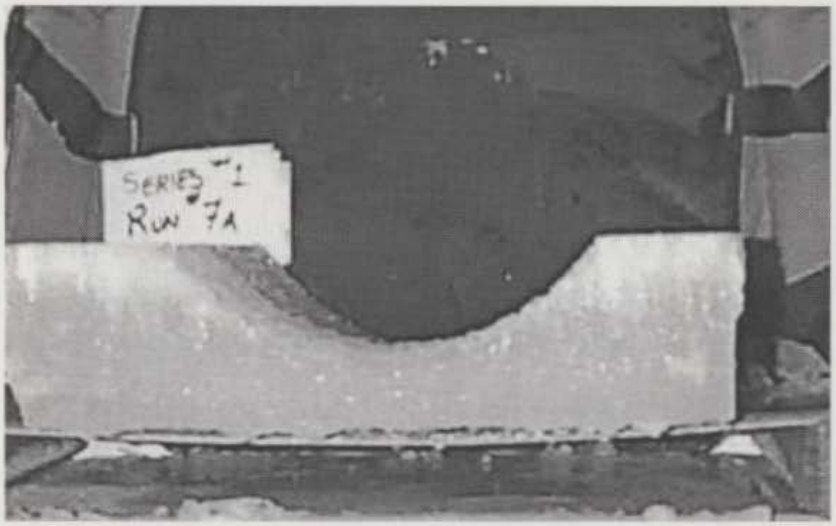

Figure 19: Ice Sample #2

The results from series 1,3 and 5 are presented in Figures 20 and 25. The solid black circles represent the experimental means for the thrust and torque coefficients and the solid line through these points represent lines of best fit. The open circles represent the maximum values measured during the test program and the open triangles

represent the minimum values measured. Dashed lines represent lines of best fit through the maximum and minimum values for each coefficient, and a solid line is used to represent a line of best fit through the mean values.. In addition, the open water values for the thrust and torque coefficients at each J are plotted as a solid horizontal line, which can be used a reference.

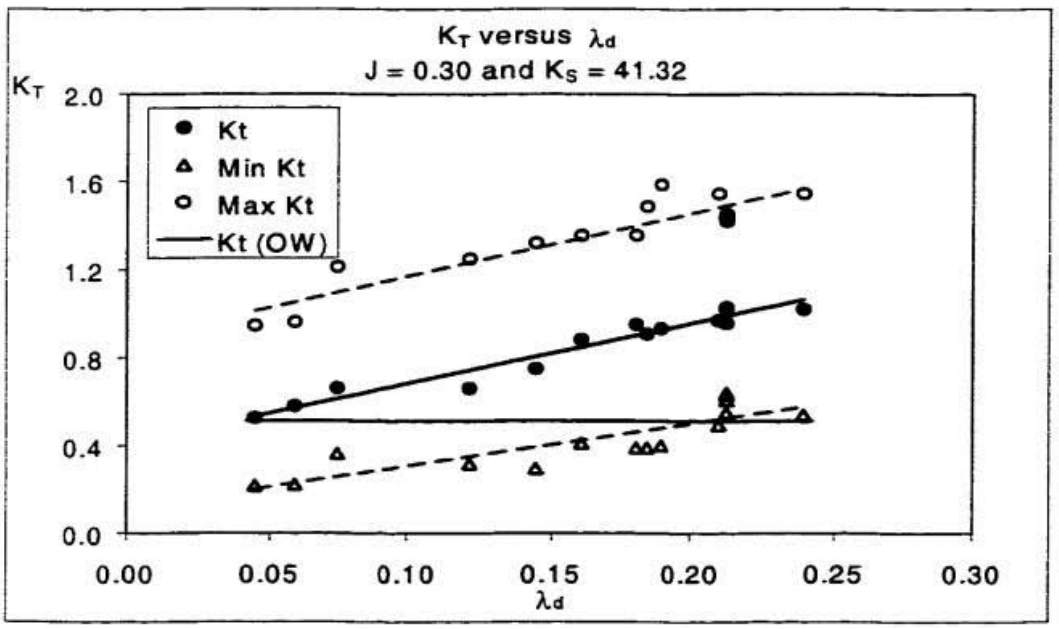

Figure 20: K_T vs. λ_d for J = 0.3 and K_S = 41.32

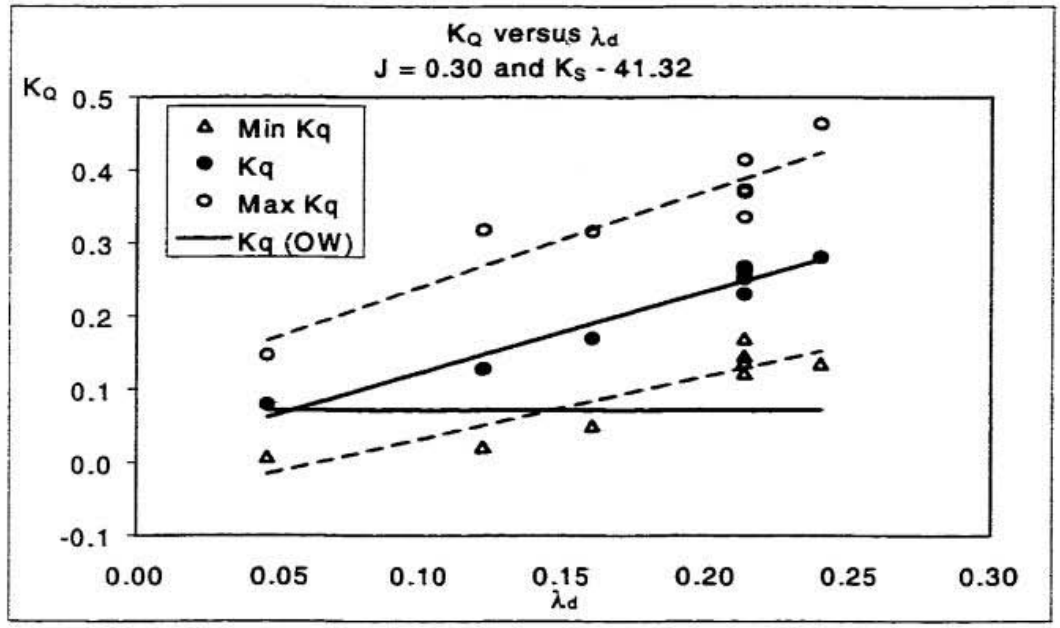

Figure 21: K_Q vs. λ_d for J = 0.3 and K_S = 41.32

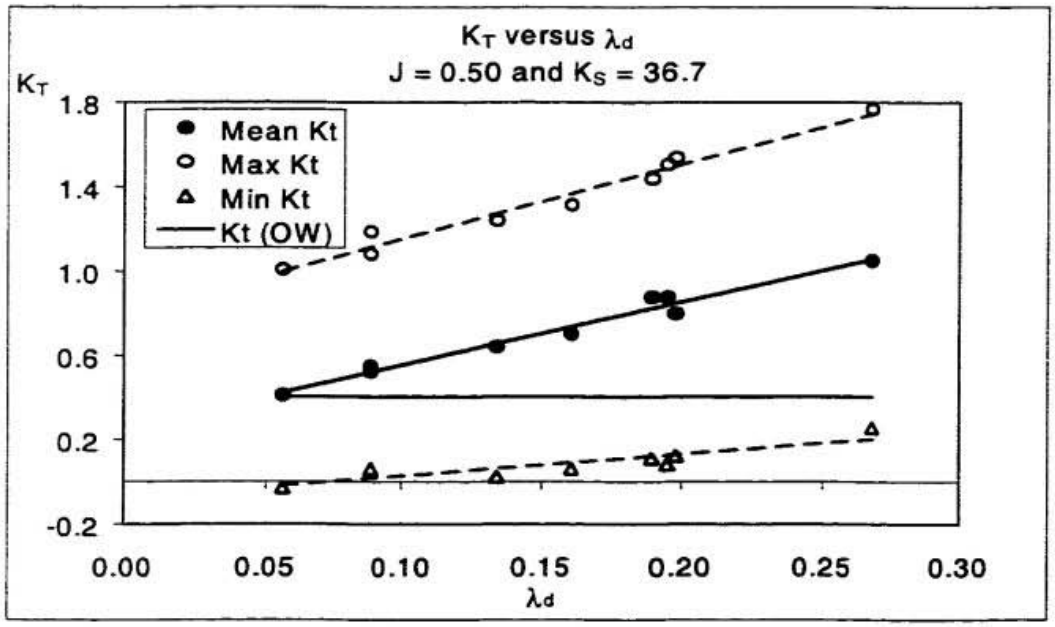

Figure 22: K_T vs. λ_d for J = 0.5 and K_S = 36.70

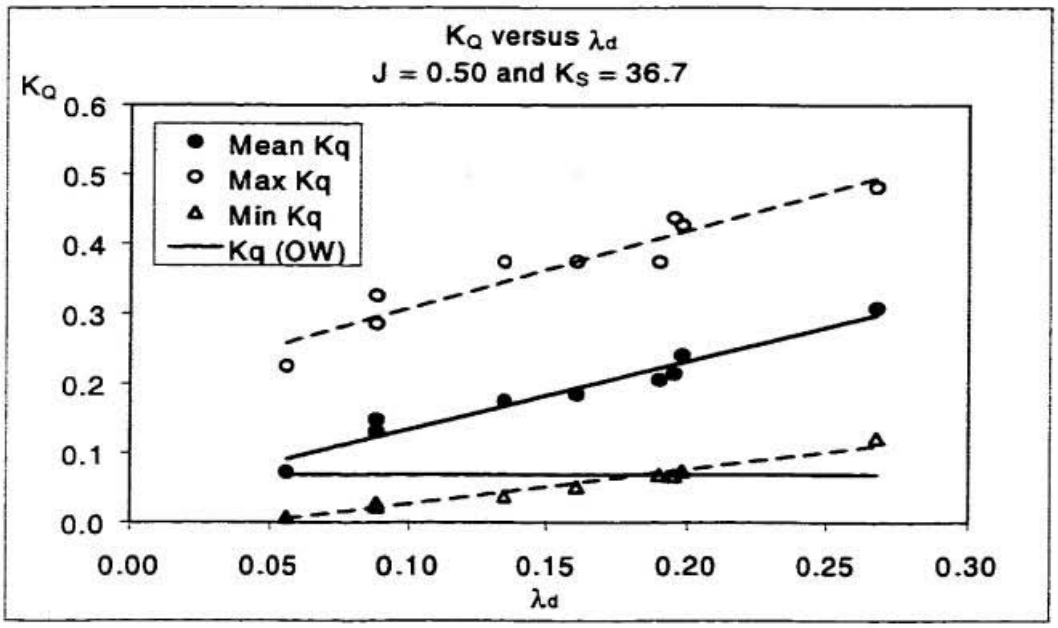

Figure 23: K_Q vs. λ_d for J = 0.5 and K_S = 36.70

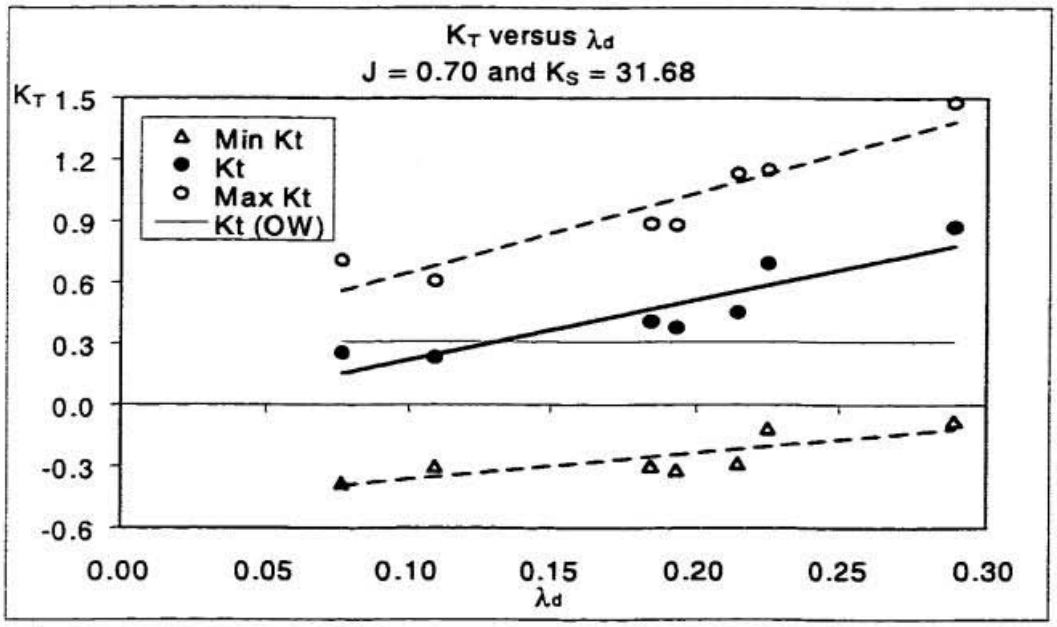

Figure 24: K_T vs. λ_d for J = 0.7 and K_S = 31.68

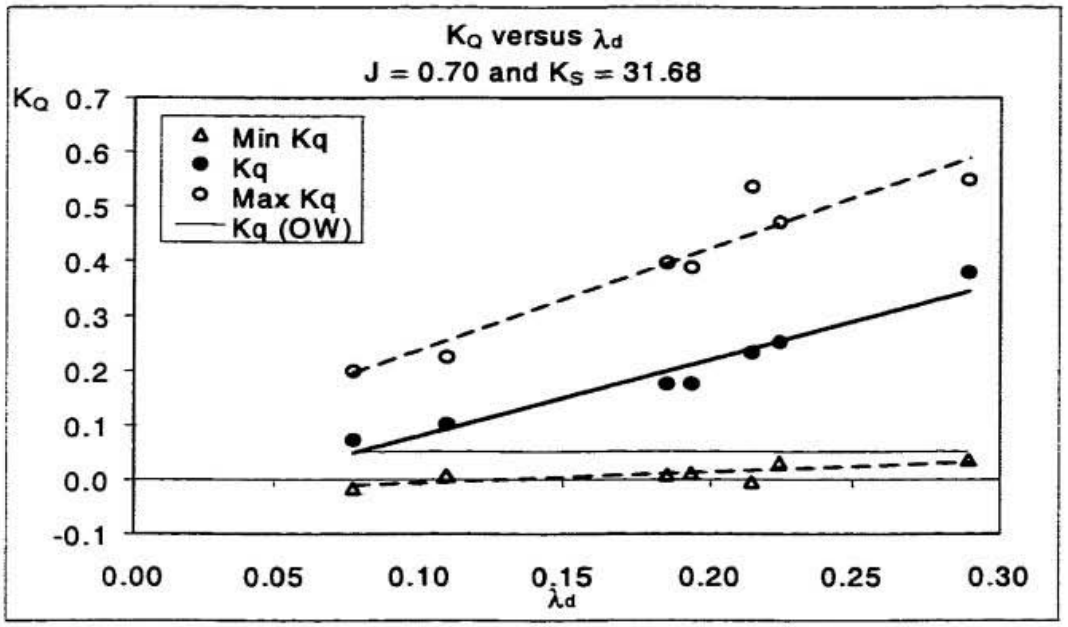

Figure 25: K_Q vs. λ_d for J = 0.7 and K_S = 31.68

Operation of the propeller at a constant advance coefficient for a range of λ_d resulted in an approximately linear relationship between both the mean K_T and K_Q versus λ_d. This is illustrated in Figures 20 and 21 for J = 0.3, where the slopes of the mean K_T and mean K_Q versus λ_d lines are

$$\frac{\Delta K_T}{\Delta \lambda_d}(J = 0.3) = 2.61 \qquad [23]$$

$$\frac{\Delta K_Q}{\Delta \lambda_d}(J = 0.3) = 1.02 \qquad [24]$$

Corresponding slopes for mean K_T and K_Q versus λ_d at J = 0.5 were 3.06 and 1.04. Likewise, for J = 0.7 the slopes were 3.30 and 1.12. The maximum and minimum values followed trends similar to the mean values. Further, the difference between the mean and maximum values, and the mean and minimum values is approximately equal. This reflects the underlying oscillatory behaviour of the loads about a single mean value.

3.2.4 Variations in Advance Coefficient

Series 2 and 4 considered the effects of variation in advance coefficient on propeller thrust and torque. Three runs at different cut depths were made for each series with the advance coefficient ranging from J = 0.1 to 0.8 in increments of 0.1. Each test was done in rapid succession to minimise the effects of ice strength variations. Figures 26 to 35 represent the thrust and torque coefficients versus advance coefficient for different values of λ_d. The solid black circles are the experimental means for the thrust and torque coefficients and the curves through these points are 3rd order polynomial lines of best fit. The open circles are the maximum values measured during the test program and the open triangles are the minimum values. The lines of fit through the maximum and minimum data points are 3rd order polynomials. The open water curves for thrust and torque coefficients are plotted on the respective charts for reference.

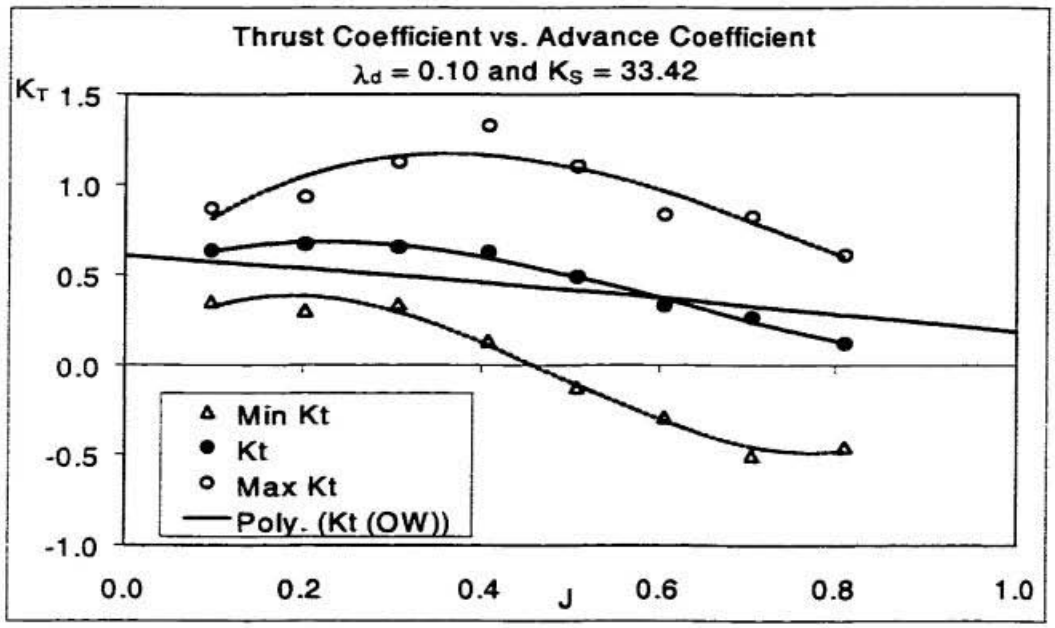

Figure 26: K_T vs. J for $\lambda_d = 0.10$ and $K_S = 33.42$

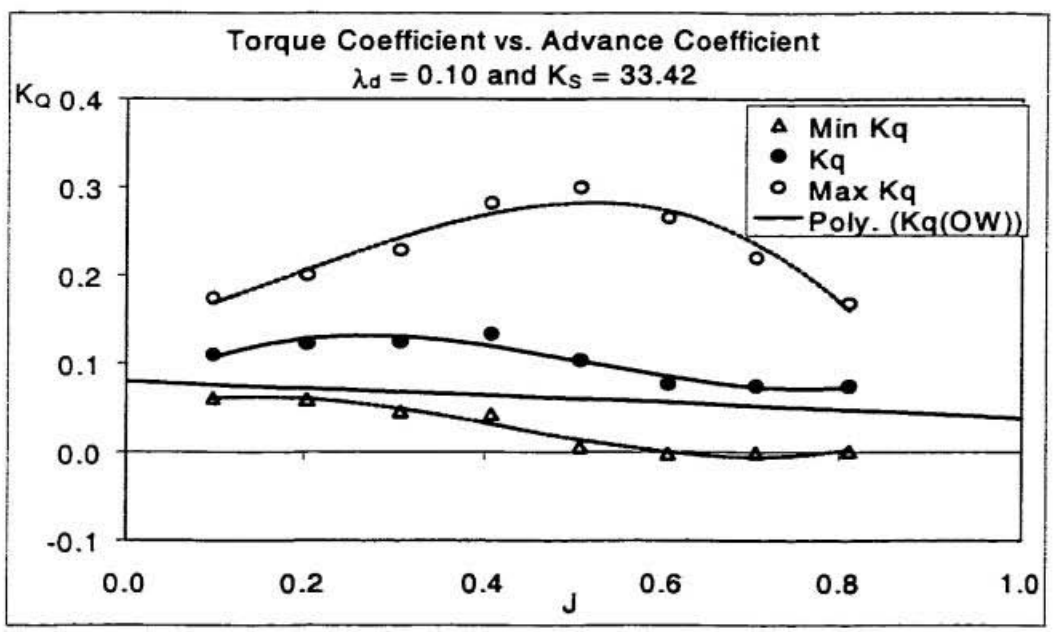

Figure 27: K_Q vs. J for $\lambda_d = 0.10$ and $K_S = 33.42$

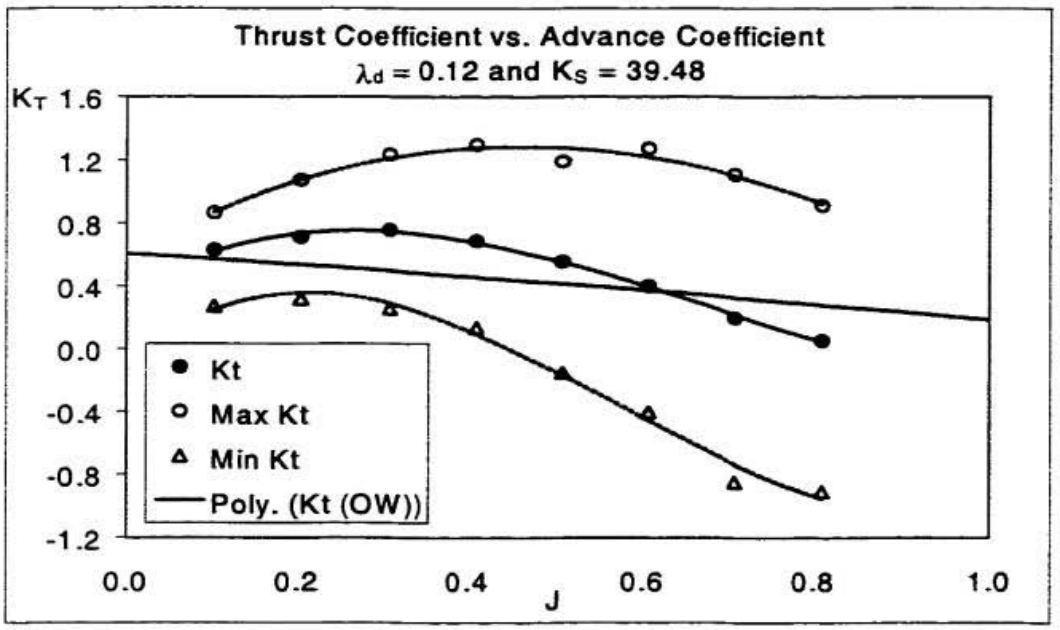

Figure 28: K_T vs. J for $\lambda_d = 0.12$ and $K_S = 39.48$

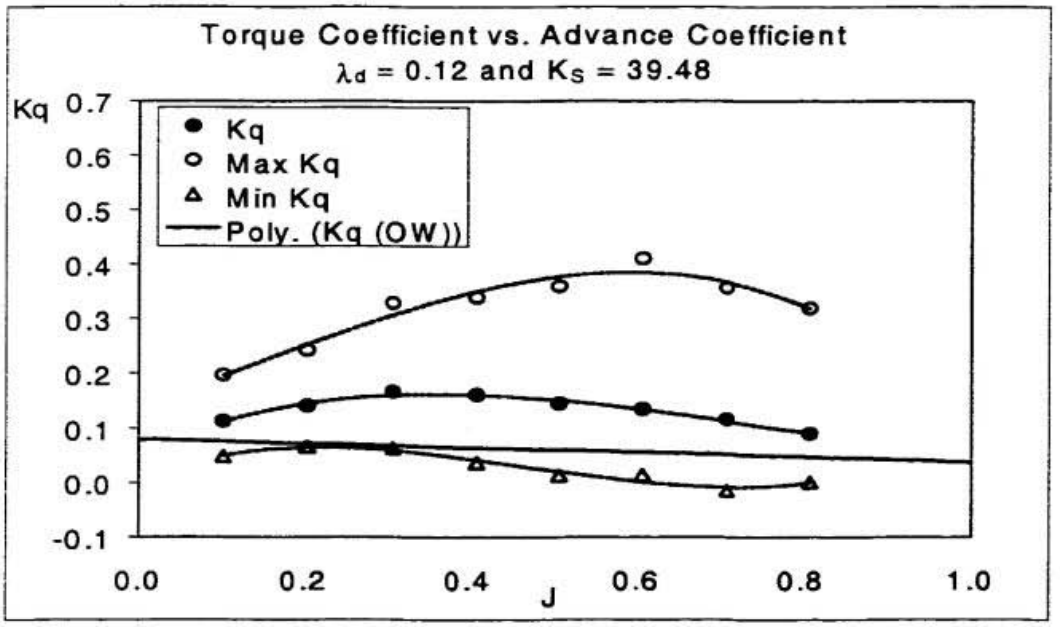

Figure 29: K_Q vs. J for $\lambda_d = 0.12$ and $K_S = 39.48$

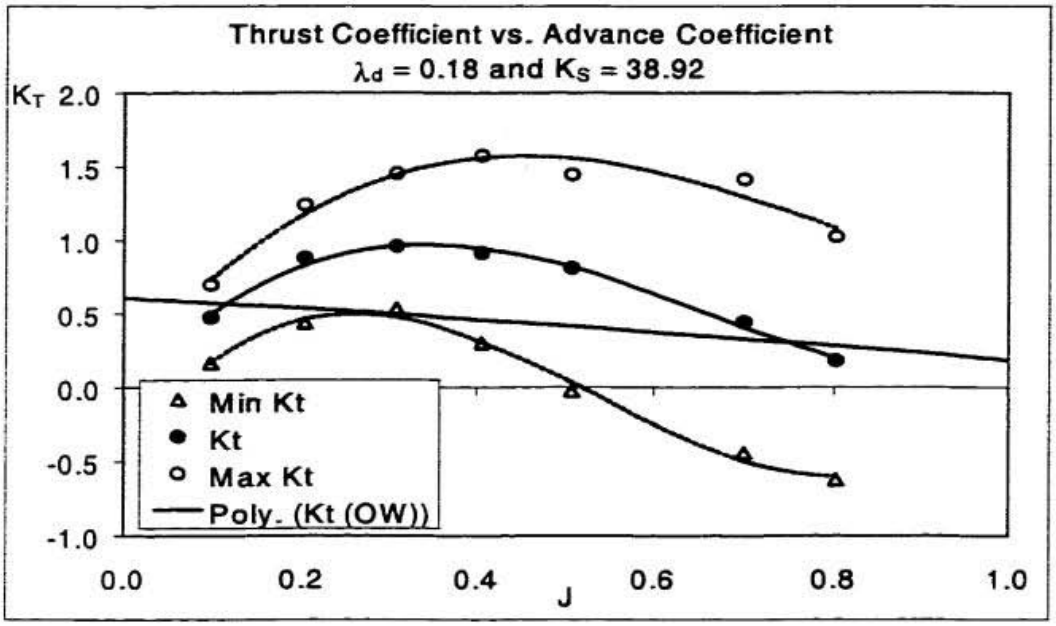

Figure 30: K_T vs. J for $\lambda_d = 0.18$ and $K_S = 38.92$

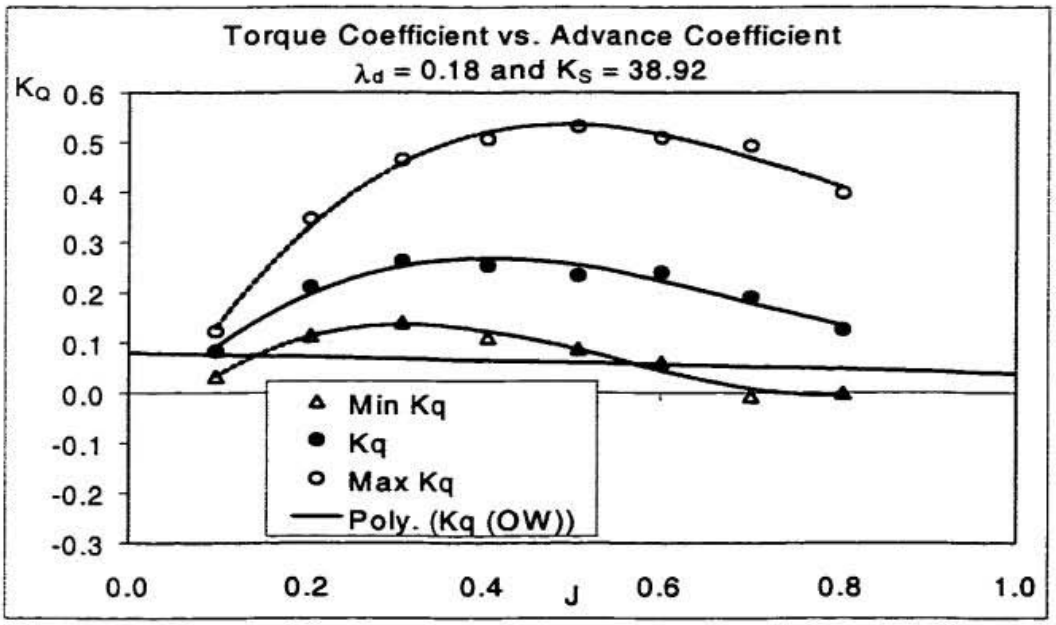

Figure 31: K_Q vs. J for $\lambda_d = 0.18$ and $K_S = 38.92$

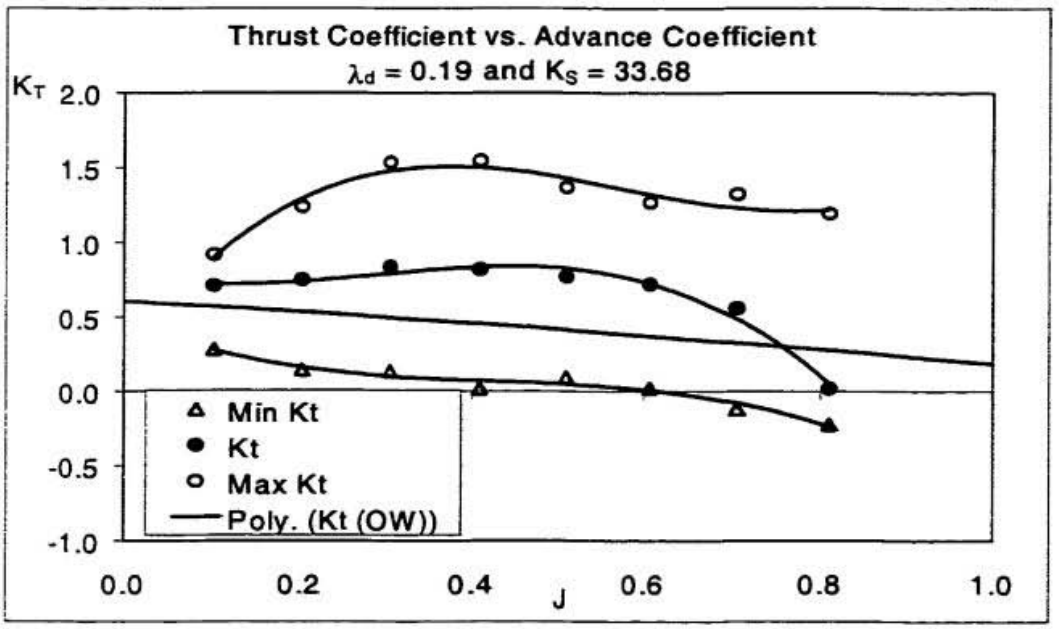

Figure 32: K_T vs. J for $\lambda_d = 0.19$ and $K_S = 33.68$

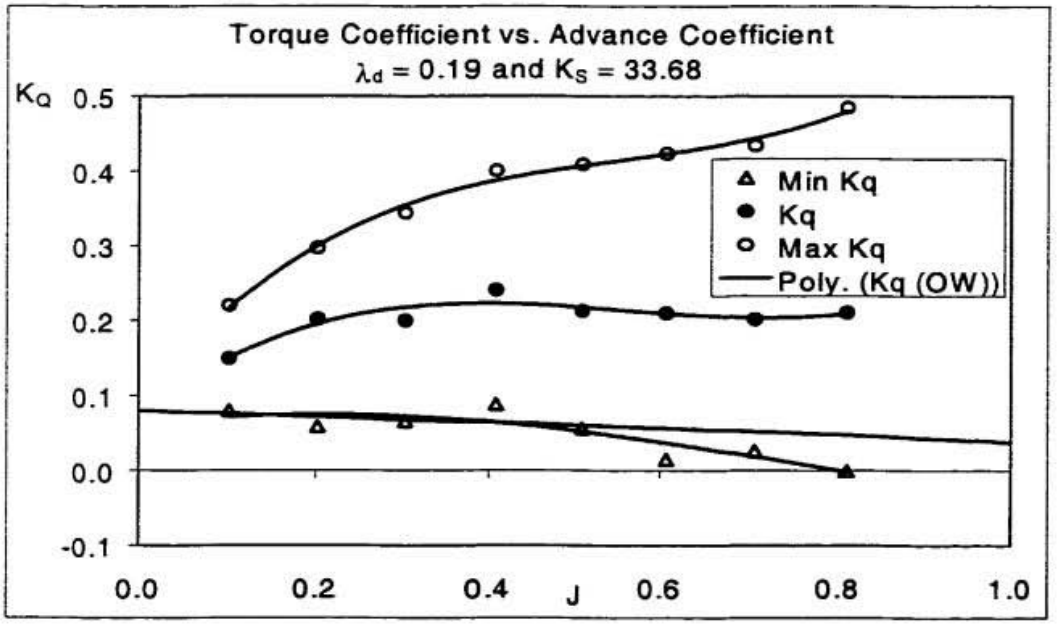

Figure 33: K_Q vs. J for $\lambda_d = 0.19$ and $K_S = 33.68$

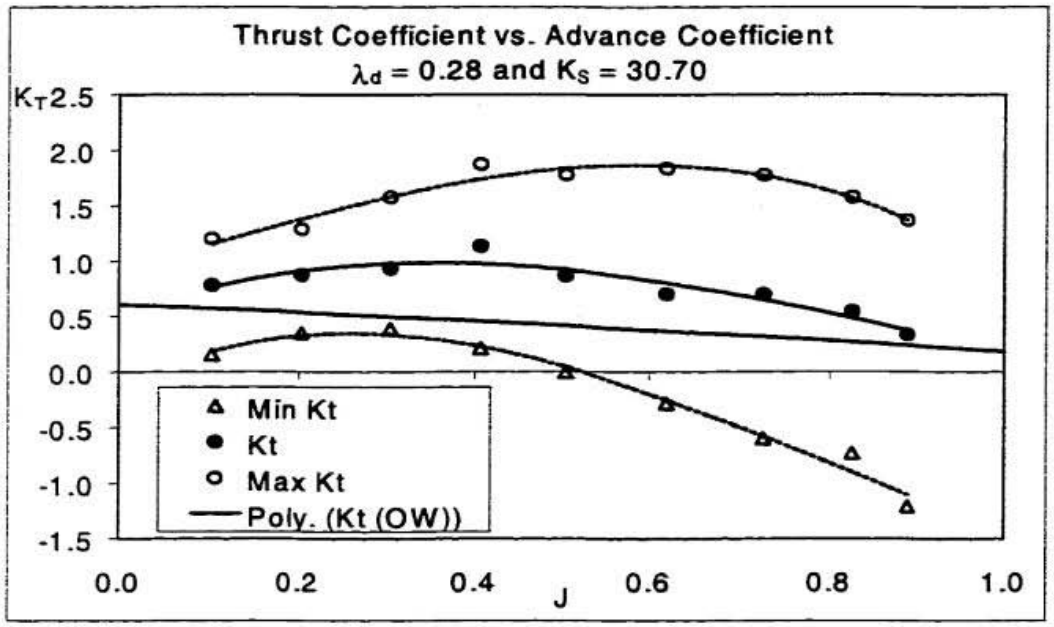

Figure 34: K_T vs. J for $\lambda_d = 0.28$ and $K_S = 30.70$

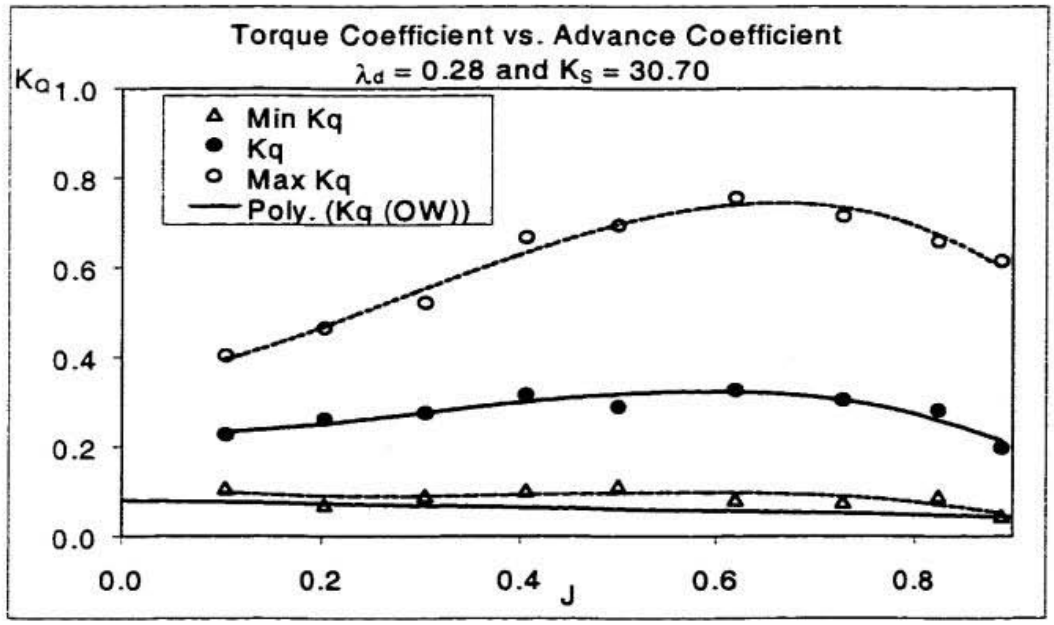

Figure 35: K_Q vs. J for $\lambda_d = 0.28$ and $K_S = 30.70$

Starting at low advance coefficient, the mean thrust coefficient first increases until a maximum is reached at approximately J = 0.3 to 0.4, then it diminishes gradually, approaching a value of zero above J = 0.8. This behaviour in the thrust load occurred for all of the runs except for the run at a cut depth of 48.3mm ($\lambda_d \cong 0.19$). During this run, ice blocks slipped prior to contact with the propeller blades which caused the thrust and torque loads to behave erratically.

The same trend can be seen in the mean torque coefficient, which has a maximum reading at approximately J = 0.4 then decreases as advance coefficient increases, but does not drop to zero over the range of J investigated. Why the thrust and torque loads behave in this manner can be attributed to the load mechanics behind the propeller-ice contact, which is described in the next paragraph.

For the portion of the mean load curves that are above the open water curves, the resultant load acts on the pressure side of the blade, as shown in Figure 36a, creating an increase in both the total thrust and torque loads. When the mean K_T curve intersects the open water curve the resultant force acts close to the leading edge of the blade, as shown in Figure 36b, such that there is a torque component to the contact load, but the thrust component is, on average, insignificant and the total thrust load consists of only the hydrodynamic component. As advance coefficient increases above this point, the resultant force moves back along the suction side of the blade, as shown in Figure 36c, creating at first a negative thrust component combined with a

positive torque component. Eventually the resultant force shifts far enough along the suction side, as shown in Figure 36d, that both the thrust and torque components can go negative.

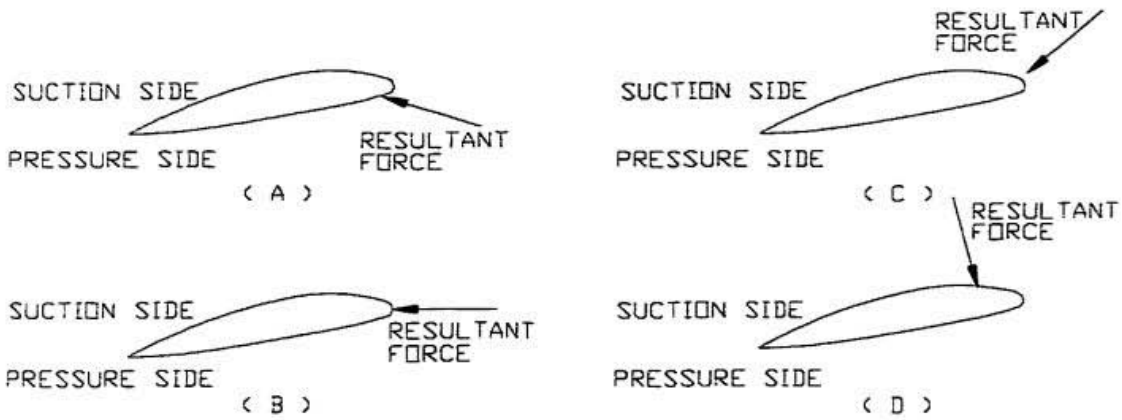

Figure 36: Location of Resultant Contact Force

In addition, the experiments indicated that the thrust and torque loads are oscillatory. The thrust load displayed maximum and minimum loads with equal components to either side of the mean load, while the torque displayed unequal components to either side of the mean with the maximum component being the larger. This finding supports the statement made by Bose et al. (1997) who suggested that the ice load is primarily oscillatory in nature and fatigue implications should be considered in the design approach.

3.2.5 Comparison of Model Damage to Full Scale Damage

During the course of testing, the model propeller sustained damage to the blade tips, which caused the test program to be cut short, and did not allow for a complete investigation of ice strength effect as had been planned. Observations showed that the blade tips were bent backwards and the leading edge of the blades had formed a cup about the pressure side of the blade. Figures 37 and 38 are shown to illustrate the damage to the model propeller. Additional photographs are presented in Appendix B.

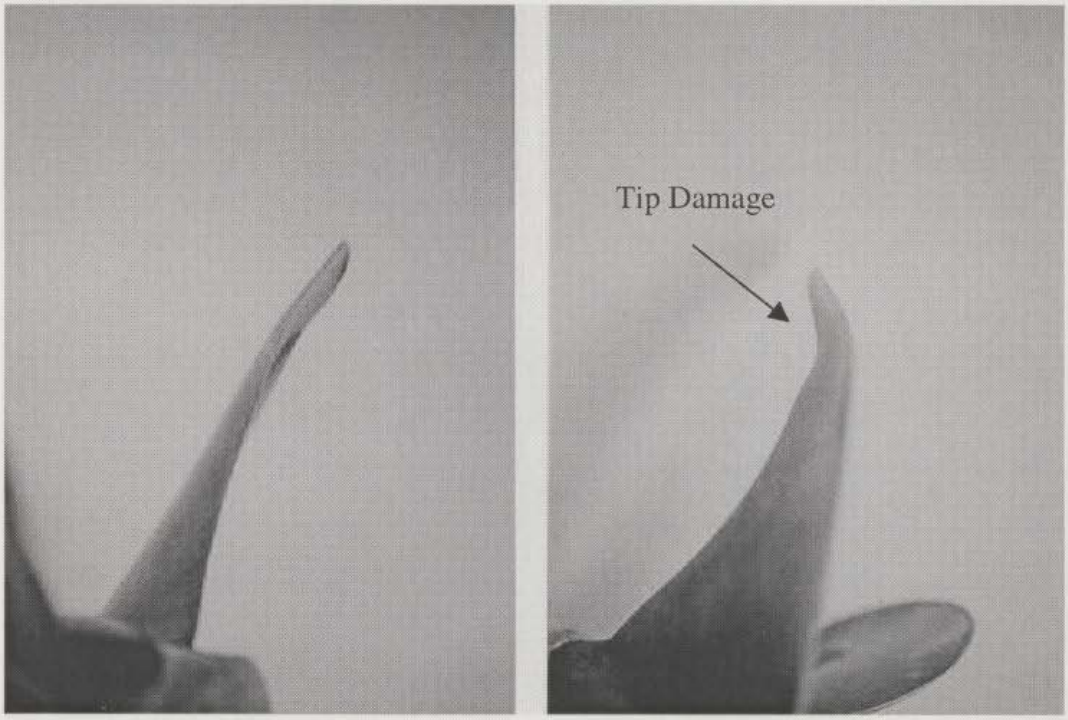

Figure 37: Damage to Model Propeller

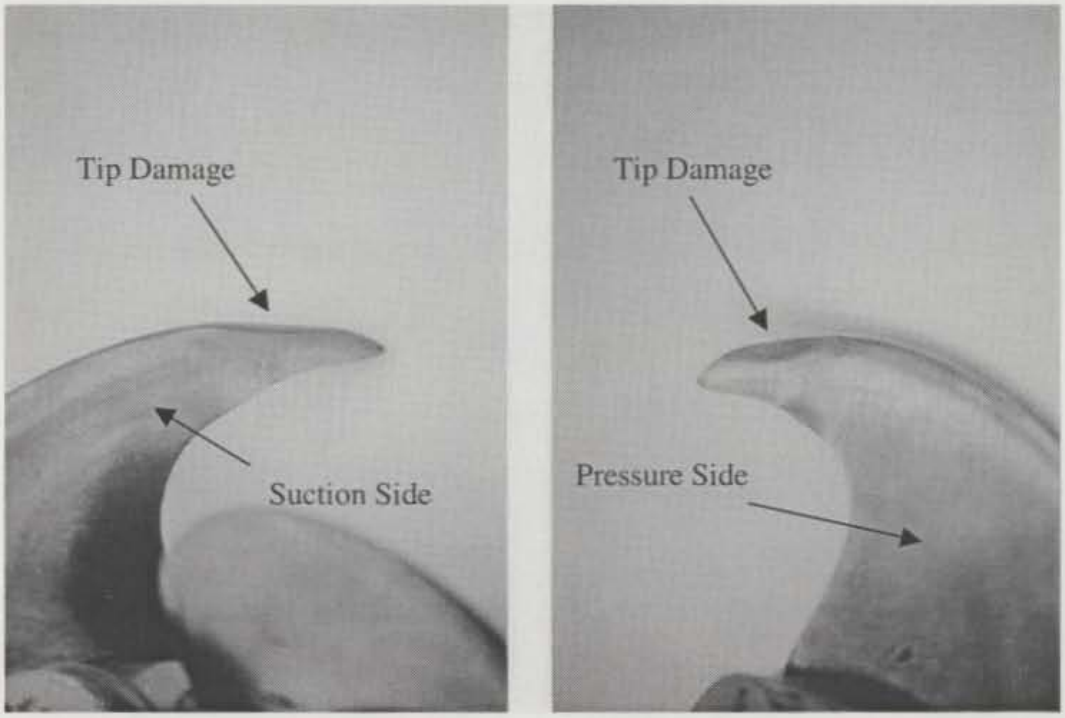

Figure 38: Damage to Model Propeller

The test run during which the model was damaged involved an advance coefficient of J = 0.8 while cutting ice at a λ_d of approximately 0.28. Although this was a rather high load case, it was not considered extreme and it raised questions regarding the full scale propellers. Through conversation with the propeller manufacturers and the vessel owners it was learned that the 5.25m propellers onboard the *M/V Caribou* and the *M/V Joseph and Clara Smallwood* had sustained damage during operation. Upon examination of the propellers it was found that the damage to the full scale propellers was very similar to that observed on the model propeller. Figures 39 and 40 illustrate the damage to the full scale propellers. Appendix C contains additional photographs of the full scale damage.

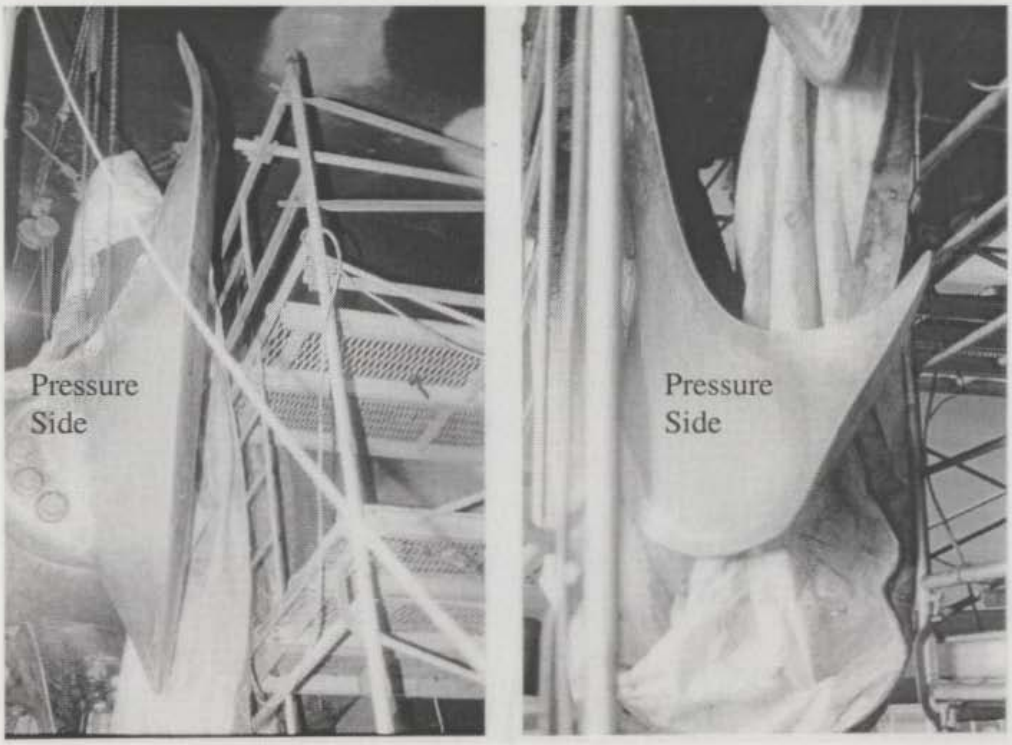

Figure 39: Damage to Full Scale Propeller

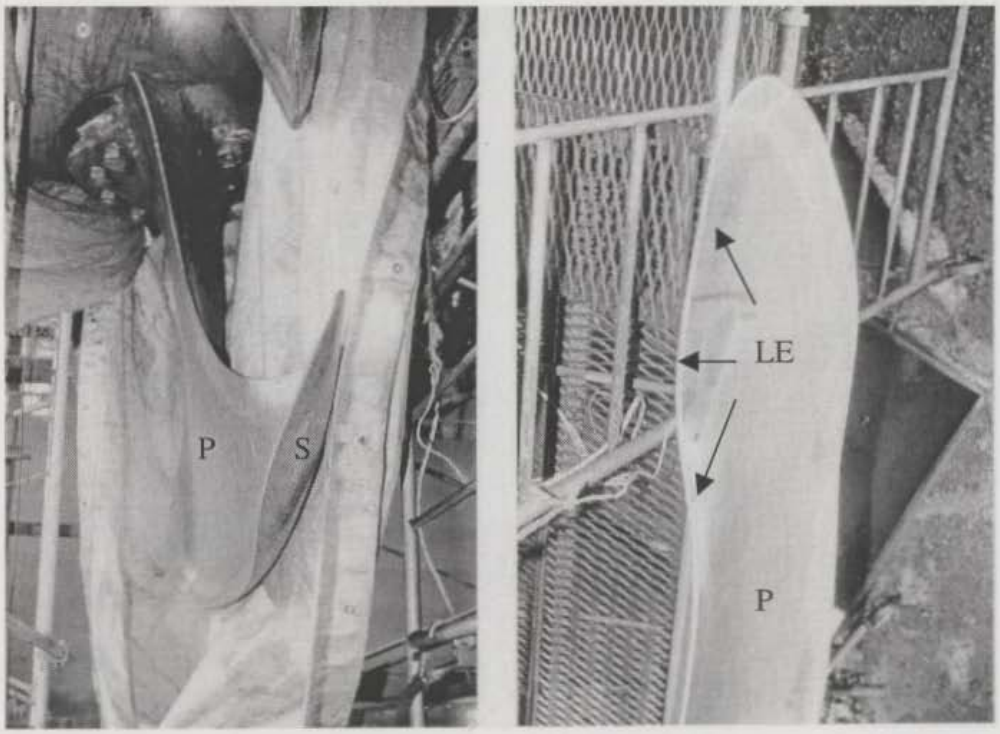

Figure 40: Damage to Full Scale Propeller

Based on these observations, questions can be raised with regard to the strength requirements and blade tip design of highly skewed propellers meant for operation in ice. It would appear that highly skewed propellers are susceptible to damage, particularly at the blade tips, when operating in such conditions. Future design of these propellers could involve limiting the extreme skew or redesigning the blade tips such that the thickness and perhaps chord length at the tips is increased, which would increase their ability to withstand this loading and possibly avoid the tip bending illustrated here.

3.3 Results: *R-Class* Propeller Test Program

For the four-quadrant test program, the test matrix was designed to investigate the ice milling condition and cover the contact and non-contact components of the propeller ice interaction using a conventional ice-class propeller. No variation in cut depth was made, but tests were done over four quadrants of operation. As with the *Caribou* propeller tests, a range of model ice strengths and ice mechanical properties were measured throughout the test program. Previous work with the *R-Class* propeller included open water hydrodynamic tests (Luznik, 1994) and the results from that work have been included to observe how propeller thrust and torque are affected by the presence of ice. The results from the *R-Class* propeller test program are presented in the following subsections.

3.3.1 Distribution of Load during Contact Period

To examine how the load is distributed during contact, the same measuring set-up used in the *Caribou* propeller test program was employed. The time series for the milling event for a section of run R1_T1_T8_001 is shown in Figure 41, where approximately seventy consecutive blade passes through the ice can be detected. The sample was recorded at an advance coefficient of J = 0.3 and a cut depth of 25mm (λ_d = 0.125). In addition to the time history, the probability density histograms of the thrust and torque loads for this run are given in Figures 42 and 43. For each test run, the maximum and minimum values were determined and 50 evenly spaced cell ranges were constructed between the extreme data points. This procedure was conducted for each test run. Additional time histories and load density distributions are presented in Appendix D.

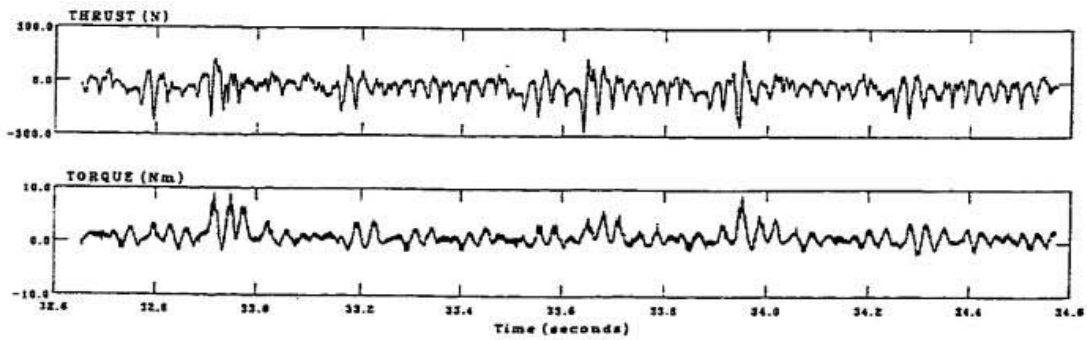

Figure 41: Time Series for R1_T1_T8_001

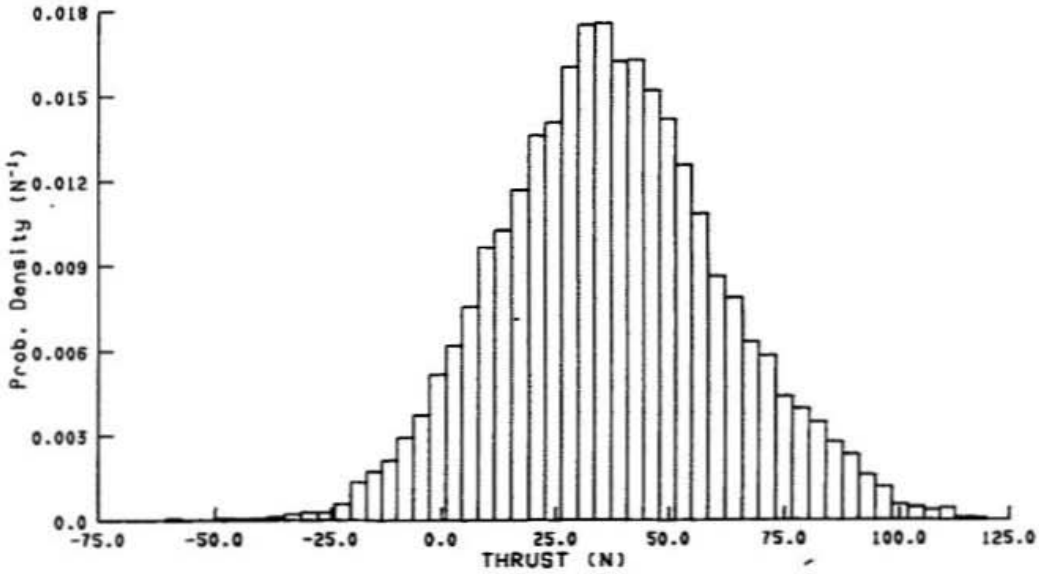

Figure 42: Thrust Distribution during run R1_T1_T8_001

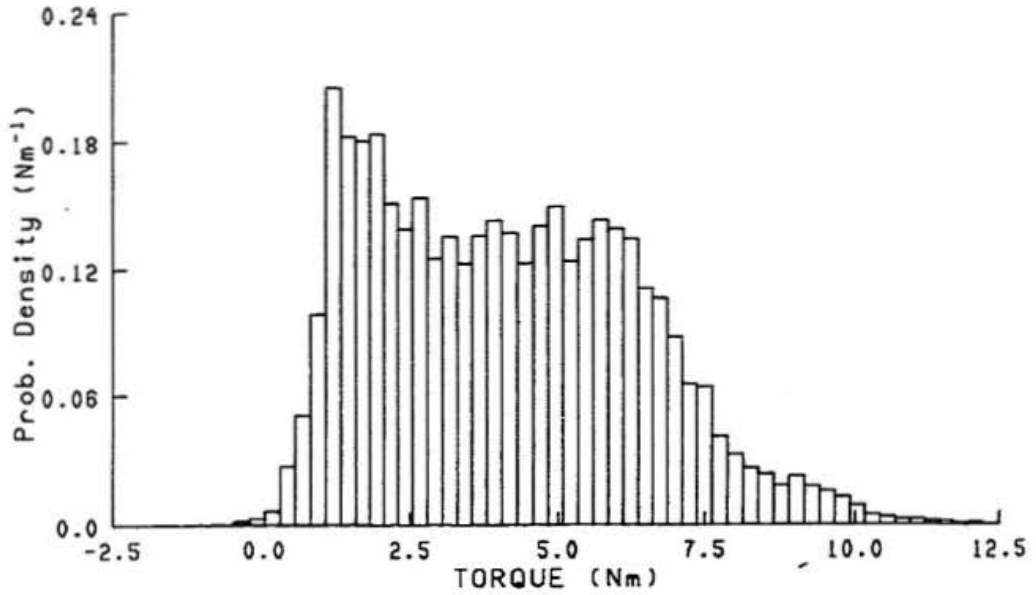

Figure 43: Torque Distribution during run R1_T1_T8_001

Like the results obtained during the *Caribou* propeller tests, the distribution was dependent on the magnitude of the load measured. The larger the load, the larger the unsteadiness of the load and in turn the wider the range. Where the torque loads were relatively high, the torque distribution was more broadly spread and showed a tendency towards a double peaked distribution. This was possibly a result of two primary torque peaks resulting from hydrodynamic loads and ice contact loads.

3.3.2 Open Water Test Results

As stated, open water hydrodynamic tests were previously conducted with the *R-Class* propeller (Luznik, 1994). An uncertainty analysis of the experimental results (Bose and Luznik, 1994.) indicated levels of uncertainty in the thrust coefficient of ±0.001-0.003, for torque coefficient ±0.0003-0.0004 and for the advance coefficient approximately ±0.002-0.004. The results from the open water tests of the *R-Class* propeller are plotted in Figure 44.

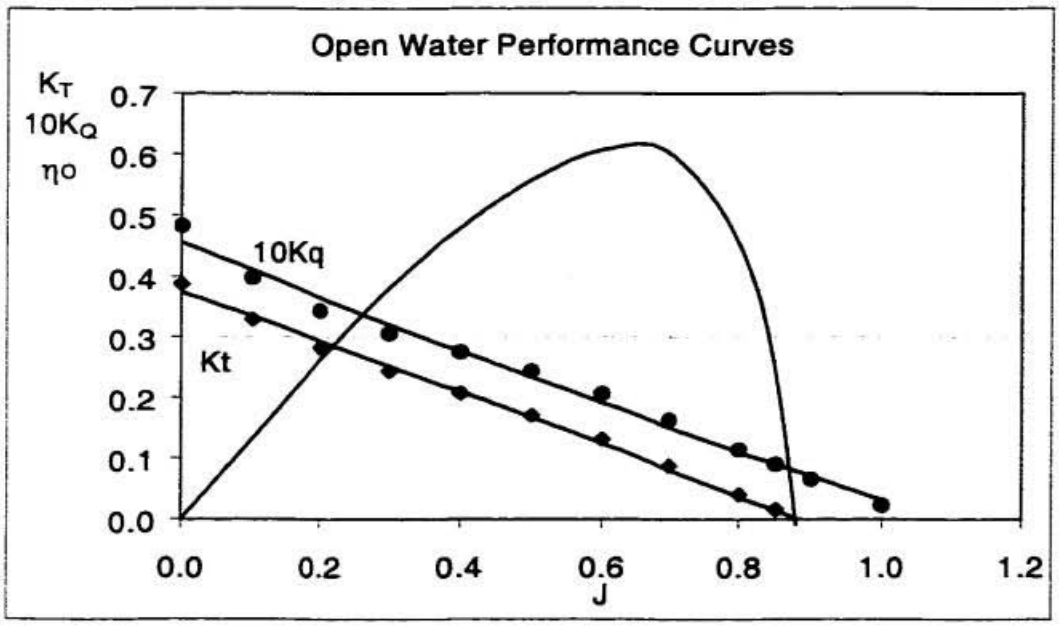

Figure 44: Open Water Performance Curves for *R-Class* Propeller

3.3.3 Quadrant 1: Test Results

Quadrant 1 is defined as the propeller in the forward operating condition where the advance speed is positive and the shaft is rotating in a positive direction. As quadrant 1 is the most frequent operating condition, it was also the most investigated. A total of 5 runs were completed. Two main variables were investigated: the effects of J and the effects of S_C. The results are presented in the following subsections.

3.3.3.1 Variations in Advance Coefficient

For the test runs in quadrant 1, the cut depth was held constant at 25 mm ($\lambda_d = 0.125$) while the propeller was run the length of the ice tank over a range of J. J was varied

by fixing the shaft speed and varying the advance speed of the propeller. The test series was conducted at three different ice strengths: 91kPa, 66kPa and 58kPa. The results for each value of S_C are presented in Figures 45 to 50. The solid black circles represent the experimental means for the K_T and K_Q and the solid line through these points represent lines of best fit. The open circles represent the maximum values measured during the test program, the open triangles represent the minimum values measured and the lines through each of these data sets represent lines of best fit for the maximum and minimum K_T and K_Q. In addition, the open water performance curves are plotted on the applicable charts. Each of the lines fitted through the data is modelled by a 3rd order polynomial.

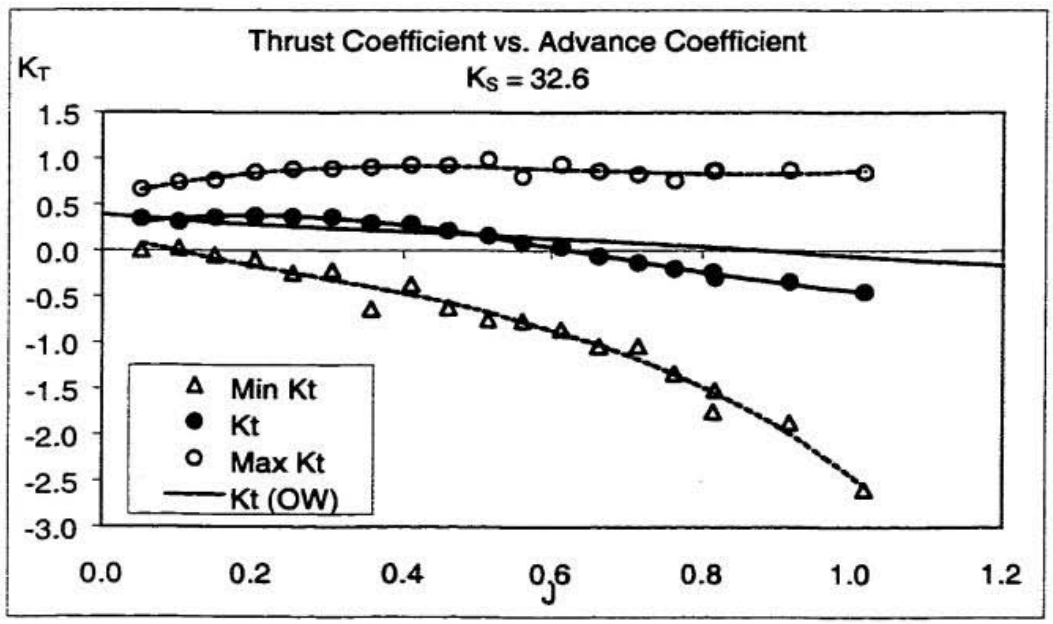

Figure 45: K_T vs. J for $K_S = 32.6$

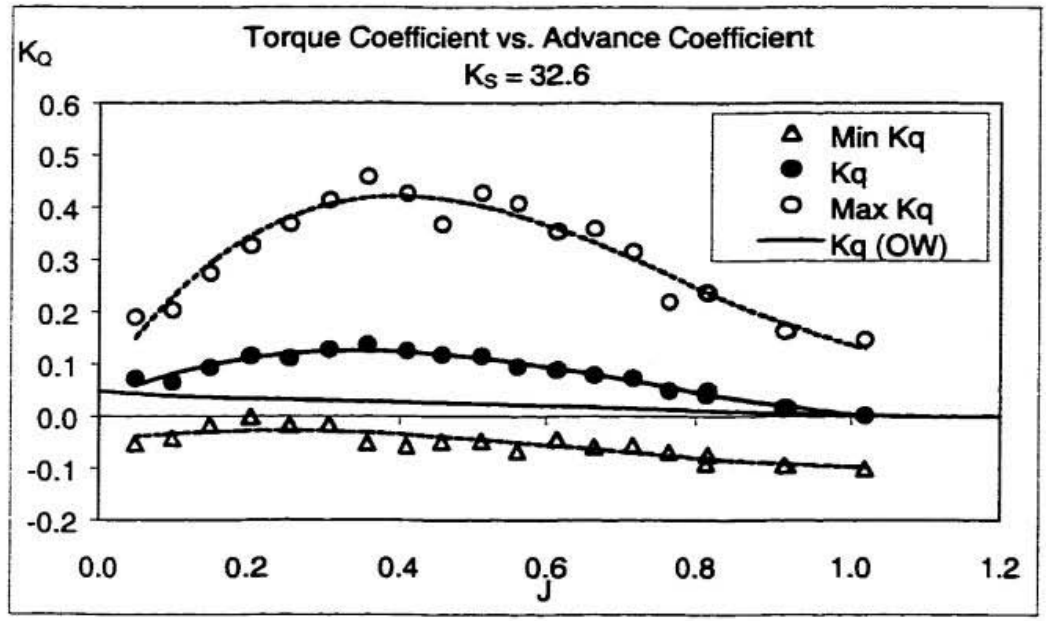

Figure 46: K_Q vs. J for $K_S = 32.6$

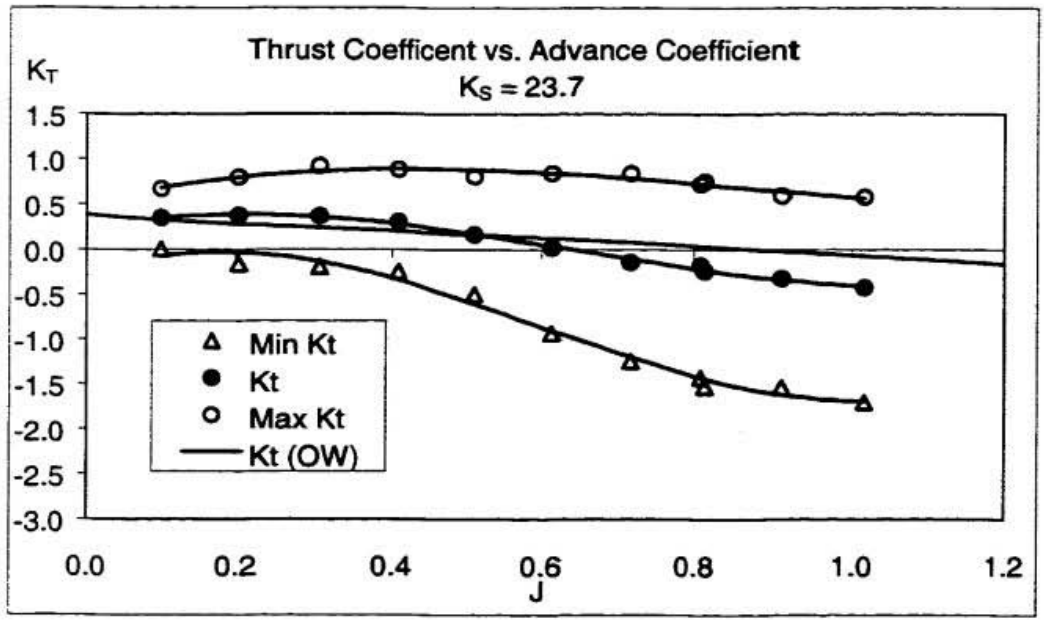

Figure 47: K_T vs. J for $K_S = 23.7$

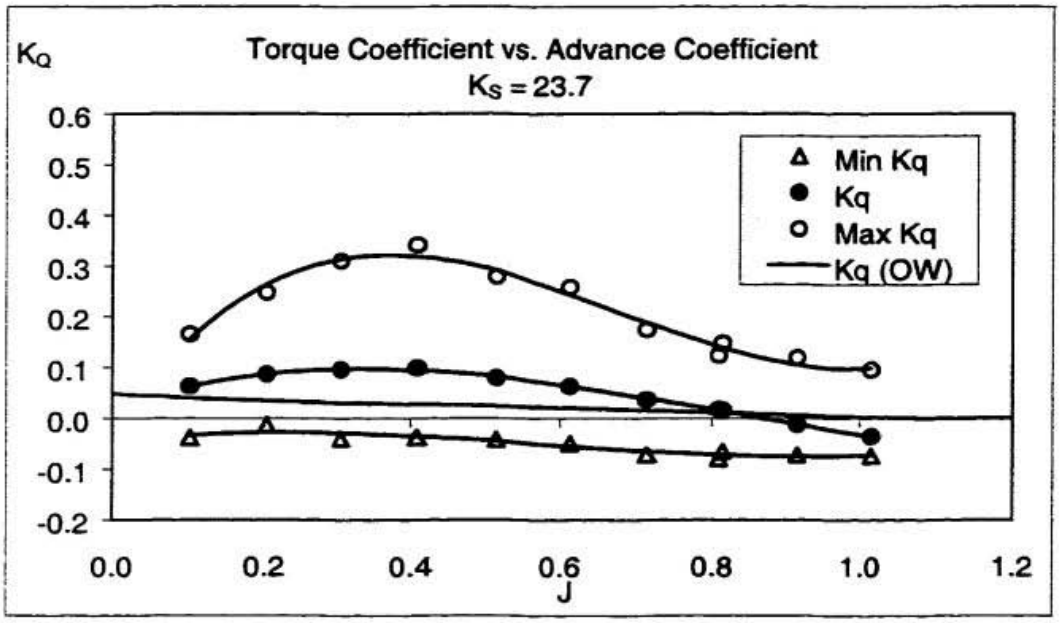

Figure 48: K_Q vs. J for $K_S = 23.7$

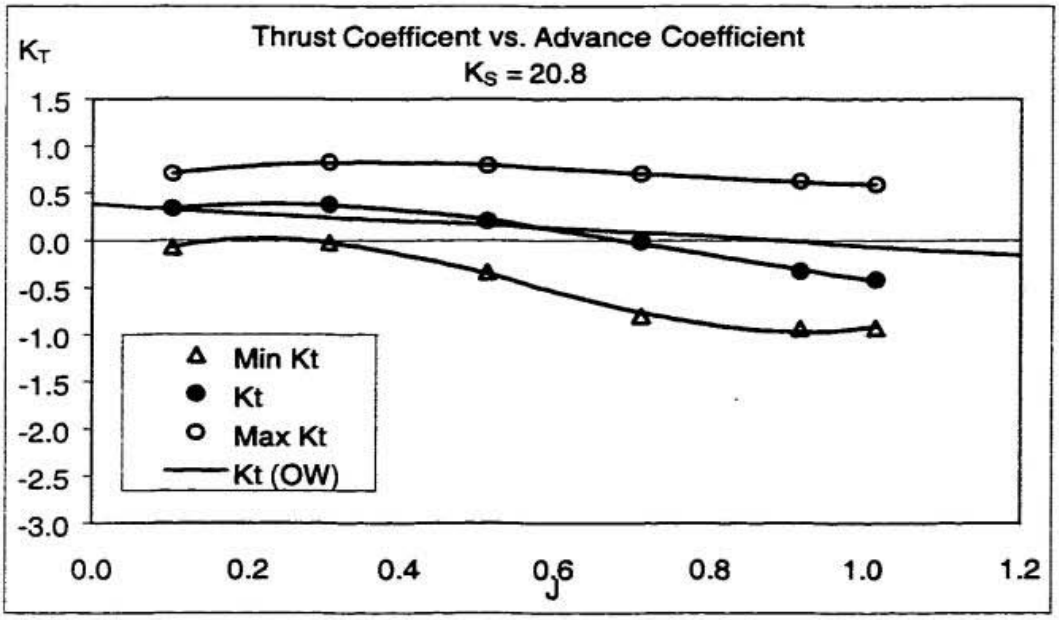

Figure 49: K_T vs. J for $K_S = 20.8$

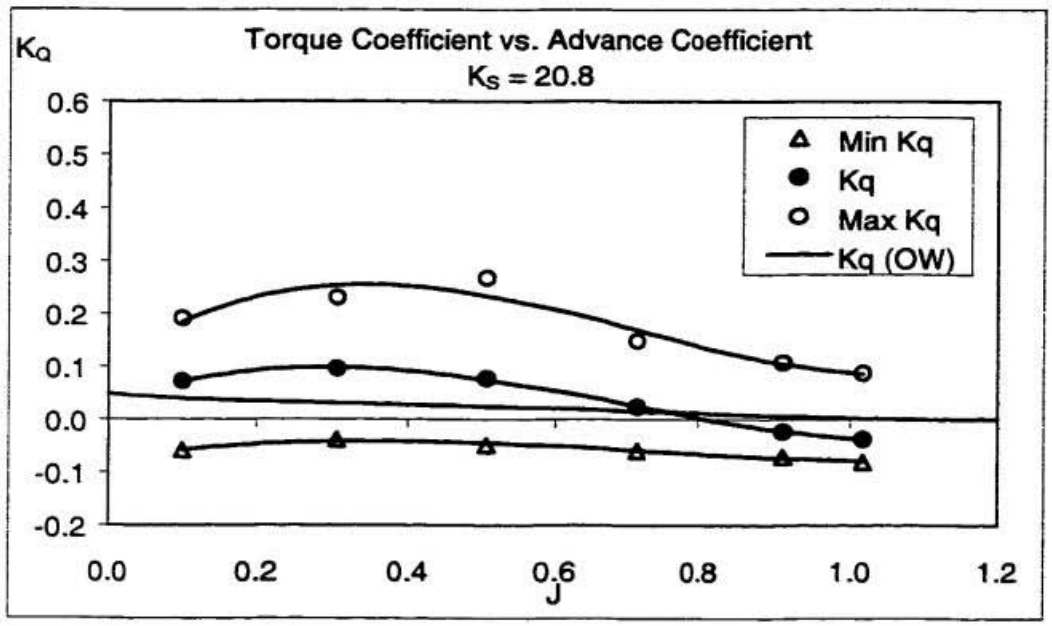

Figure 50: K_Q vs. J for $K_S = 20.8$

Starting at low advance coefficient, the thrust coefficient increases until a maximum is reached at approximately J = 0.3, then it diminishes gradually, going zero at approximately J = 0.6 for S_C = 91kPa, J = 0.65 for S_C = 66kPa and J = 0.7 for S_C = 58kPa. The same trend can be seen in the mean torque coefficient, which has a maximum reading at approximately J = 0.3 then decreases as advance coefficient increases. With the decrease in J, the point at which torque coefficient goes negative decrease from J = 1.0 for S_C = 91kPa, J = 0.9 for S_C = 66kPa and J = 0.8 for S_C = 58kPa.

In comparison to the open water thrust coefficient, the mean thrust coefficient for the *R-Class* propeller behaves similarly to the *Caribou* propeller. The mean K_T curve is

larger in magnitude at low J, but with increasing J the mean K_T curve intersects with the open water K_T curve and the open water K_T becomes the larger of the two coefficients. The mean K_Q curves also demonstrate a similar behaviour to that experienced with the *Caribou* propeller, except the tests were done over a high enough range of J for the *R-Class* propeller to cause the mean K_Q curve to go negative. Why the ice causes an original increase in the total load then gradually decreases can be attributed to the load mechanics behind the propeller-ice contact as described in section 3.2.4.

In addition, the experiments indicated that the thrust and torque loads for the *R-Class* propeller are oscillatory, which agrees with the *Caribou* propeller findings. The thrust load displayed maximum and minimum loads with equal components to either side of the mean load, while the torque displayed unequal components to either side of the mean with the maximum component being the larger.

3.3.3.2 Variation in Ice Strength

To investigate the effects of ice strength, tests at three different ice strengths are compared: 91kPa, 66kPa, and 58kPa. For each run, the cut depth was held at 25mm ($\lambda_d = 0.125$) and the same range of J was investigated for each. The results from these tests are shown in Figures 51 to 54.

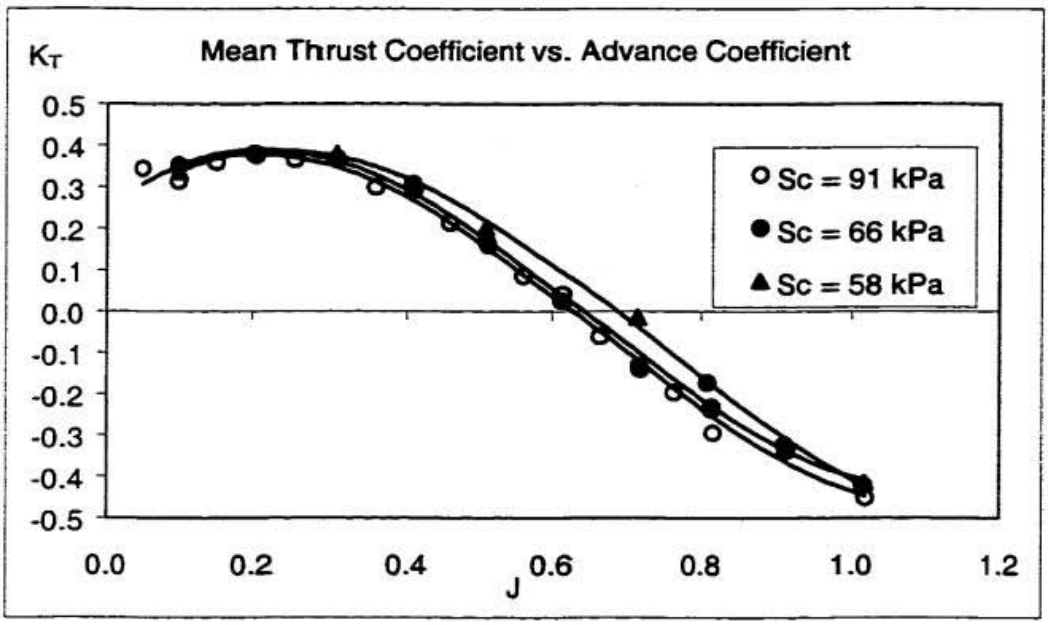

Figure 51: Mean K_T vs. J (Ice Strength Effects in Quadrant 1)

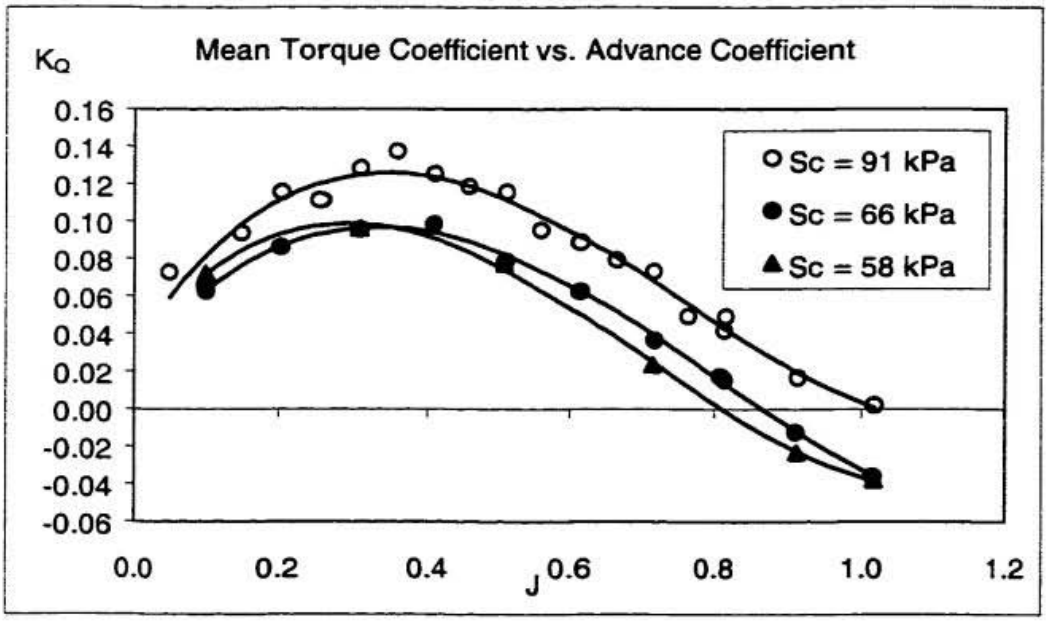

Figure 52: Mean K_Q vs. J (Ice Strength Effects in Quadrant 1)

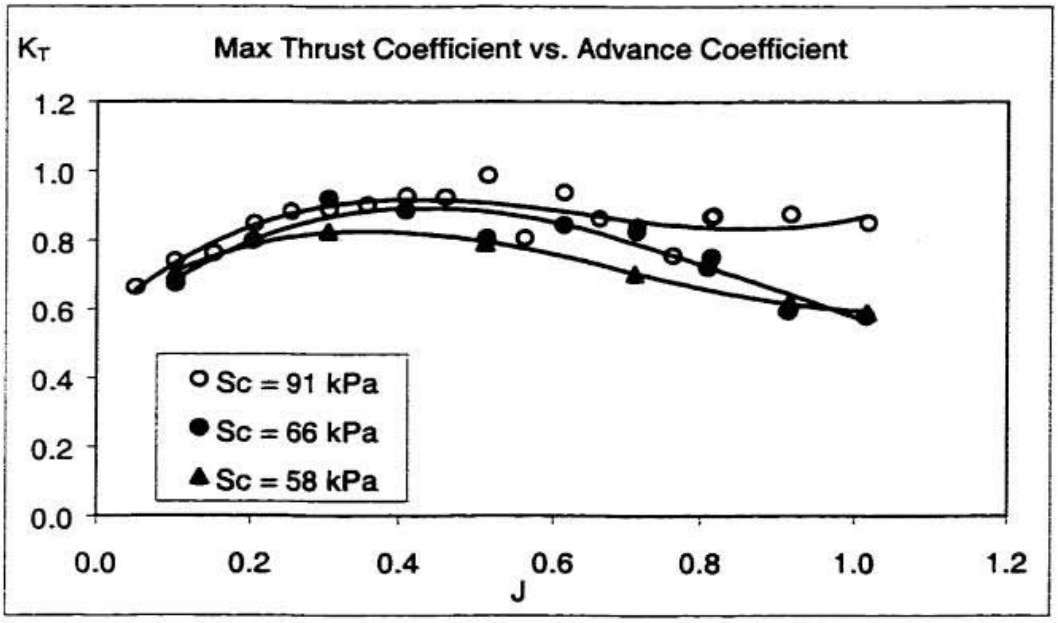

Figure 53: Max K_T vs. J (Ice Strength Effects in Quadrant 1)

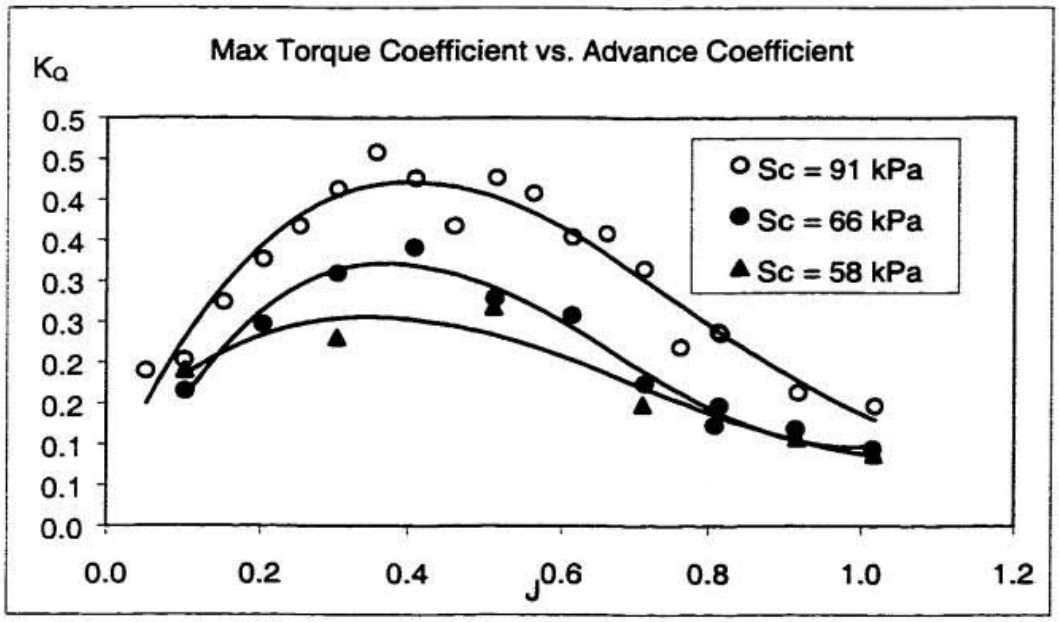

Figure 54: Max K_Q vs. J (Ice Strength Effects in Quadrant 1)

Other than the maximum K_T data at large values of J, the thrust data behaved in such a manner that would suggest that ice strength has little effect on thrust. A 27% change in S_C resulted in only a 3% change in mean K_T and a 7% change in the max K_T. Conversely, there was a much larger change in the torque reading with the variation in ice strength, indicating that torque is highly dependent on the ice strength. A 38% change in S_C resulted in a 32% change in the mean K_Q and a 29% change in the max K_Q. The data in Figures 51 and 52 is replotted in Figures 55 and 56 showing the propeller thrust and torque coefficients versus compressive ice strength index for different constant values of J.

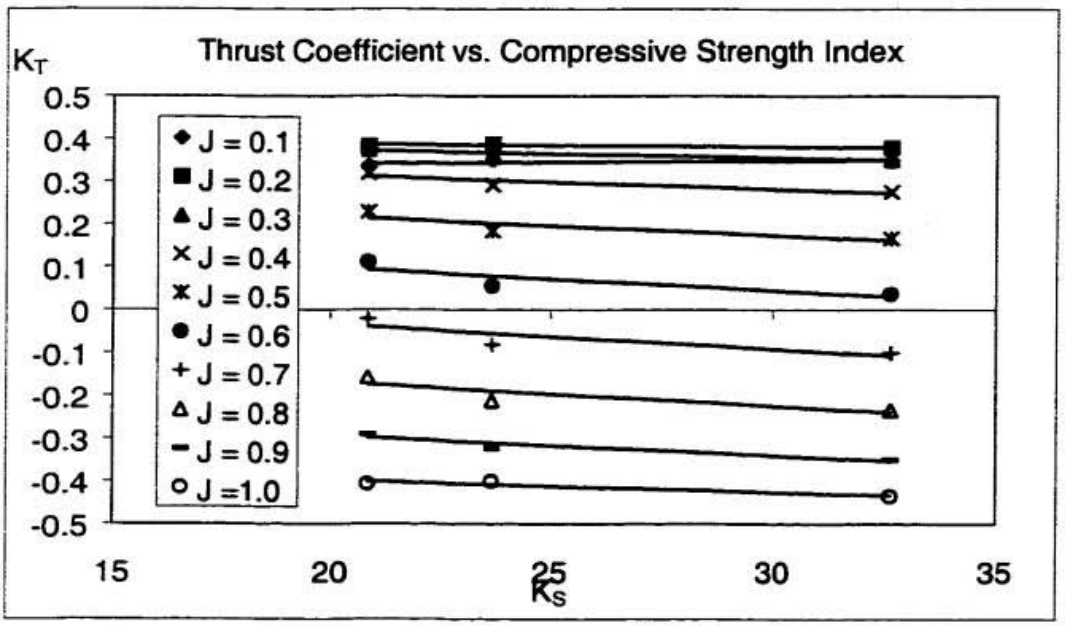

Figure 55: K_T versus K_S for values of J

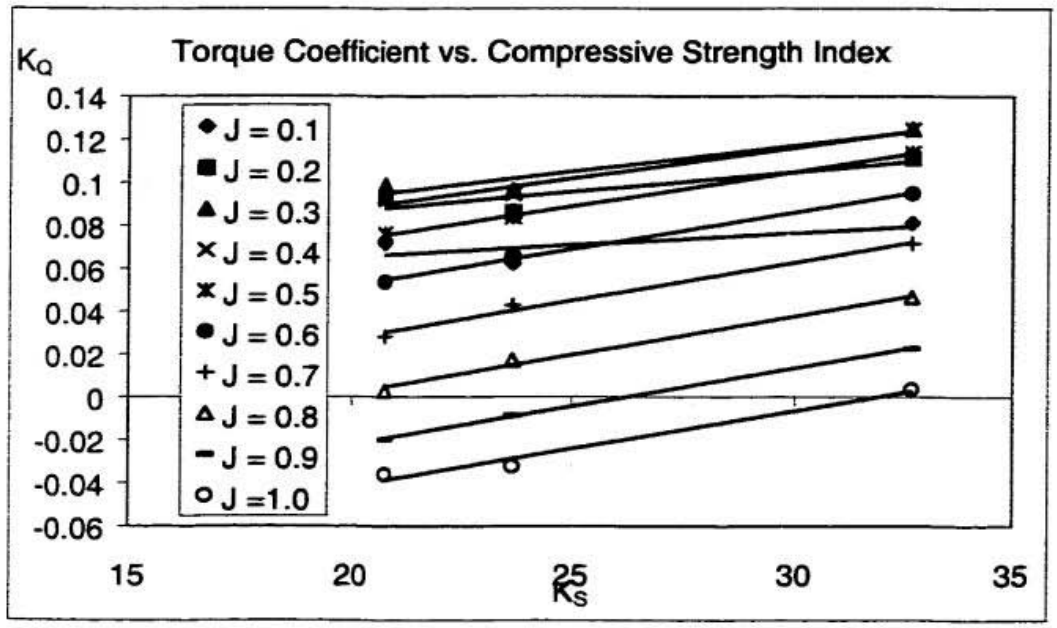

Figure 56: K_Q versus K_S for values of J

As illustrated in Figure 55, variations in the compressive ice strength index (K_S) have minimal effect on the thrust coefficient while Figure 56 suggests that the torque coefficient is linearly related to changes in the compressive ice strength index. The dimensional analysis conducted in Chapter 2 showed that thrust and torque coefficients for a marine propeller operating in ice can be represented by equations [5] and [6] respectively. Each of these equation consist of linear functions of Froude number, Reynolds number, advance coefficient, depth of cut ratio, compressive strength index and ratios of ice modulus, ice tensile and flexural strengths to compressive strength.

Ignoring the K_T and K_Q results for J = 0.1 and 0.2, the results support a linear variation of K_T and K_Q versus K_S with a slope of -4.21×10^{-3} on average for K_T and a slope of 3.27×10^{-3} on average for K_Q. For these results Froude number, Reynolds number and depth of cut ratio were all constant for each advance coefficient tested. The experimental propeller performance at low advance coefficient such as J = 0.1 and J = 0.2 is less reliable than at higher advance coefficient due to the large angles of attack of the propeller sections in this condition and the very low speed of advance. The latter in particular can be important in propeller-ice work as at these very low advance speeds, modelling the ice block acceleration ahead of the propeller accurately is difficult and this can have a large influence on the propeller loads.

Making the assumption that the last three variables developed in the dimensional analysis have only minor effects on the propeller loads and compressive strength is the governing ice property when investigating propeller-ice interaction, it is possible to extrapolate the results to full scale and make estimates of the thrust and torque loads of the full scale propeller for different values of compressive ice strength.

The full scale propeller has a diameter of 4.12m and a shaft rotation of 2 rps. Taking S_C = 6MPa, 4MPa and 2MPa, $\rho_I = 900 kg/m^3$ and keeping $h_I/D = 0.125$, K_S is calculated to be 98.2, 65.5, and 32.7 respectively. The K_T and K_Q curves for the values of K_S at full scale are plotted with the model K_S values in Figures 57 and 58.

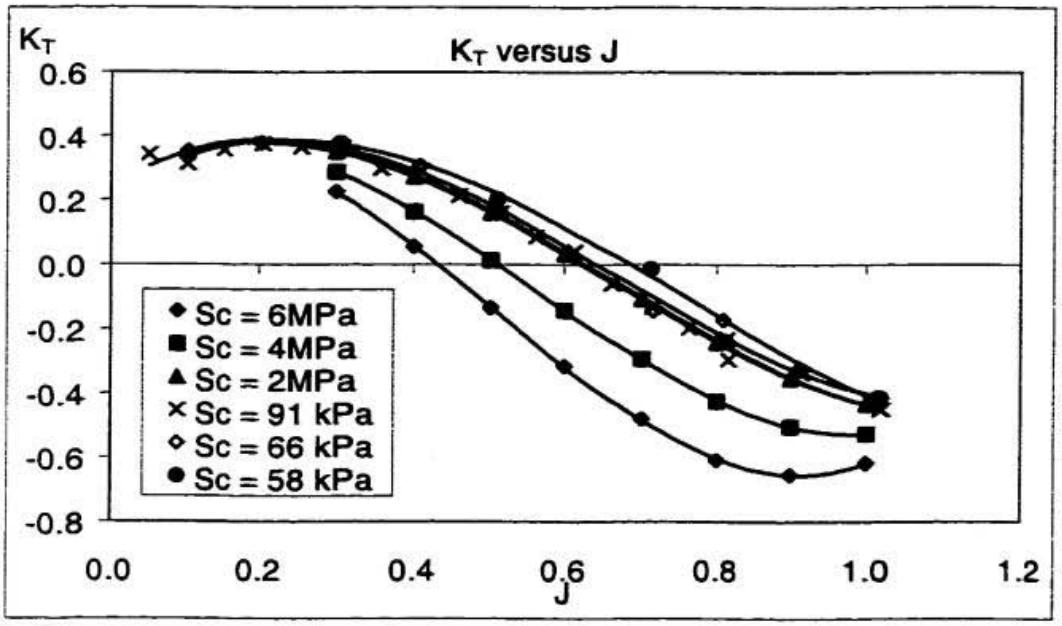

Figure 57: K_T vs. J for values of S_C

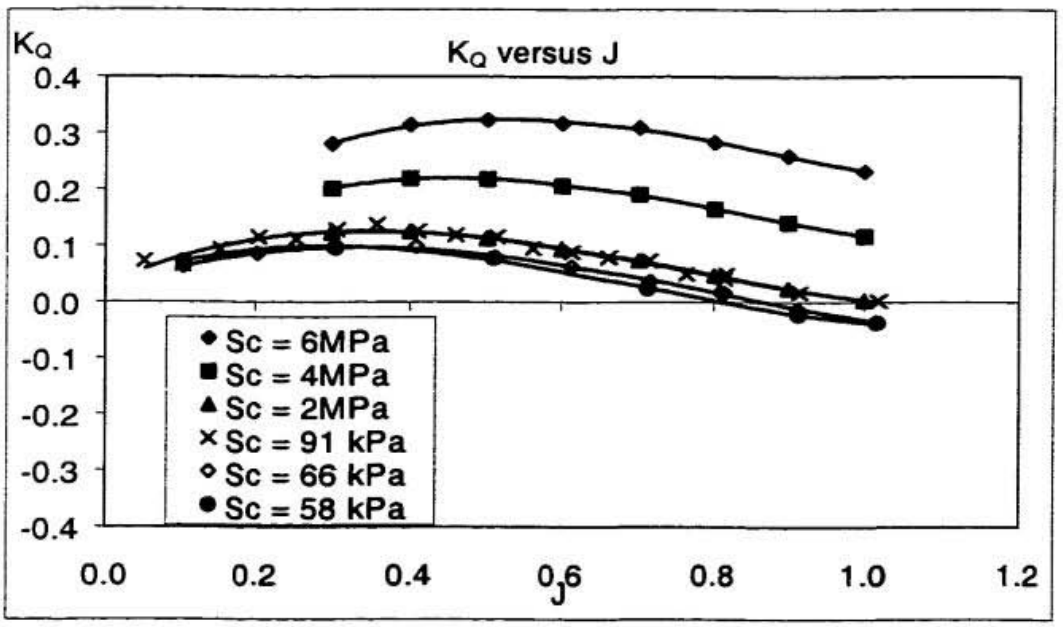

Figure 58: K_Q vs. J for values of S_C

As expected, the full-scale extrapolations have a similar form to the model results on which they were based. The model scale results fall within the full-scale extrapolations as the compressive ice strength index for the model results fall within the values calculated for full scale. For the higher full-scale compressive ice strengths, the results are an extrapolation. Model tests at higher ice strengths are required to fill in the gaps. Full scale data in ice of known strength and for known cut depth would help validate the extrapolations. Model scale data for other cut depths would be beneficial and expand the work.

Based on the test results, the following equations can be derived to demonstrate an initial relationship between the full and model scale K_T and K_Q values for this propeller at a cut depth ratio of $h_I/D = 0.125$.

$$Mean: K_{T(FS)} = -4.21x10^{-3} \cdot (K_{S(FS)} - K_{S(MS)}) + K_{T(MS)} \quad [19]$$

$$Mean: K_{Q(FS)} = 3.27x10^{-3} \cdot (K_{S(FS)} - K_{S(MS)}) + K_{Q(MS)} \quad [20]$$

3.3.4 Quadrant 2: Test Results

Quadrant 2 is defined as the propeller having a negative advance speed in combination with a positive shaft speed. It is defined as an off-design condition but one that is relevant as some vessels, like icebreakers, operate in these conditions while manoeuvring or during ramming operations. Two independent runs were

performed to investigate the propeller operating from J = -0.05 to J = -0.4 at steps of -0.05. Two main variables were investigated: the effects of advance coefficient and the effects of ice strength. The results of both are presented in the following subsections.

3.3.4.1 Variations in Advance Coefficient

Operation of the propeller at a constant cut depth over a range of advance coefficient resulted in close to linear relationships for both thrust and torque versus advance coefficient as illustrated in Figures 59 and 61. In addition, operation in quadrant 2 led to much larger thrust and torque loads on the propeller than those recorded in quadrant 1. This result is of concern as the majority of the design methods proposed for the design of ice class propellers use the loads encountered in quadrant 1 as their design criteria. From the results presented here, it would appear that this might not be the most appropriate design criterion, as it is not the operating condition where the propeller receives its maximum loads.

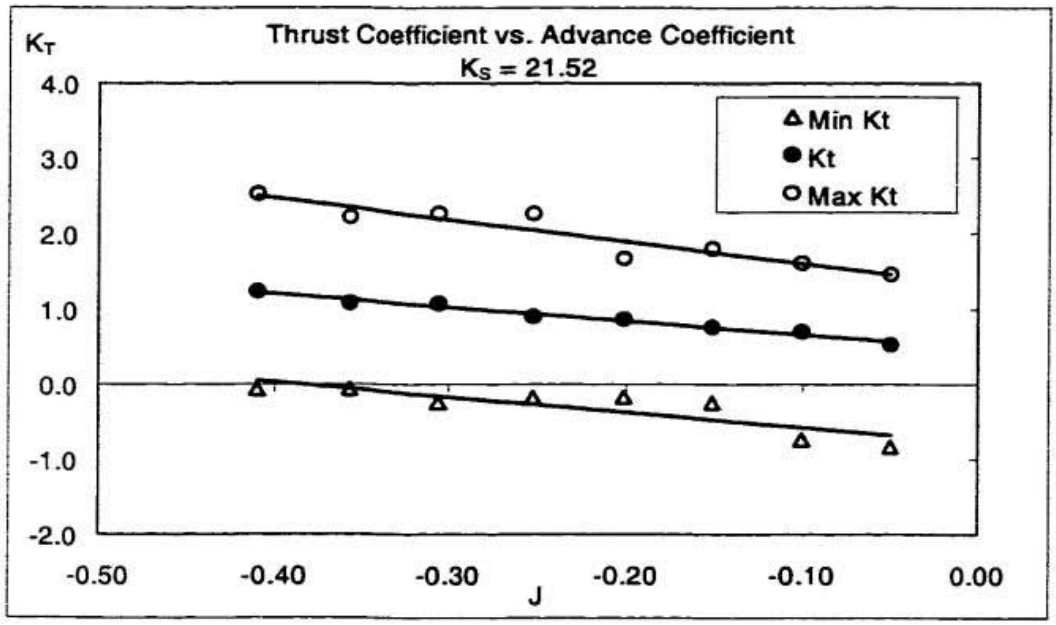

Figure 59: K_T vs. J for $K_S = 21.52$

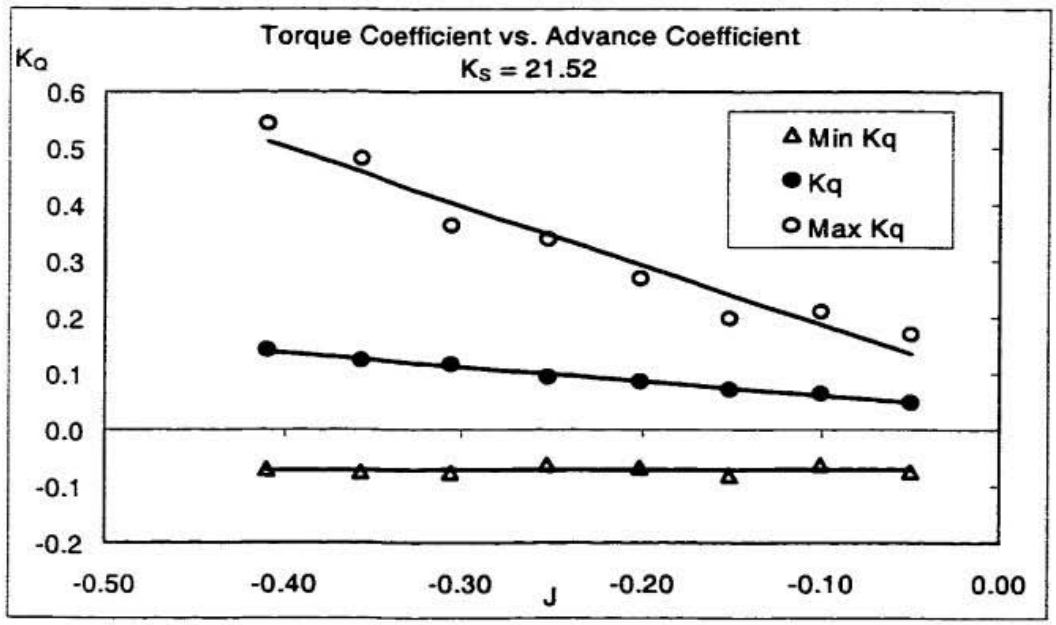

Figure 60: K_Q vs. J for $K_S = 21.52$

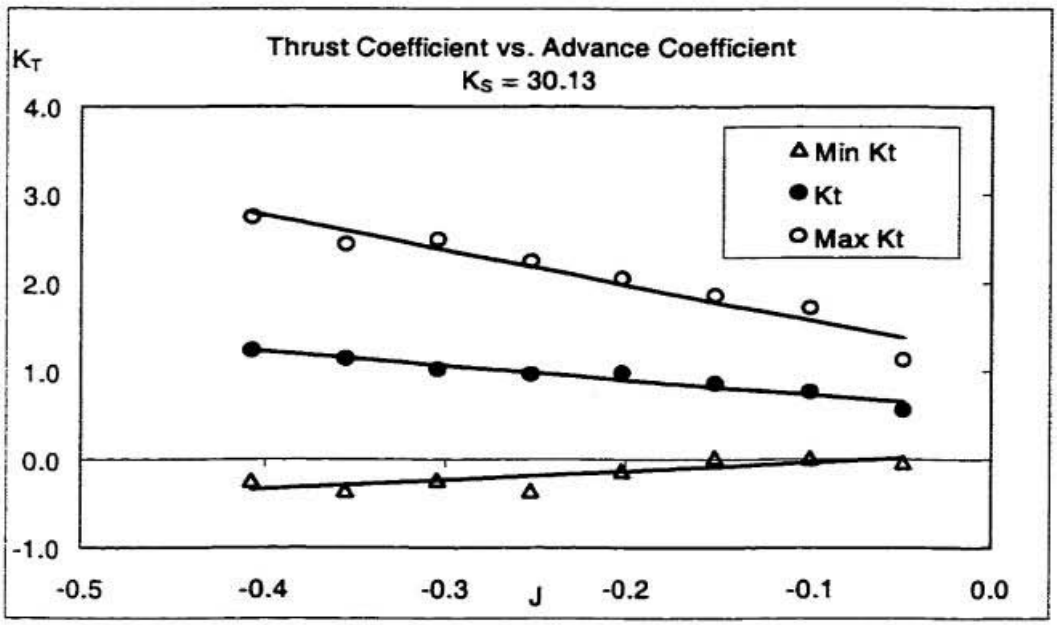

Figure 61: K_T vs. J for K_S = 30.13

The K_Q vs. J for K_S = 30.13 is not shown as problems were encountered with the data acquisition system during this test run and it was not possible to collect the torque data.

3.3.4.2 Variations in Ice Strength

As previously stated, problems were encountered with the torque data acquisition during one of the runs and it was not possible to repeat this run at a later date, so the effects of ice strength on torque in quadrant 2 are not presented. However, it was possible to acquire the thrust data and the ice strength effects on the mean and max thrust coefficients are presented in Figures 62 and 63.

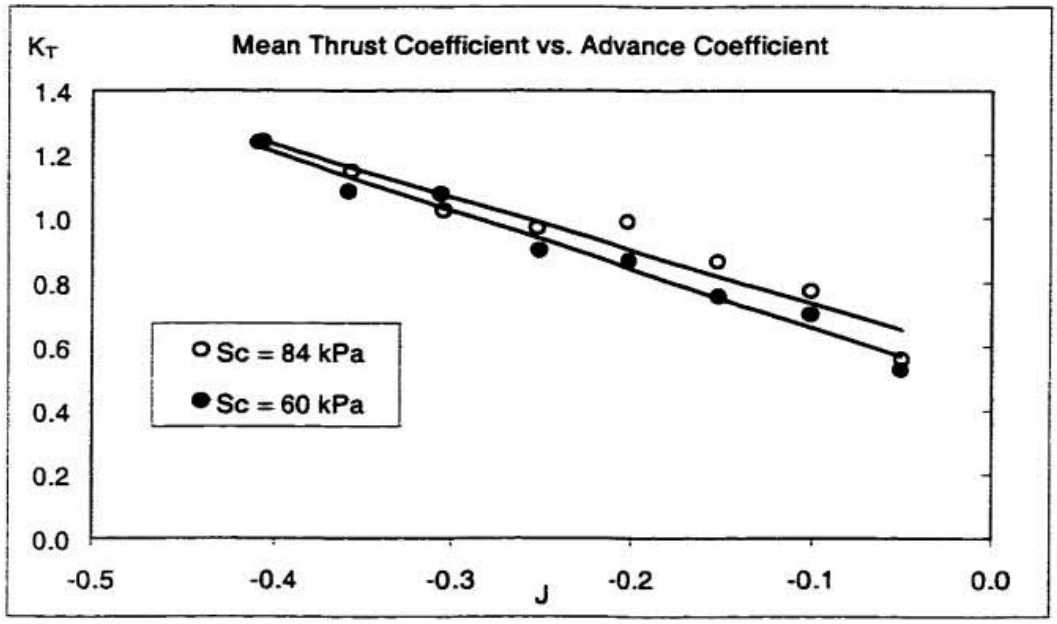

Figure 62: Mean K_T vs. J (Ice Strength Effects in Quadrant 2)

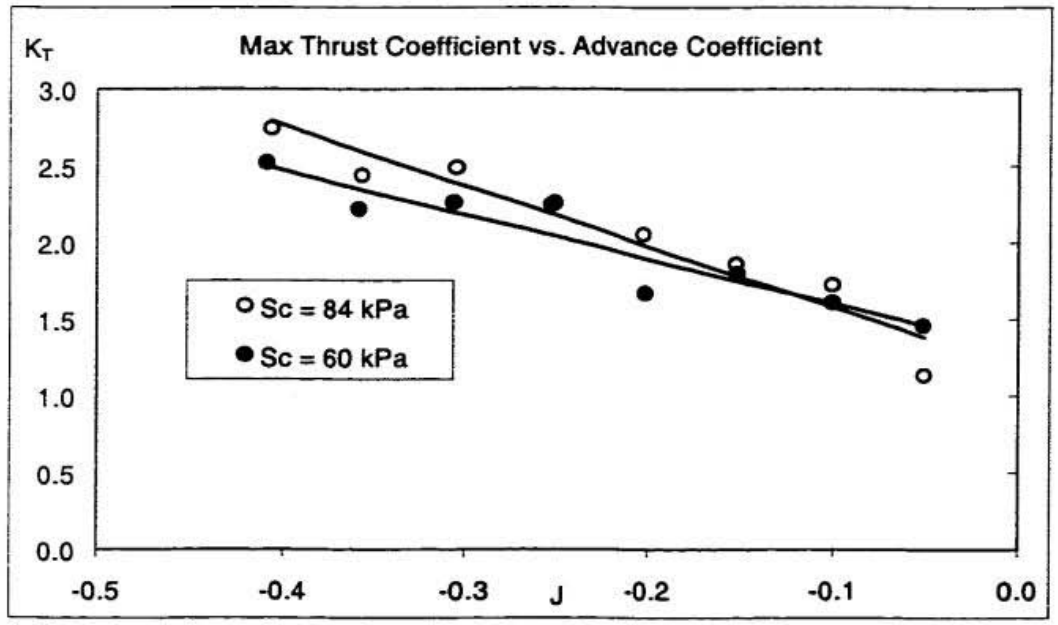

Figure 63: Max K_T vs. J (Ice Strength Effects in Quadrant 2)

In the above figures, the K_T versus J curves are plotted for two different values of compressive ice strength: 84kPa and 60kPa. From the results it was concluded that ice strength variation has minimal effect on the propeller thrust during operation in quadrant 2. A 29% change in S_C resulted in only a 7% change in the mean K_T and a 5% change in the max K_T.

3.3.5 Quadrant 3: Test Results

Quadrant 3 is defined as the propeller having a positive advance speed in conjunction with a negative shaft speed. Two independent runs were performed to investigate the propeller operating from J = -0.05 to J = -0.3 at steps of -0.05. Two main variables were investigated: the effects of advance coefficient and the effects of ice strength. The results of both are presented in the following subsections.

3.3.5.1 Variations in Advance Coefficient

The results of quadrant 3 proved to be similar to those of quadrant 2. Operation of the propeller in quadrant 3 resulted in close to linear relationships for both thrust and torque versus advance coefficient, as illustrated in Figures 64 to 67. With the increase in load magnitude, the load coefficients developed a larger range, which lead to high loads on the propulsion system. Like the loads experienced in quadrant 2, the high loads associated with quadrant 3 operation are not accounted for in the current design rules for ice class propellers. As stated previously, these findings raise concern and

indicate that current design models may require modifications before they can be used reliably for all states of operation for the design of ice-class propellers.

It is recognised that quadrants 2 and 3 are off-design operating conditions and normal vessel manoeuvres do not involve these quadrants, but there are instances when vessels are in these situations i.e. icebreakers during ramming cycles or crash stopping during emergencies. If propellers are to be designed to survive ice contact during operation then it is necessary to design propellers to withstand the maximum probable loads they could encounter during operation and for some ice-class propellers these loads occur during quadrant 2 and 3.

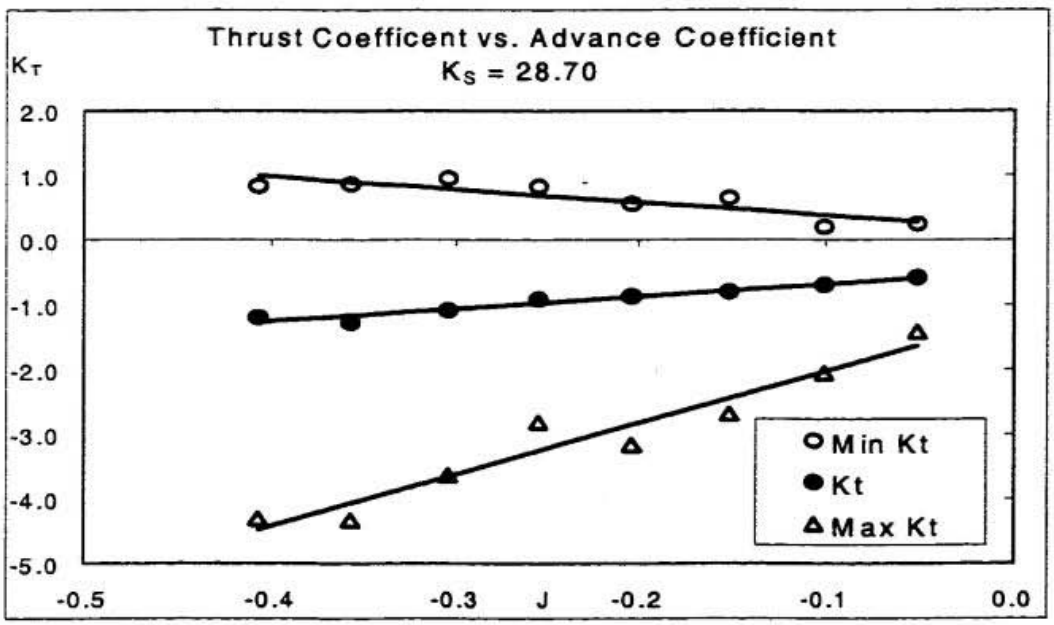

Figure 64: K_T vs. J for $K_S = 28.70$

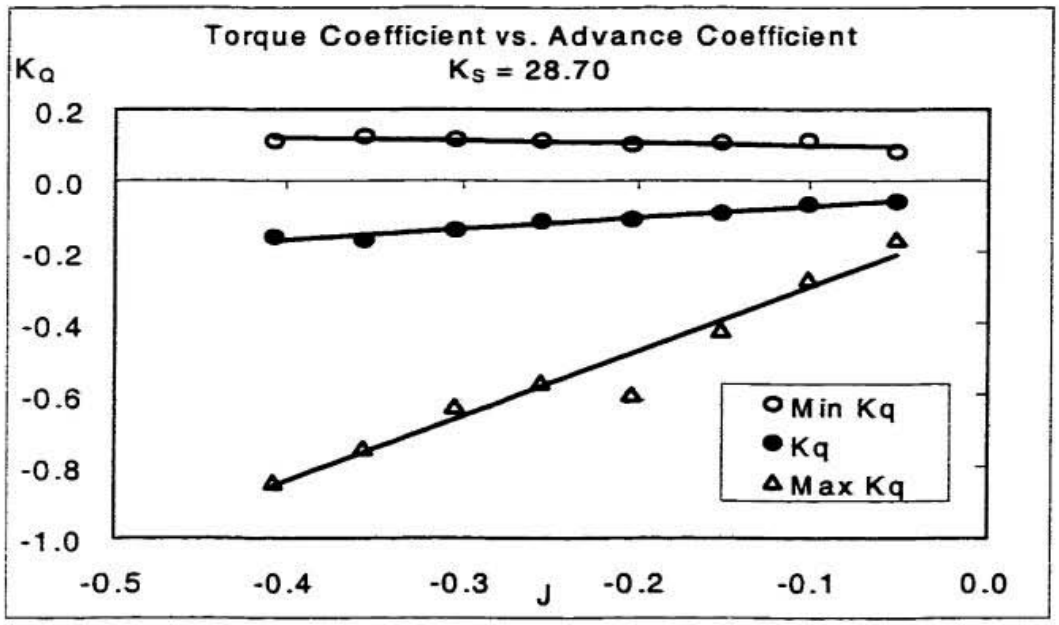

Figure 65: K_Q vs. J for K_S = 28.70

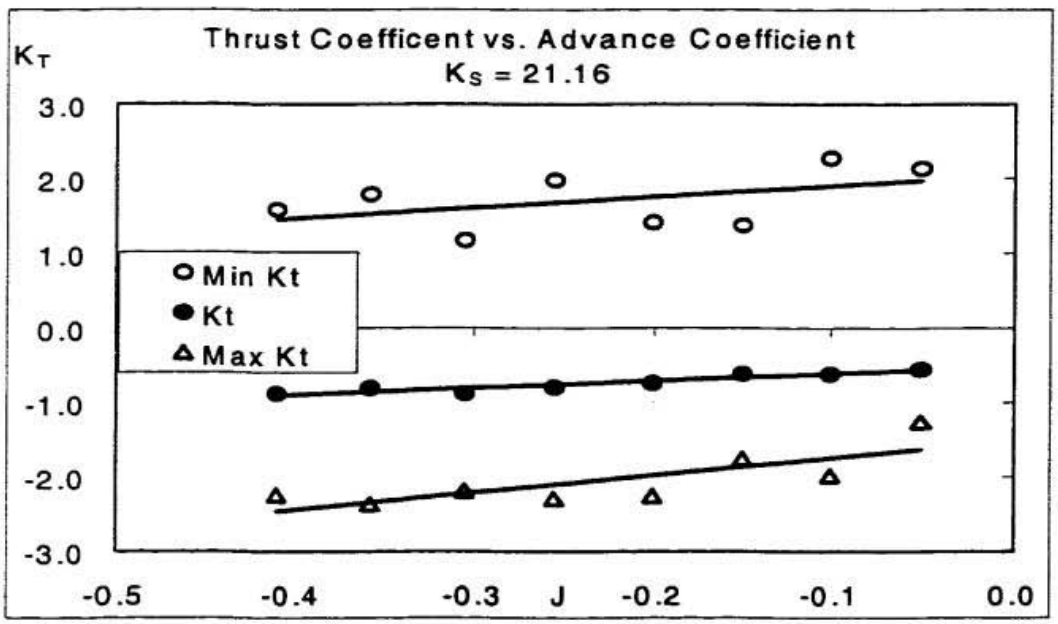

Figure 66: K_T vs. J for K_S = 21.16

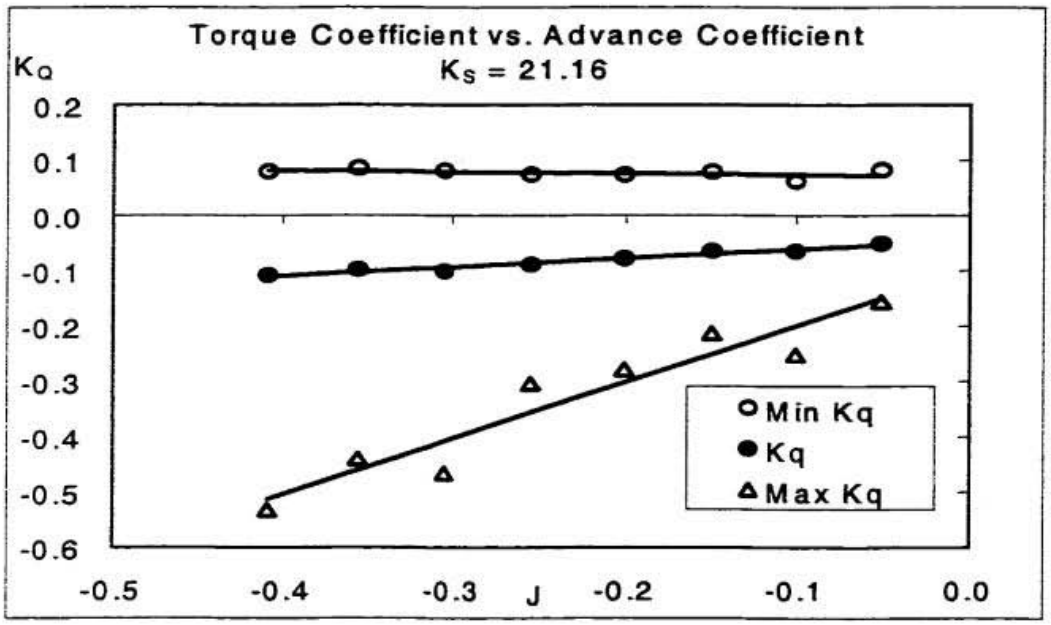

Figure 67: K_Q vs. J for $K_S = 21.16$

3.3.5.2 Variations in Ice Strength

To investigate the effects of ice strength, two runs were completed in quadrant 3 at two values of compressive ice strength: 80kPa and 59kPa. The maximum and mean K_T and K_Q versus J for each run are presented in Figures 68 to 71. Based on the presented data, the propeller thrust behaves differently in quadrant 3 compared to quadrant 1. The propeller thrust is affected by variations in ice strength and increases with an increase in ice strength. As there is no previous work with which to compare this result, it is not possible to confirm this relationship. A 26% change in S_C resulted in a 23% change in the mean K_T and a 40% change in the max K_T.

Up to a point, the K_Q curves behaved as witnessed in other quadrants, but as the absolute J increased the curves began to diverge, which was not witnessed in quadrant 1. Over the range of J investigated, a 26% change in S_C resulted in a 34% change in the mean K_T and a 60% change in the max K_T. The change in the loads due to S_C becomes larger the higher J is investigated because of the divergence in the curves.

Why K_T and K_Q behave in this manner could be due to how the propeller and the ice interact during operations in quadrant 3. At lower J (i.e. > J = -0.3), the propeller could be acting as more as an indenter rather than a cutting tool allowing the ice strength to have a greater effect on both load coefficients than it would if the propeller acted as a cutting tool.

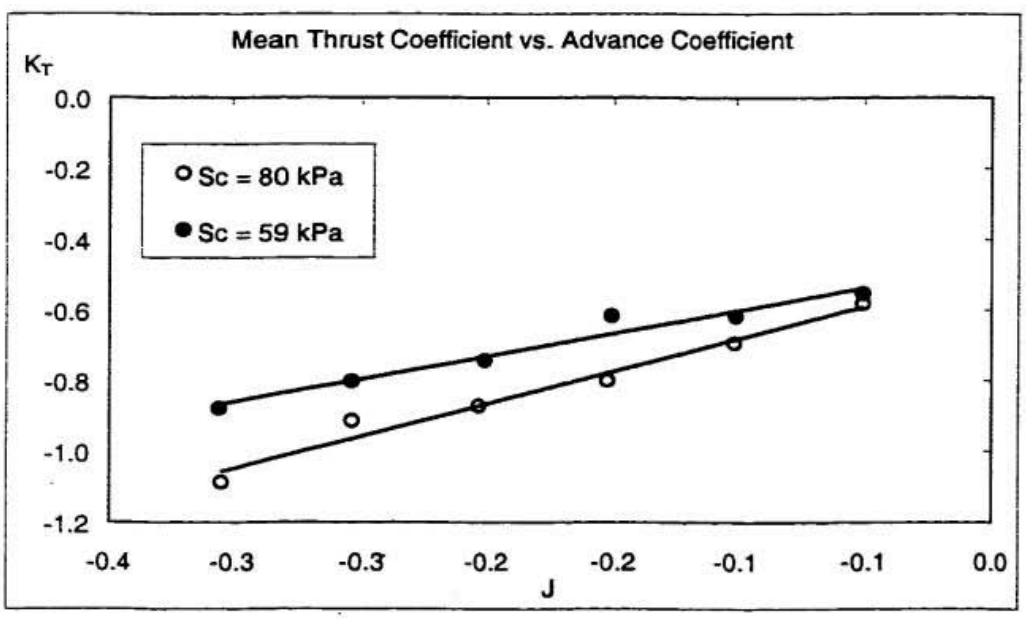

Figure 68: Mean K_T vs. J (Effects of Ice Strength in Quadrant 3)

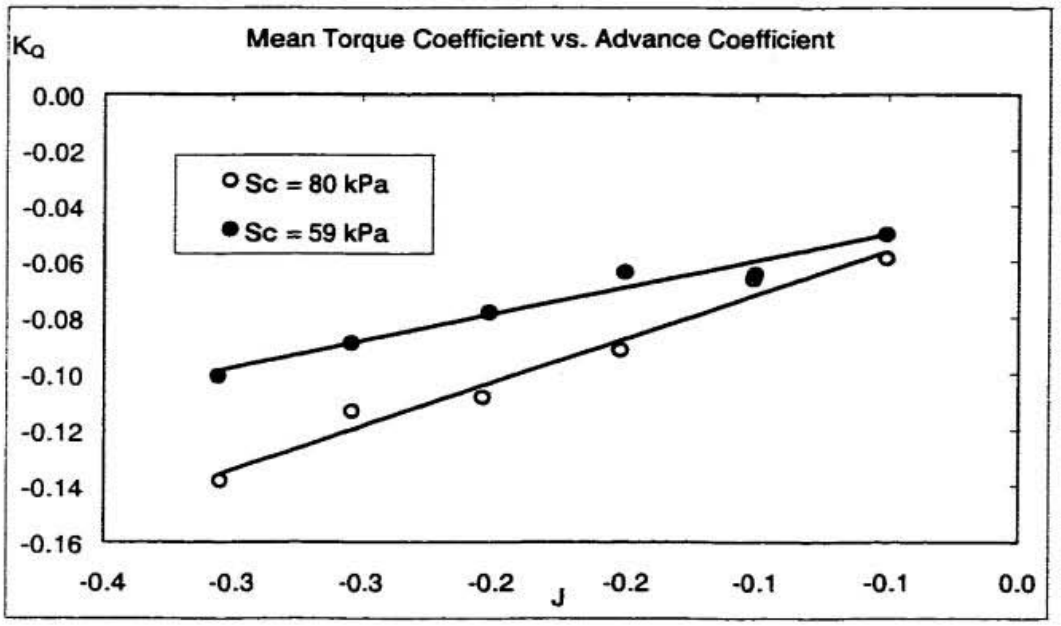

Figure 69: Mean K_Q vs. J (Effects of Ice Strength in Quadrant 3)

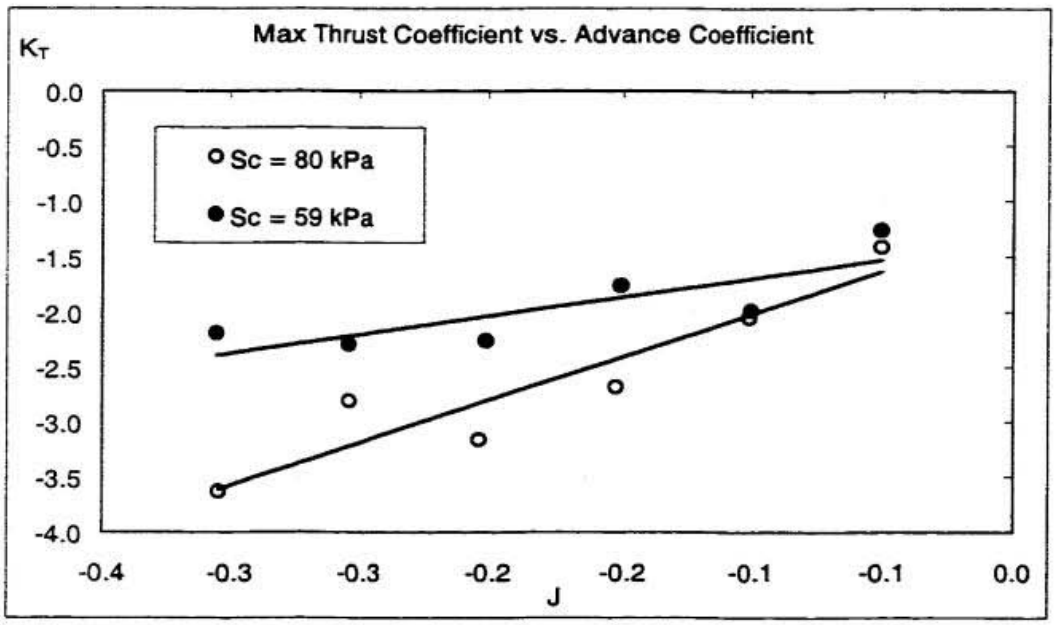

Figure 70: Max K_T vs. J (Effects of Ice Strength in Quadrant 3)

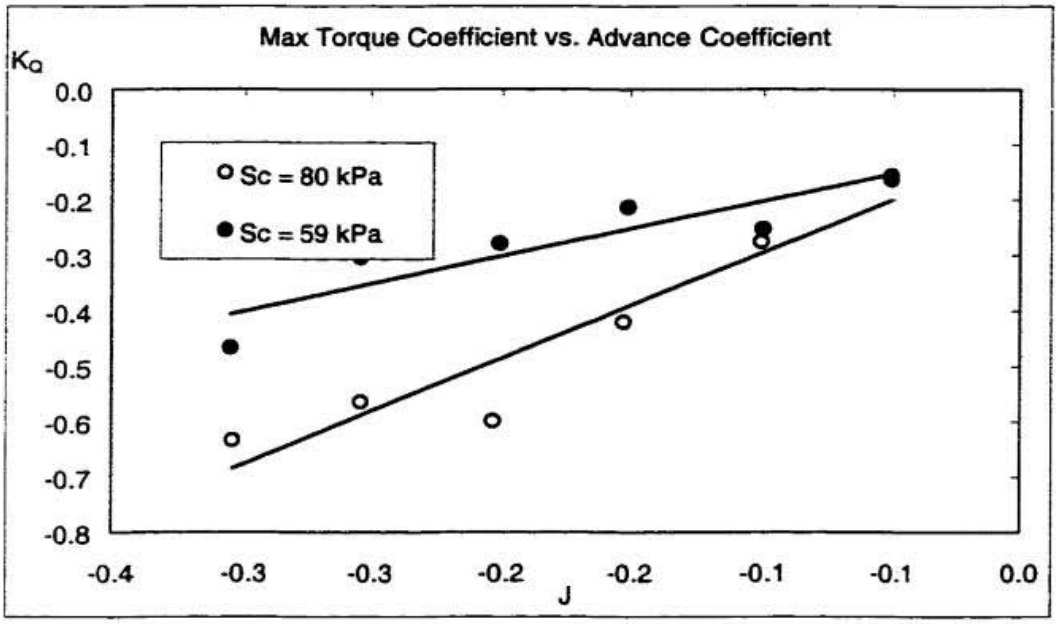

Figure 71: Max K_Q vs. J (Effects of Ice Strength in Quadrant 3)

3.3.6 Quadrant 4: Test Results

Quadrant 4 is defined as the reversing condition. For quadrant 4, the advance coefficient was investigated from J = 0.1 to 1.1 and a total of 5 test runs were conducted to investigate the propeller loads. As with the other quadrants, two main variables were investigated: the effects of advance coefficient and the effects of ice strength. The results of both are presented in the following subsections.

3.3.6.1 Variations in Advance Coefficient

For the test runs in Quadrant 4, the cut depth was held constant at approximately 25 mm ($\lambda_d = 0.125$) while the propeller was run the length of the ice tank over a range of J. The test series was conducted at two different compressive ice strengths, S_C = 71kPa and S_C = 63kPa. The K_T and K_Q versus J plots for each compressive ice strength are presented in Figures 72 to 75. The results obtained in quadrant 4 are similar in magnitude to the results of quadrant 1 but behave in the opposite direction. The solid black circles represent the experimental means for the thrust and torque coefficients and the solid line through these points represent lines of best fit. The open circles represent the maximum values measured during the test program, the open triangles represent the minimum values measured and the lines through each of these data sets represent lines of best fit for the maximum and minimum thrust and torque coefficients. Each of the lines fitted through the data is modelled by a 3rd order polynomial.

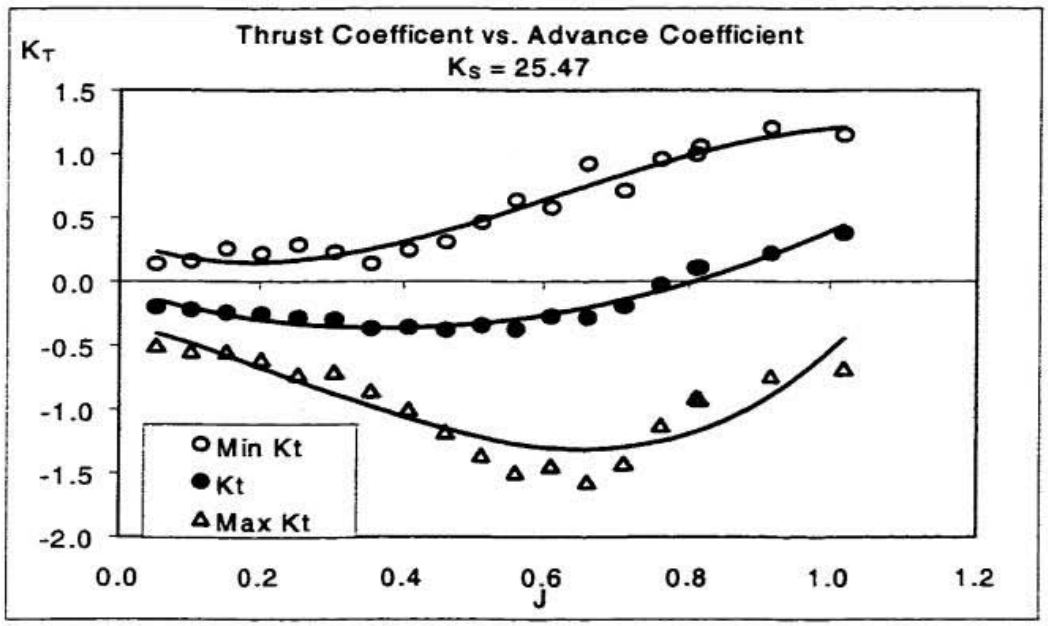

Figure 72: K_T vs. J for $K_S = 25.47$

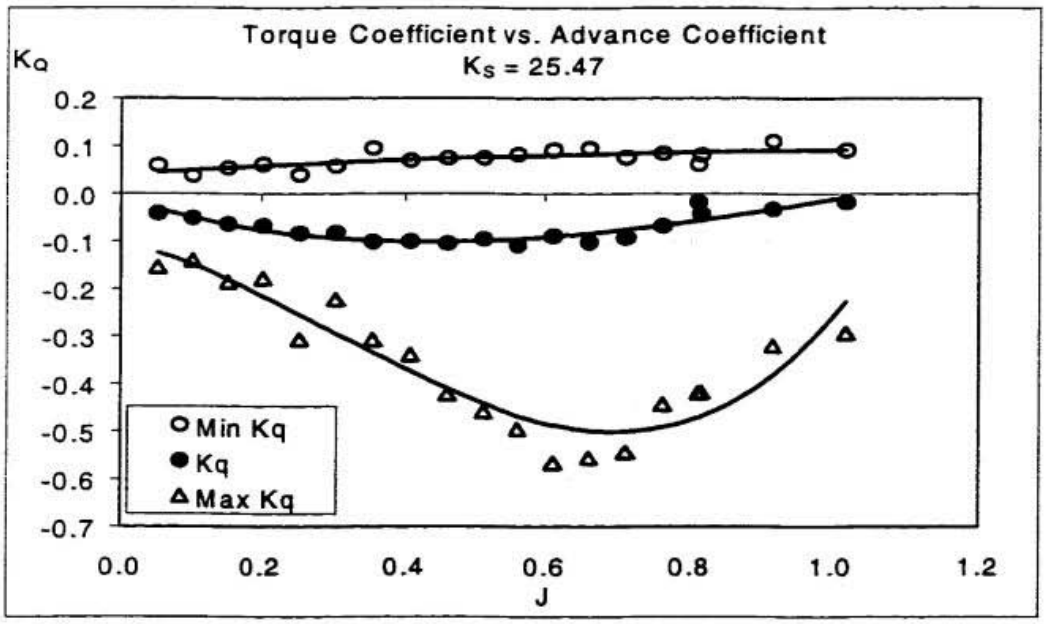

Figure 73: K_Q vs. J for $K_S = 25.47$

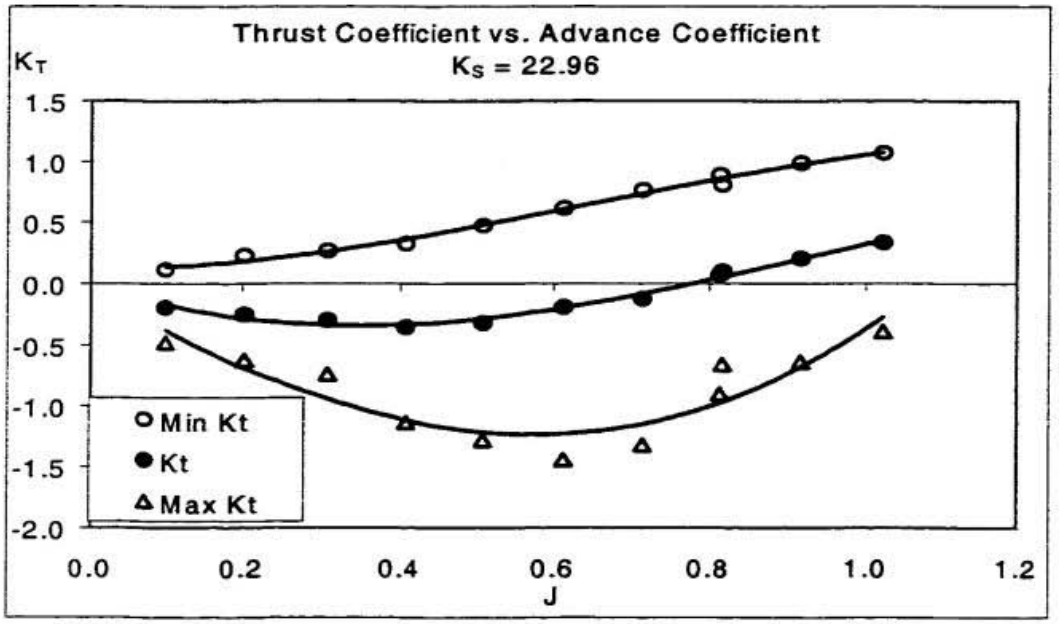

Figure 74: K_T vs. J for K_S = 22.96

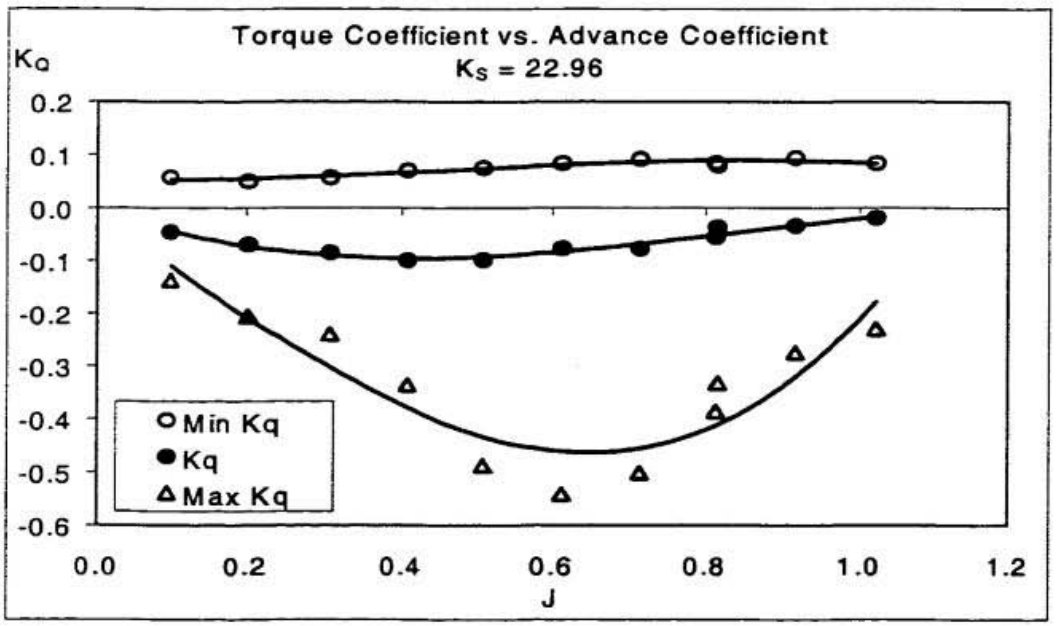

Figure 75: K_Q vs. J for K_S = 22.96

3.3.6.2 Variations in Ice Strength

As stated, tests were conducted at two different ice strengths: 71kPa, 63kPa. For each run, the cut depth was held at 25mm (λ_d = 0.125) and the same range of J was investigated for each. The max and mean K_T and K_Q versus J are presented in Figures 76 to 79 to investigate the effects of compressive strength.

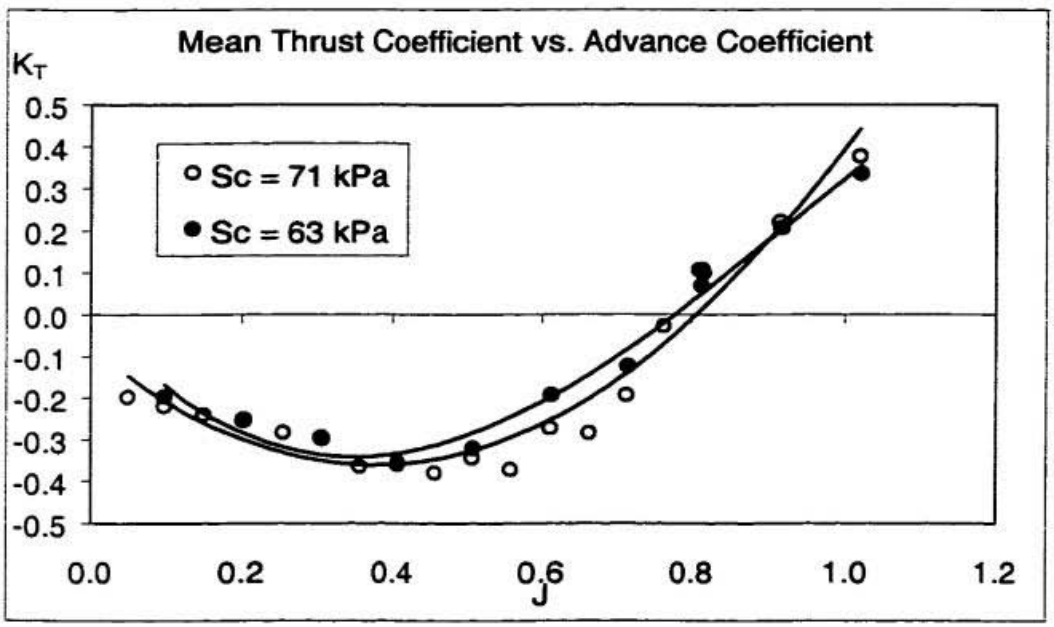

Figure 76: Mean K_T vs. J (Ice Strength Effects in Quadrant 4)

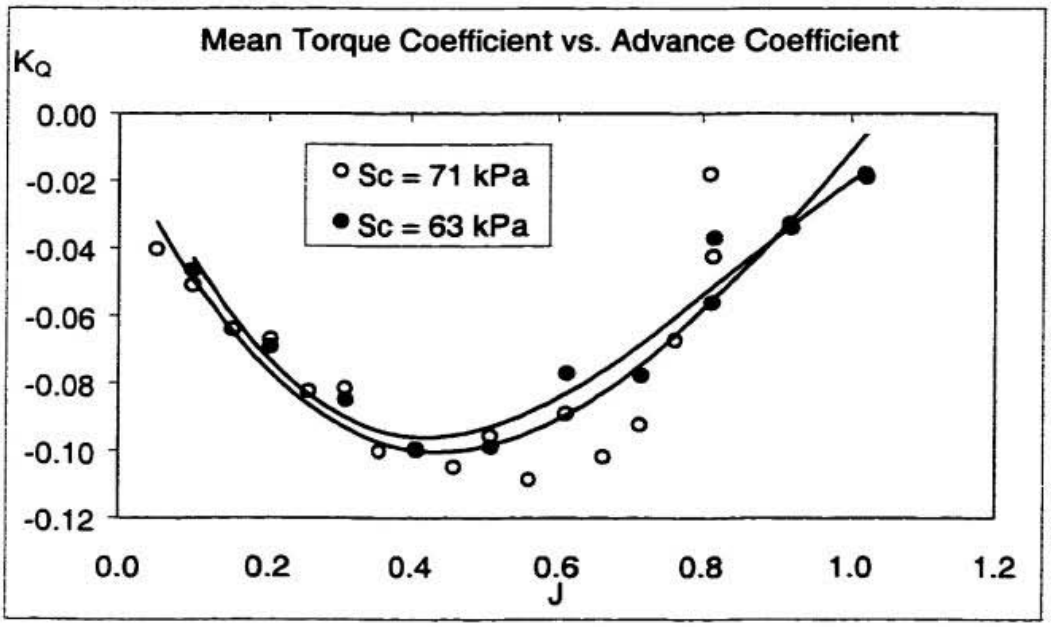

Figure 77: Mean K_Q vs. J (Ice Strength Effects in Quadrant 4)

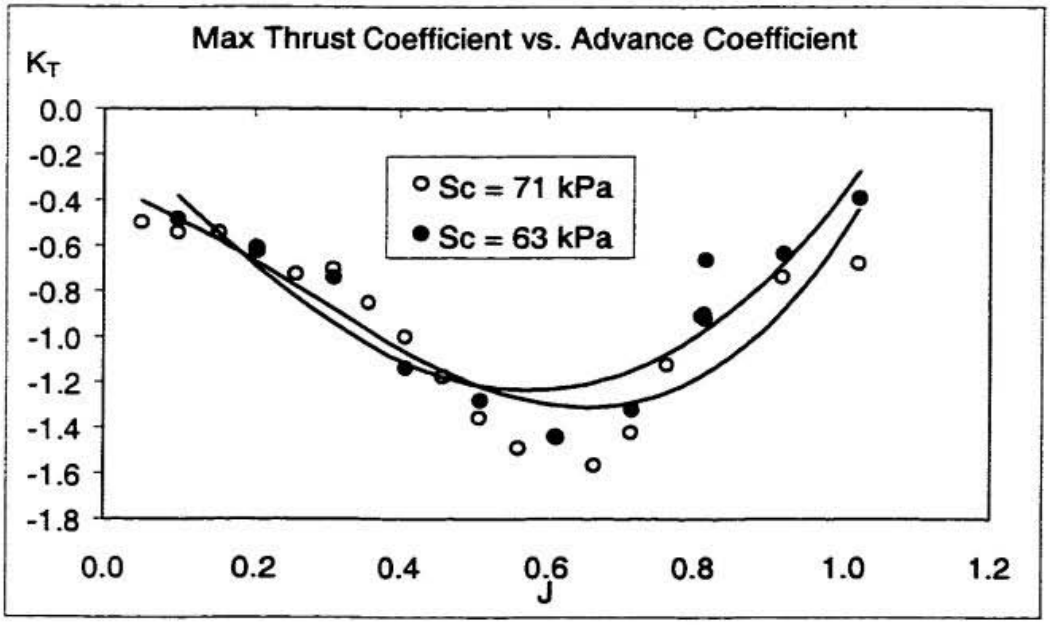

Figure 78: Max K_T vs. J (Ice Strength Effects in Quadrant 4)

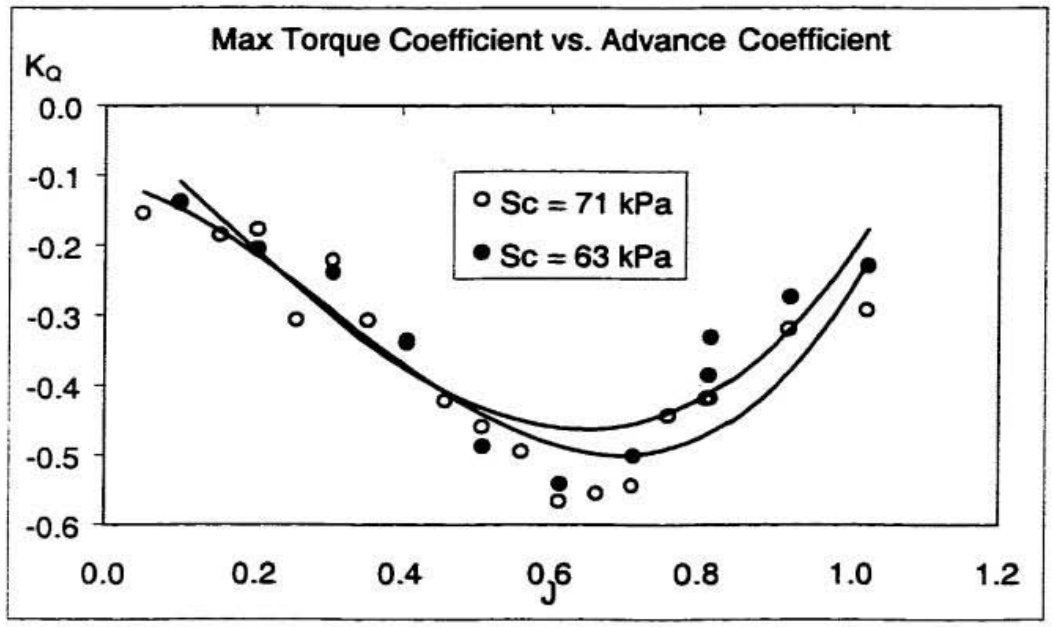

Figure 79: Max K_Q vs. J (Ice Strength Effects in Quadrant 4)

As illustrated in the above figures, it is not possible to confirm the effects of ice strength in quadrant 4. Although it appears that there is little variation in the results, which would indicate a minimal effect of ice strength, it must be noted that the range of ice strength investigated in this quadrant was small: 8kPa. As there were time constraints during testing, not enough time was available between repeats in quadrant 4 to reduce ice strength further between runs. As stated previously, quadrant 1 was the most frequent operating condition, thus efforts were made to get the maximum strength differences to occur between runs in that quadrant. In doing so testing of ice strength effects in quadrant 4 was limited.

3.3.7 Overall Picture of Four Quadrants

To illustrate the propeller thrust and torque loads in the four quadrants and how they compare to one another, Figures 80 to 83 have been provided. The maximum and mean load coefficients have been plotted versus advance coefficient. For each run the cut depth was held at 25mm (λ_d = 0.125) and the variation in ice strength was approximately 7kPa. It varied from S_C = 66kPa in quadrant 1 to S_C = 59kPa in quadrant 3. The plotted results neglect this small change in ice strength.

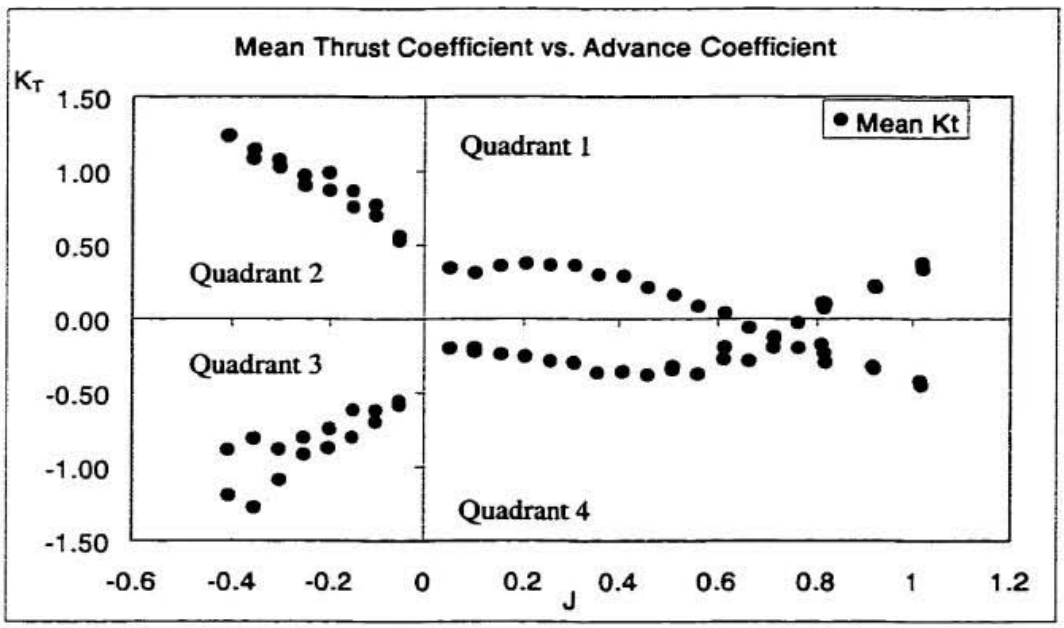

Figure 80: Mean K_T vs. J in Four Quadrants

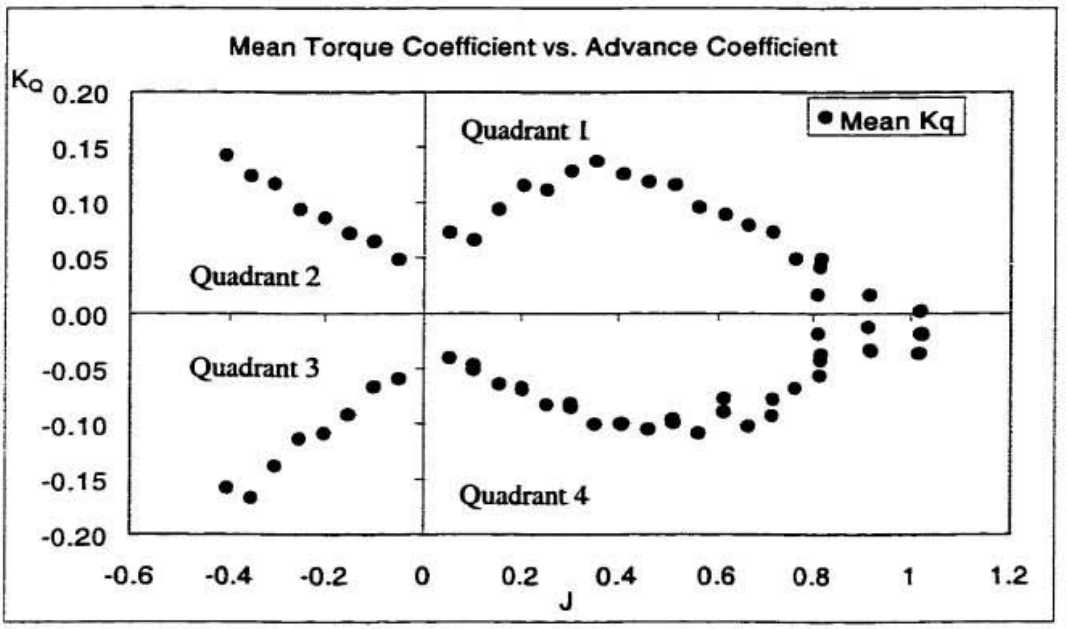

Figure 81: Mean K_Q vs. J in Four Quadrants

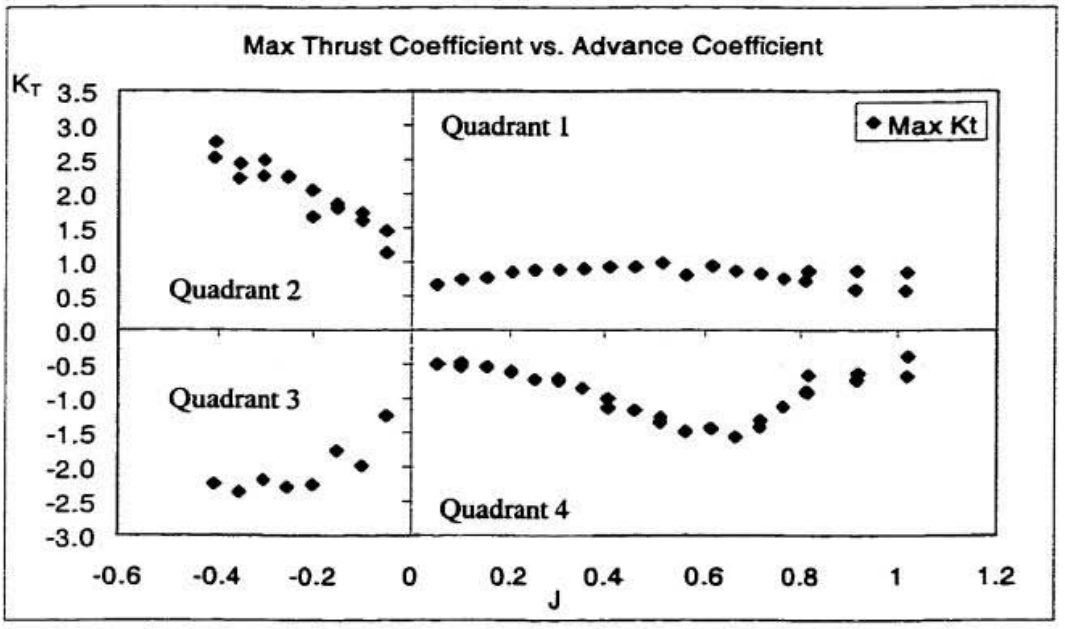

Figure 82: Maximum K_T vs. J in Four Quadrants

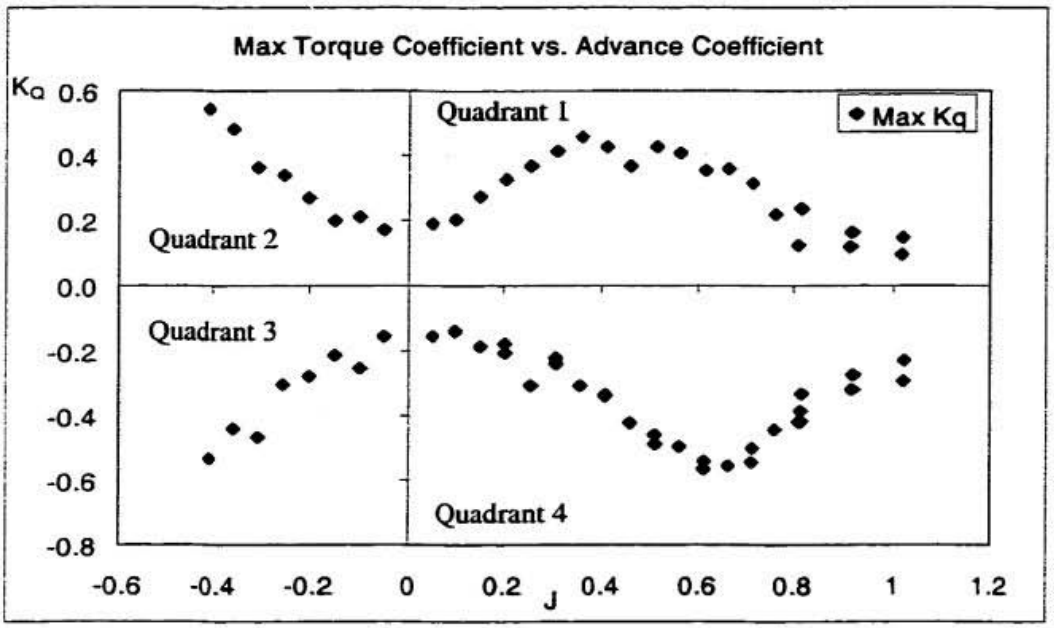

Figure 83: Maximum K_Q vs. J in Four Quadrants

As illustrated in the plots, the loads experienced in quadrant 2 and 3 are much larger than those experienced in quadrants 1 and 4. In addition, the loads in quadrants 2 and 3 are close to linearly related to advance coefficient while the loads in quadrants 1 and 4 show close to cubic relationships.

Based on the results of this test program, it would appear that modification should be made to existing design models to take into account the severe loads that some ice-class propellers may experience during operations in quadrants 2 and 3 if damage is to be avoided.

Chapter 5

Conclusions

The main results from two series of propeller-ice interaction tests in an ice tank have been reported. Recently proposed methods for dimensioning ice-class propellers have focussed on the more traditional ice-class propeller geometry and arrangements so that unconventional designs, such as highly skewed propeller blades, have been excluded and must be treated as special cases. Also, these design methods are based on work that has concentrated on propeller operation in quadrant 1, which may not necessarily be the correct criterion as the loads experienced in quadrants 2 and 3 are both larger than the loads experienced in quadrant 1.

To address some of these issues, an experimental investigation was undertaken in the ice tank at the Institute for Marine Dynamics (IMD) using two different propeller models. A model of the propeller on the passenger ferry *MV Caribou* was tested

specifically to investigate a highly skewed propeller under ice loading over a range of operating and ice conditions. The second propeller tested was a more conventional ice-class propeller from the *R-Class* icebreaker which was tested over a wide range of operating conditions to give loading characteristics in all four quadrants.

Measurements were made of the propeller advance speed, shaft speed, shaft thrust and shaft torque. A major improvement in this test program, compared to previous work, included using a much higher sampling frequency of 5000Hz. The higher sampling frequency aided in developing a clearer picture of the propeller-ice interaction and the loads experienced by the propeller due to these interactions.

The *Caribou* propeller test program investigated two main parameters: the effects of cut depth and the effects of advance coefficient. The test program resulted in two important conclusions. First, a close to linear relationship exists between propeller loads and the depth of cut into the ice piece. The deeper the cut depth, the greater the thrust and torque loads. Three values of J were investigated and the same trends were found for each series. At low cut depths, the mean values of thrust and torque were approximately equal to the open water hydrodynamic components and increased proportionally with the increased depth of cut. These results can be used by design methods to investigate propeller classes by defining the classes in terms of design ice thickness and estimating the exposure of propellers in terms of the operational profiles of the different classes. Secondly, the propeller loads were found to be

strongly dependent on the propeller's operating condition. The thrust and torque relationships against advance coefficient initially increased relative the open water to a maximum at a J = 0.3 to 0.4. Above this value of J, the K_T and K_Q reduced steadily, eventually approaching or dropping below the open water hydrodynamic values. The trends in the data showed that a zero value of K_T and K_Q would be reached at an advance coefficient value lower than that experienced in open water, which would indicate that the contact component of the load acts in the opposite direction to the hydrodynamic component at higher values of J. In addition, the experiments indicated that the thrust and torque loads are oscillatory, which supports suggestions that these propellers should be designed to withstand fatigue from the oscillating load.

Overall, highly skewed propellers behave in a similar fashion to conventional propellers interacting with ice, but questions can be raised with regard to their strength requirements and especially their blade tip design. Highly skewed propellers appear to be susceptible to damage. If these propellers are meant for use in ice conditions, it may be required to limit the extreme skew or redesign the blade tips to increase their ability to withstand loading and possibly avoid the tip bending illustrated here.

The focus of the experimental work involving the *R-Class* model was to provide insight into propeller-ice interaction in off-design conditions and investigate the effects of ice strengths. Tests were conducted in all four quadrants of propeller

operation and the main result from the test program was quadrant 1 is not the operating condition where propellers experience the greatest loads and may not necessarily lead to appropriate loads in proposed design methods. Based on the experimental results, quadrants 2 and 3 both experience loads greater than those experienced in quadrant 1. Although quadrants 2 and 3 are considered off-design conditions, it must be acknowledged that an ice class vessel can find itself in these conditions during its operating life. Propeller design should not be entirely based on quadrant 1 loads; the design criteria should be based more on the exposure of a propeller to each condition. If the vessel spends a proportion of its operating life in these off-design conditions, then it should be required that the propeller be designed for those loads. Exactly what proportion of its operating life is deemed reasonable is a decision that would need to be made by the regulatory bodies. Consequently, the results of this test program suggest that modifications should be made to existing design models to take into account the severe loads that some ice-class propellers may experience during operations in quadrants 2 and 3.

From the tests investigating variations in compressive ice strength it was concluded that thrust is minimally effected by variations in compressive ice strength while the torque load demonstrates a higher dependence on compressive ice strength. A dimensional analysis showed that thrust and torque coefficients for a marine propeller operating in ice are dependent on a set of non-dimensional coefficients including Froude number, Reynolds number, advance coefficient, depth of cut ratio,

compressive ice strength index, and ratios of ice elastic modulus, ice tensile and flexural strengths to compressive strength. Using the test results, together with results from the dimensional analysis, a method to extrapolate the thrust and torque characteristics to full scale ice compressive strengths was described.

The work presented here is the first published ice tank work that has investigated highly skewed propellers and four quadrant operations in ice. Additional work in both these areas would be beneficial. Particularly if more sophisticated models could be used, which allowed the experimenters to instrument the blades and obtain data as to how the blades react directly to interaction with ice.

References

Antonides, G., Hagen, A., and Langrock, D., (1981), *"Full Scale Icebreaking Stresses on Propellers of the Polar Star"*, Propellers '81 Symposium, The Society of Naval Architects and Marine Engineers, Virginia Beach.

Barr, D.I.H., (1969), *"Method of Synthesis - Basic Procedures for the New Approach to Similitude"*, Water Power, pp. 148-153, 183-8, April and May.

Belyashov, V.A. & Shpakov, V.S., (1983), *"On Mechanics of Ice Crushing by Propeller Blades"*, (trans.) Ice Mechanics and Physics, Nauka, Academy of Sciences of the USSR, Moscow.

Belyashov, V., (1993), *"An Investigation on Fracture Mechanics and Ice Loads During Cutting Freshwater Ice by Indenters simulating propeller blades"*, Proceedings POAC '93, Hamburg.

Bose, N. and Luznik, L., (1996), *"Uncertainty Analysis in Propeller Open Water Tests"*, International Shipbuilding Progr. Vol. 43, No. 435, pp. 237-246.

Bose, N., (1996), *"Ice Blocked Propeller Performance Prediction Using a Panel Method"*, Transactions of the Royal Institution of Naval Architects, Vol. 138.

Bose, N., Veitch, B., and Doucet, M., (1998), *"Proposals for Design of Ice-Class Propellers"*, TP 13213E, Transportation Development Centre.

Bose, N., Veitch, B., and Doucet, J.M., (1998), *"A Design Approach for Ice Class Propellers"*, Trans. of the Society of Naval Architects and Marine Engineers.

Browne, R.P., Keinonen, A., and Semery, P., (1991a), *"Ice Loading on Open and Ducted Propellers"*, Proceedings of 1st ISOPE, Edinburgh.

Brown, R.P. and Keinonen, A., (1991b), *"Icebreaker Propulsion Systems, Propulsive Performance and Ice Loading for Design"*, Proceedings of 1st Marine Dynamics Conference, St. John's.

Bulat, V., Majid, I., and Goosens, L., (1985), *"Experimental Determination of Factors Affecting Loads Imposed on Propellers in Ice"*, Transport Canada Publication TP 6812E.

Carlton, J.S., (1994), *"Marine Propellers and Propulsion"*, Butterworth-Heinemann Ltd., Oxford.

Chernuka, M.W., Jategaonkar, R.P., Norwood, M.E., and Warner, J.L., (1989), *"Development of a Procedure for Predicting Propeller-Ice Interaction Forces"*, Transport Canada Publication TP 9850E.

Doucet, J.M., (1996), *"Cavitation Erosion Experiments in Blocked Flow with Two Ice-Class Propeller Models", M.Eng.* Master's Thesis, Memorial University of Newfoundland, St. John's, Newfoundland, Canada.

Doucet, J.M., Bose, N., Veitch, B., and Liu, P., (1997), *"Experimental Results and Theoretical Predictions of Loading on an Ice-Class Ducted Propeller"*, 4th Canadian Marine Hydrodynamic & Structures Conference, Ottawa.

Doucet, J.M., Liu, P., and Bose, N., (1998), *"Numerical Prediction of Ice-Induced Loads on Ice-Class Screw Propellers using a synthesised Contact/Hydrodynamic Code"*, Ocean Engineering Research Centre, OERC Report No. OERC-1998-004.

Duff, J., Kirby, K., and Laskow, V., (1985), *"Measurement of Ice-Propeller Interaction Parameters: M.V. Robert LeMeur: Main Report"*, Transport Canada Publication TP 6839E.

Edwards, R.Y., (1976), *"Methods for Predicting Forces Encountered by Propellers During Interactions with Ice"*, Intl. Shipbuilding Progress, Vol. 23, No. 268.

Enkvist, E. and Johansson, B.M., (1968), *"On Icebreaker Screw Design"*, European Shipbuilding, Vol. 16, No. 1, Oslo.

Gabel, D.G., Parsons, M.G., and Kaldjian, M.J., (1979), *"Finite Element Structural Analyses for Displacements Occurring in the Hub of a Polar Class Icebreaker Controllable Pitch Propeller Operating in Ice "*, Dept of Naval Architecture and Marine Engineering Report No. 217, The University of Michigan.

Harvald, Sv. Aa., (1983), *"Resistance and Propulsion of Ships"*, John Wiley & Sons, Toronto.

Ignatjev, M.A., (1964), *"Determination of Ice Loads Encountered by Ship Propeller Blades"*, (trans.), Problems of the Arctic and Antarctic, No. 15, pp.41-51.

Ignatjev, M.A., (1966), *"Screw Propellers for Ships Navigating in Ice"*, (trans), Sudostroenie.

ITTC, (1978), *"Report of the Resistance and Flow Committee,"* 15th International Towing Tank Conference, Ottawa, Canada.

Jagodkin, V.Y., (1963), *"Analytical Determination of the Resistance Moment of a Propeller During Its Interaction with Ice"*, (trans.) Problems of the Arctic and Antarctic, Vol. 12, pp.78-88.

Jones, S.J., (1987), *"Ice Tank Test Procedures at the Institute for Marine Dynamics"*, Report No. LM-AVR-20, Institute for Marine Dynamics, NRC, St. John's.

Jussila, M., (1983), *"Ice Loads on the Propulsion System of an Icebreaking Tug"*, POAC '83, Espoo.

Jussila, M. and Koskinen, P., (1989a), *"Ice Loads on CP-Propeller Shaft of Small Ferry and their Statistical Distributions during Winter '87"*, OMAE, The Hague.

Jussila, M. and Koskinen, P., (1989b), *"Ice Loads on Propeller Blade of Small Car Ferry"*, POAC '89 Vol. 2, LuleΣ.

Jussila, M. & Soininen, H., (1991), *"Interaction between Ice and Propeller"*, Research Notes 1281, Technical Research Centre of Finland, Espoo.

Kannari, P., (1988), *"Full Scale and Model Tests Performed with a Nozzle and Open Propeller Simultaneously"*, IAHR Symposium, Sapporo.

Katzmann, F.M., and Andriushin, A.V., (1997), *"Strength Rates for Blades as Intended for the Propellers of Ice-Breakers and Ice Ships"*, Russian Maritime Register of Shipping.

Keinonen. A.J., and Browne, R.P., (1990), *"Ice Propeller Interaction Forces"*, Transport Canada Publication 10401E Vol. 1.

Koskikivi, J. and Kujala, P., (1985), *"Long-Term Measurements of Ice Induced Loads on the Propulsion Machinery of Product Tanker Sotka"*, Winter Navigation Research Board Report No. 42, Finnish Board of Navigation.

Kotras, T., Humphreys, D., Baird, A., Morris, G., and Morley, G., (1985), *"Determination of Propeller-Ice Milling Loads"*, OMAE '85, Dallas, Vol. 2 pp. 336-343.

Laskow, V., Spencer, P.A., and Bayly, I.M., (1986), *'The MV Robert LeMeur Ice/Propeller Interaction Project: Full Scale Data"*, Marine Technology, Vol. 23, No. 4, Society of Naval Architects and Marine Engineers, New York.

Lindroos, H., and Bj rkestam, H., (1986), *"Hydrodynamic Loads Developed During Ice-Clogging of a Propeller Nozzle and Means to Prevent the Clogging"*,

PolarTech '86 International Offshore and Navigation Conference and Exhibition, Vol. 2, Technical Research Centre of Finland, Espoo.

Liu, P., (1996), *"A Time-Domain Panel Method for Oscillating Propulsors with Both Chordwise and Spanwise Flexibility ", Ph.D.* Doctoral Thesis, Memorial University of Newfoundland, St. John's, Newfoundland, Canada.

Luznik, L., (1994), *"Open Water Performance of a Propeller in a Uniform Flow and in a Blocked Flow from a Nearby Simulated Ice Body"*, Memorial university of Newfoundland, OERC Reprot No. WR-WTT—94001.

Luznik, L., Walker, D., Bose, N., and Jones, S.J., (1995), *"Effects of Ice Blockage Size and Proximity on Propeller Performance During Non-Contact Propeller-Ice Interaction"*, Proceedings 14th International Conference on Offshore Mechanics and Arctic Engineering, ASME, Copenhagen.

Newbury, S., Shih, L.Y., Browne, R.P., Revill, C.R., Kenny, S., and Zheng, Y., (1993), *"Experimental and Theoretical Evaluation of Hydrodynamic Pressure During Non-Contact Propeller-Ice Interaction"*, Proceeding of the 2nd Canadian Marine Conference, Vancouver.

O'Brien, T.P., (1962), *"The Design of Marine Screw Propellers"*, Hutchinson Scientific & Technical, London.

Okamoto, H., Shimoyama, N., Yamamoto, F., Nozawa, K., Iizuka, K., and Matsumura, H., (1981a), *"Experimental Study on Propeller Ice Interaction for Icebreaking Merchant Ship, 1st Report: Ice Load Model Experiments"*, Journal of the Society of Naval Architects of Japan, Vol. 149, No. 4.

Okamoto, H., Kawakami, H., Yamamoto, F., Nozawa, K., Yoshikawa, T., and Iizuka, K., (1981b), *"Experimental Study on Propeller Ice Interaction for Icebreaking Merchant Ship, 2nd Report: Static Load Test and FEM Analysis"*, Journal of the Society of Naval Architects of Japan, Vol. 150, No. 4.

Okamoto, H., Nozawa, K., Kawakami, H., Yamamoto, F., (1981c), *"Dynamic Ice Loads and Stress Analysis on the Propeller of the Arctic Ship; Model Test in Ice"*, POAC '81, Vol. 1, Quebec.

Riska, K., (1987), *"On the Mechanics of the Ramming Interaction Between a Ship and a Massive Ice Floe"*, Doctor of Technology Thesis, Technical Research Centre of Finland, Espoo.

Riska, K., Jalonen, R., Veitch, B., Nortola-Hoikkanen, A., and Wilkman, G., (1994), *"Assessment of Ice Model Testing Techniques", Proceedings of* IceTech, Calgary.

Robbins, I., Doucet, J.M., Liu, P., and Bose, N., (1998), *"Numerical Prediction of Ice-Induced Loads on Ice-Class Screw Propellers"*, Ocean Engineering Research Centre, Report Number OERC-1998-003.

Sasajima, T., Bulat, V., and Glen, I., (1981), *"An Experimental Investigation of Two Candidate Propeller Designs for Ice Capable Vessels"*, POAC '81, Vol. 1.

Sasajima, T. and Mustamaki, E., (1984), *"Ice Milling Load Encountered by a Controllable Pitch Propeller"*, IAHR Ice Symposium, Hamburg.

Sasajima, T., (1985), *"Ice Milling Loads Encountered by a Controllable Pitch Propeller"*, Mitsubishi Technical Bulletin No. 170, Mitsubishi Heavy Industries Ltd., Tokyo.

Sharp, J.J., (1981), *"Hydraulic Modelling"*, Butterworth & Co. Ltd., London.

Sharp, J.J., Deb, A. and Deb, M.K., (1992), *"Application of Matrix Manipulation in Dimensional Analysis Involving Large Numbers of Variables"*, Marine Structures Vol. 5.

Shih, L.Y., and Zheng, Y., (1992), *Constricted Hydrodynamic Flow due to Proximate Ice Blockage over a Blade Profile in Two Dimensions"*, Proceedings 2nd International Symposium on Propellers and Cavitation, Hongzou.

Shih, L.Y., and Zheng, Y., (1993), *"Application of 3-D BEM to Time Dependent Potential Flow Around a Propeller Blade Profile During Ice Contact"*, Proceedings International Shipbuilding Conference, St. Petersburg.

Soininen, H., Liukkonen, S, and Muhonen, A., (1995), *"Laboratory Tests of Propeller Blade Profile Pressure Distribution under Ice Contact"*, Research Notes 1664, Technical Research Centre of Finland, Espoo.

Soininen, H., Jussila, M., Koskinen, P., Jones, S.J., Newbury, S., and Browne, R., (1997), *"Propeller-Ice Interaction"*, Transactions of the Society of Naval Architects and Marine Engineers, Vol. 105.

Tamura, K., Kato, H., and Yamaguchi, H., (1997), *"Experimental Approach to the Interaction between Nozzle-Propeller and Ice Block"*, Joint OMAE/POAC Conference, Yokohama, Japan.

Timco, G.W., (1986), *"EG/AD/S: A New Type of Model Ice for Refrigerated Towing Tanks"*, Cold Regions Science and Technology.

Veitch, B., (1992), *"Propeller-ice Interaction"*, Licentiate of Technology Thesis, Helsinki University of Technology, Espoo.

Veitch, B., and Kivel™, J., (1993), *"Results of Ice Cutting Experiments with Cutting Tools Representing Propeller Blade Sections"* Report M-183, Ship Laboratory, Helsinki University of Technology, Espoo.

Veitch, B., (1995), *"Predictions of Ice Contact Forces on a Marine Screw Propeller During the Propeller-Ice Cutting Process"*, Acta Polytechnica Scandinavica, Mechanical Engineering Series No. 118, Helsinki.

Veitch, B., (1997), *"Effects of Propeller Size on Loads during Propeller-Ice Interaction"*, Oceanic Engineering International, Vol. 1, No. 1, pp.33-37.

Veitch, B., Bose, N., Meade, C., and Liu, P., (1997), *"Predictions of Hydrodynamic and Ice Contact Loads on Ice Class Screw Propellers"*, Proceedings of OMAE, Yokohama.

Veitch, B., (1999), *"Numerical Predictions of Propeller-Ice Contact Loads"*, OERC-1999-001, Ocean Engineering Research Centre, Memorial University of Newfoundland.

Walker, D., Bose, N., and Yamaguchi, H., (1994a), *"Hydrodynamic Performance and Cavitation of an Open Propeller in a Simulated Ice Blocked Flow"*, Journal of OMAE, Vol.116.

Walker, D., Bose, N., (1994b), *"Hydrodynamic Performance and Cavitation of an Open Propeller in Simulated Ice Blocked Flow"*, Proceedings of Propeller/Shafting '94, Virginia Beach, Paper No. 20.

Walker, D., Bose, N., and Casey, S., (1994c), *"Ducted Propeller Cavitation in Blocked Flow"*, 2nd International Symposium on Cavitation, Tokyo.

Walker, D.L.N., (1996), *"The Influence of Blockage and Cavitation on the Hydrodynamic Performance of Ice Class Propellers in Blocked Flow", Ph.D.* Doctoral Thesis, Memorial University of Newfoundland, St. John's, Newfoundland, Canada.

Wind, J., (1983), *"The Dimensioning of High Power Propeller System for Arctic Icebreaking Vessels"*, Proceedings, The 5th Lips Propeller Symposium.

Yamaguchi, H., (1993), *"Investigation on Propeller Performance in Uniform and Blocked Flow for the Lifting Surface Calculations"*, Report NRC LM-1993-11, National Research Council of Canada, St. John's.

Appendix A

Sample Time Histories and Load Density Distributions for *Caribou* Propeller Test Program

Run Name	S1A_T1_001
Advance Coefficient	0.30
Cut Depth (mm)	11.2
Compressive Ice Strength (kPa)	278

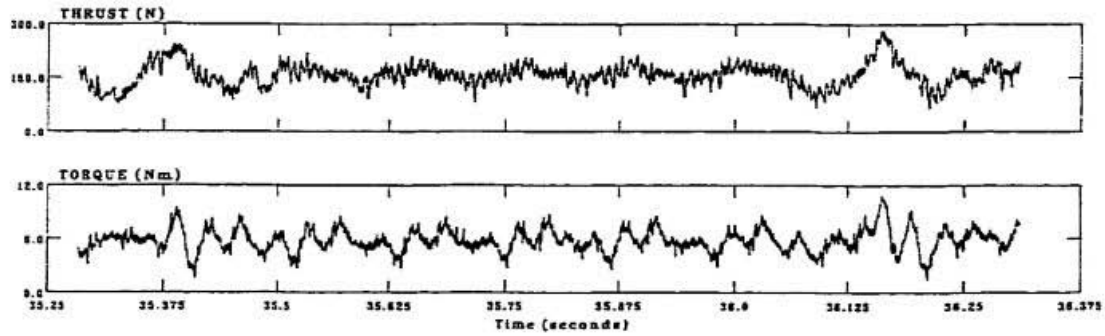

Figure 84: Time Series for Run S1A_T1_001

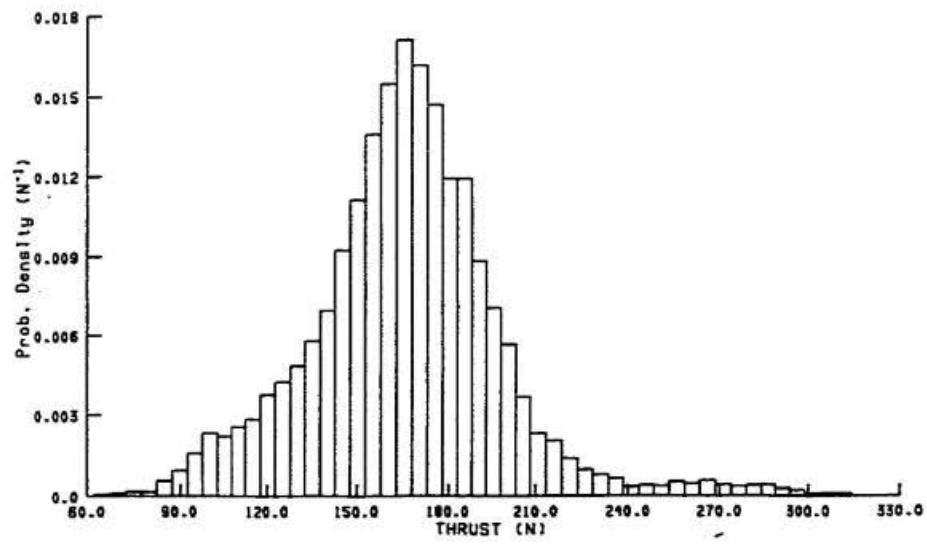

Figure 85: Thrust Distribution during run S1A_T1_001

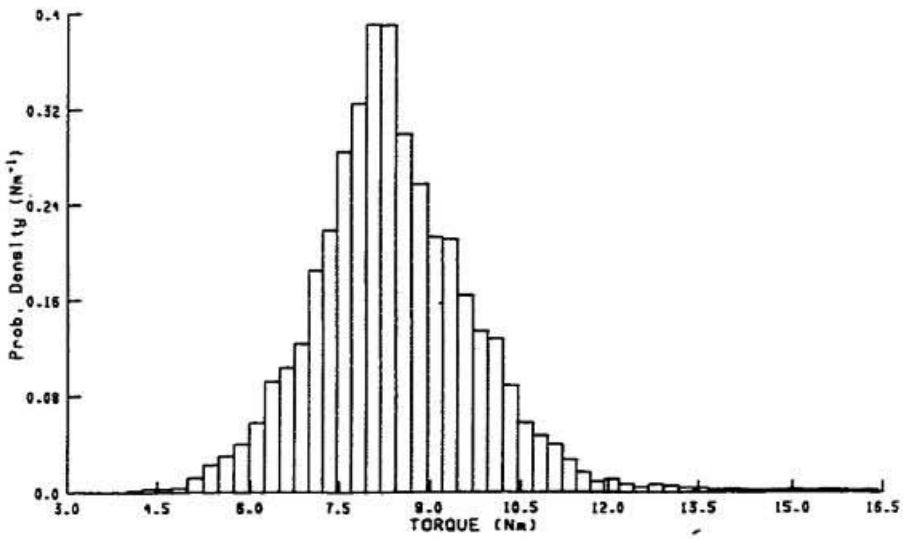

Figure 86: Torque Distribution during run S1A_T1_001

Run Name	S1A_T3_003
Advance Coefficient	0.30
Cut Depth (mm)	40.1
Compressive Ice Strength (kPa)	278

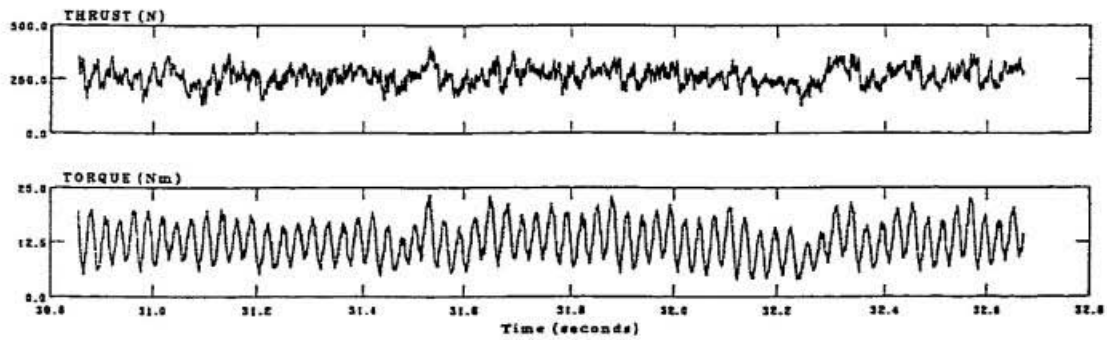

Figure 87: Time Series for Run S1A_T3_003

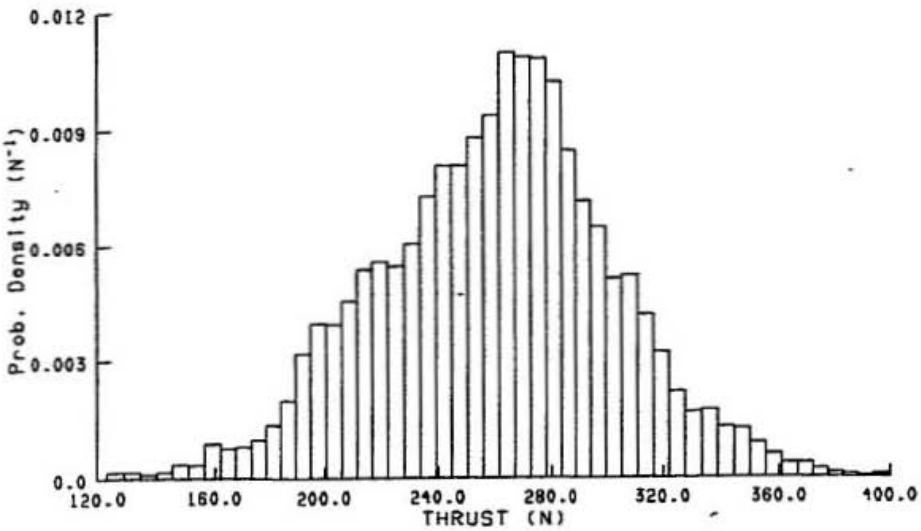

Figure 88: Thrust Distribution during run S1A_T3_003

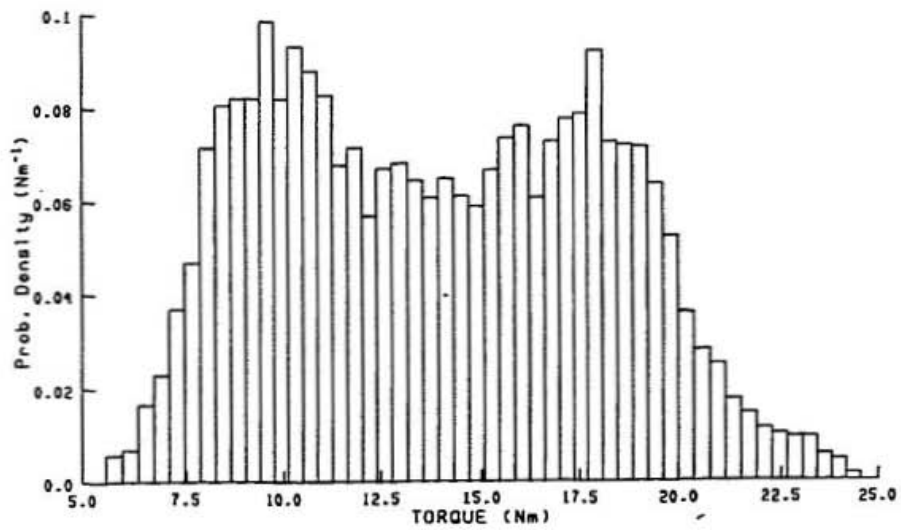

Figure 89: Torque Distribution during run S1A_T3_003

Run Name	S3_T5_005
Advance Coefficient	0.50
Cut Depth (mm)	47.5
Compressive Ice Strength (kPa)	158

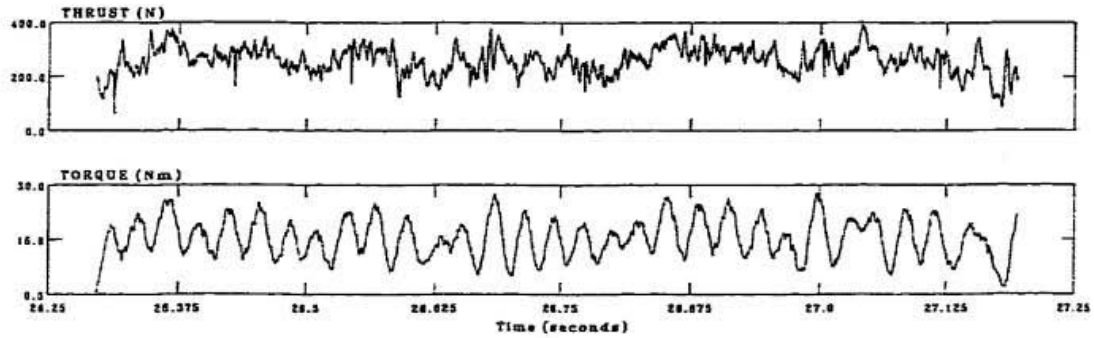

Figure 90: Time Series for Run S3_T5_005

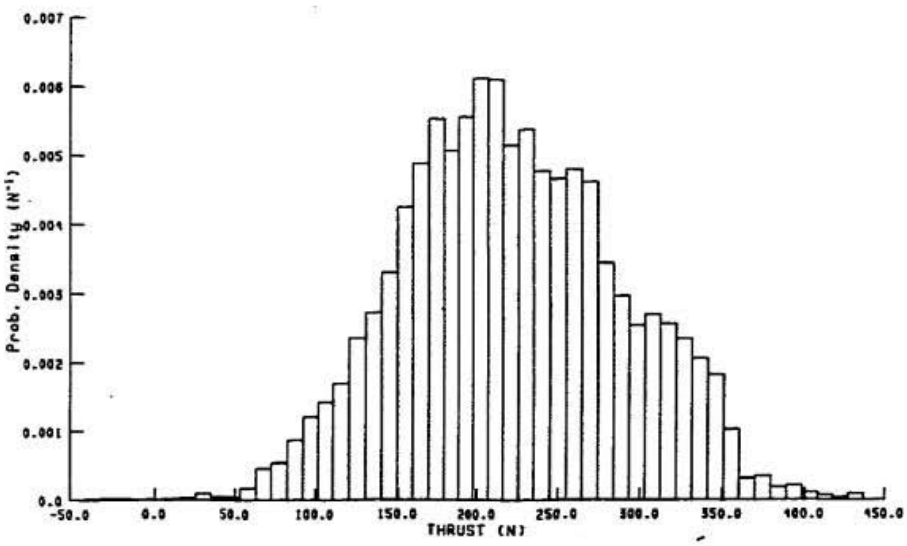

Figure 91: Thrust Distribution during run S3_T5_005

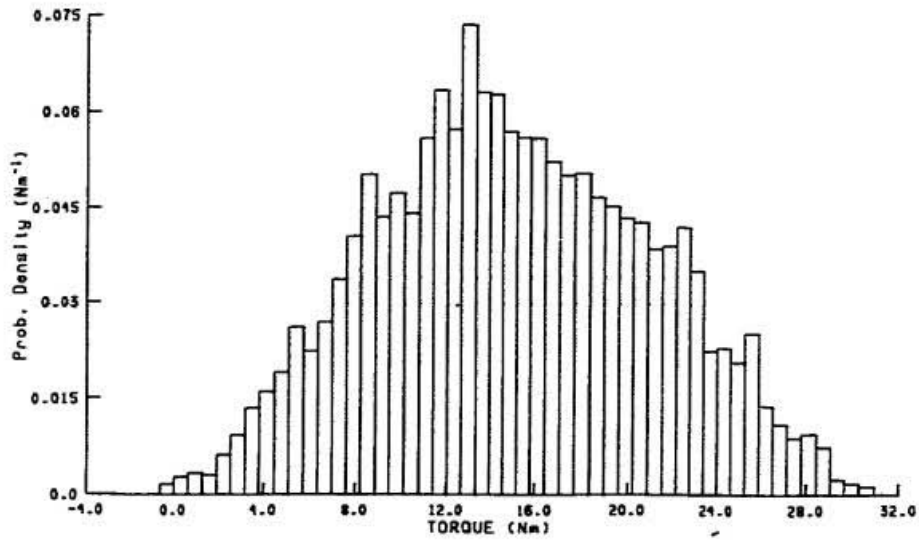

Figure 92: Torque Distribution during run S3_T5_005

Run Name	S5_T3_003
Advance Coefficient	0.70
Cut Depth (mm)	27.2
Compressive Ice Strength (kPa)	139

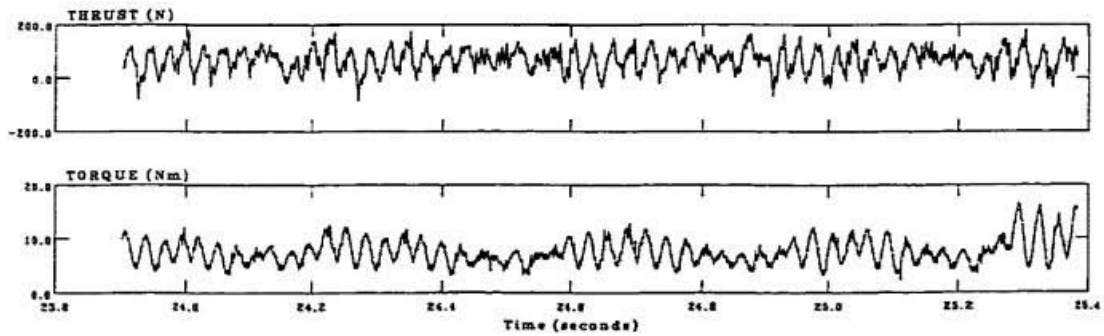

Figure 93: Time Series for Run S5_T3_003

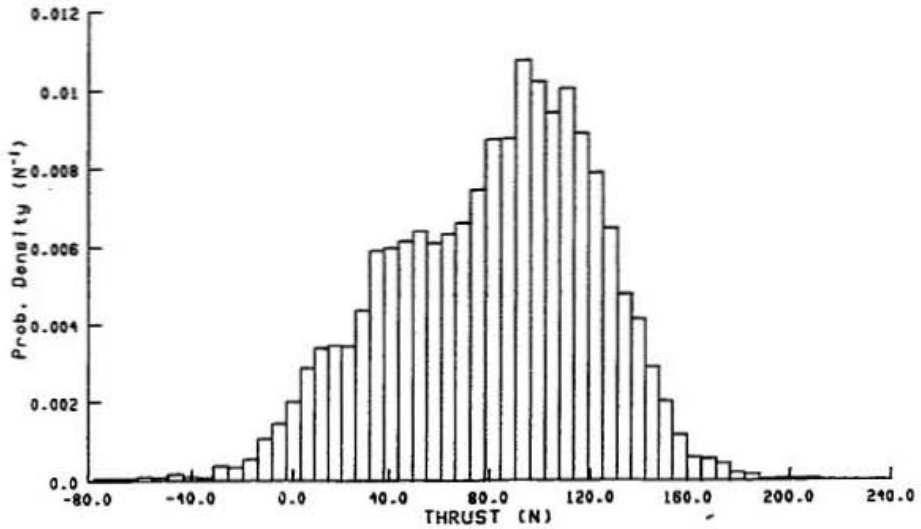

Figure 94: Thrust Distribution during run S5_T3_003

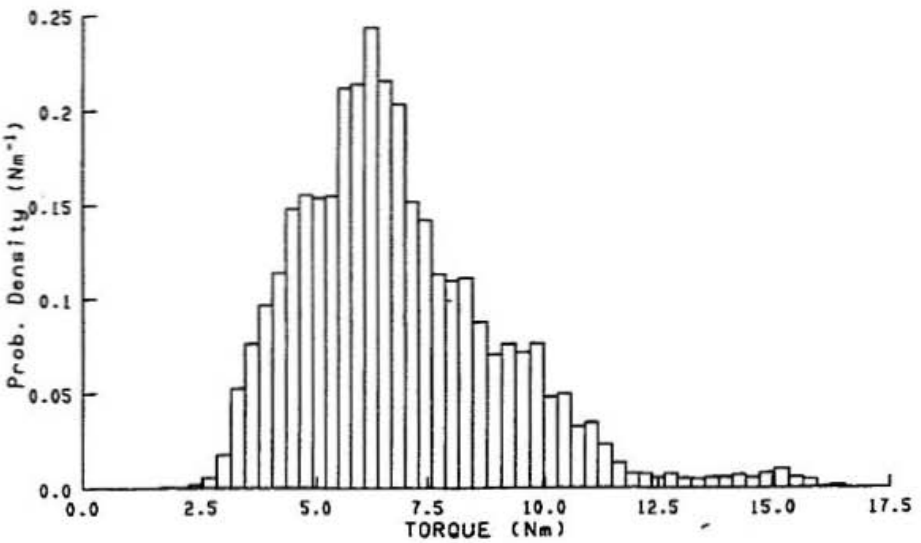

Figure 95: Torque Distribution during run S5_T3_003

Run Name	S5_T5_005
Advance Coefficient	0.70
Cut Depth (mm)	46.2
Compressive Ice Strength (kPa)	137

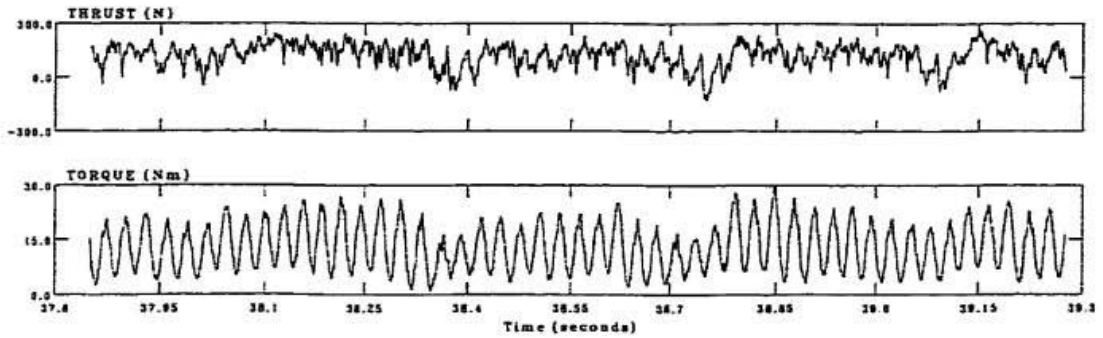

Figure 96: Time Series for Run S5_T5_005

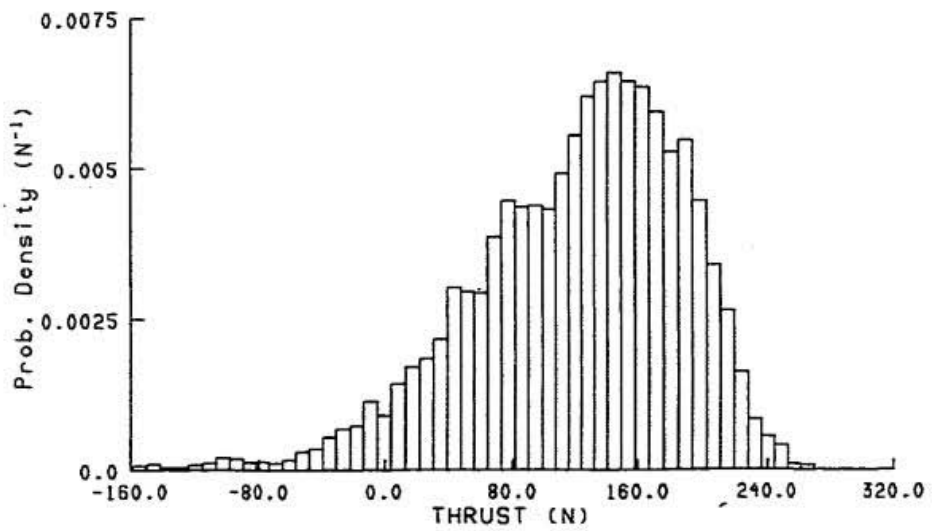

Figure 97: Thrust Distribution during run S5_T5_005

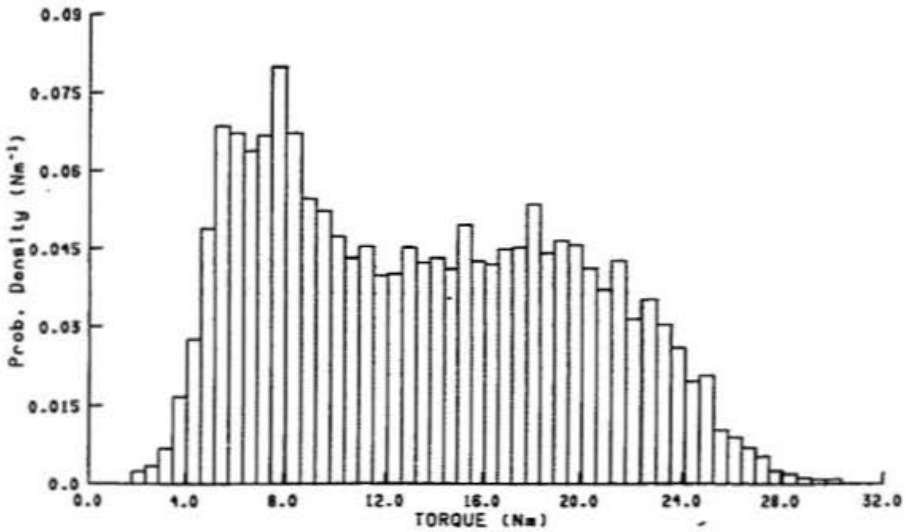

Figure 98: Torque Distribution during run S5_T5_005

Appendix B

Photographs of Damage to Model Propeller

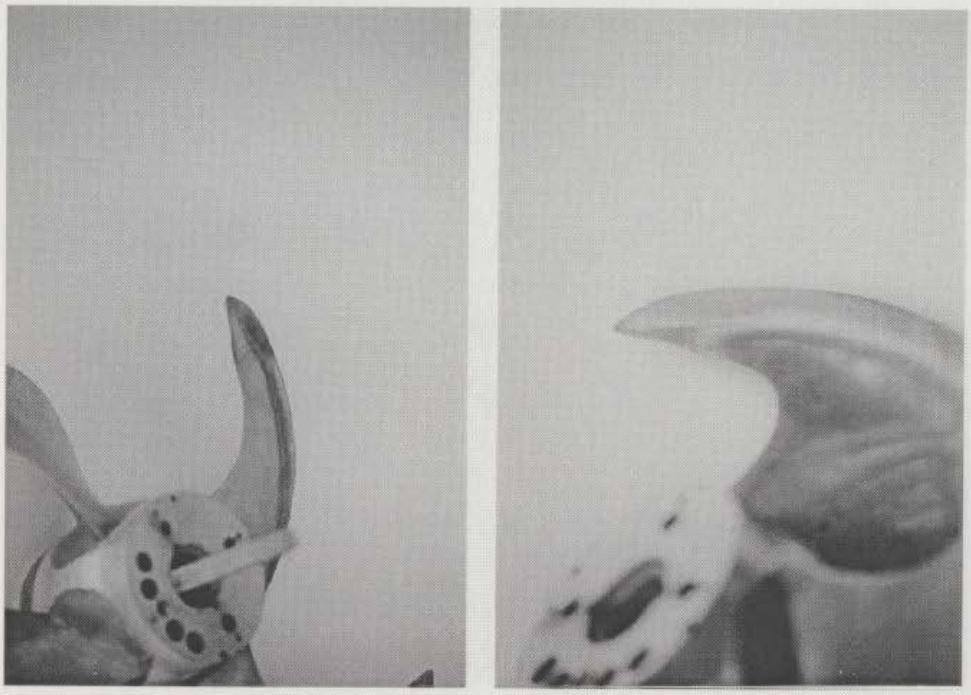

Figure 99: Photographs of Model Propeller

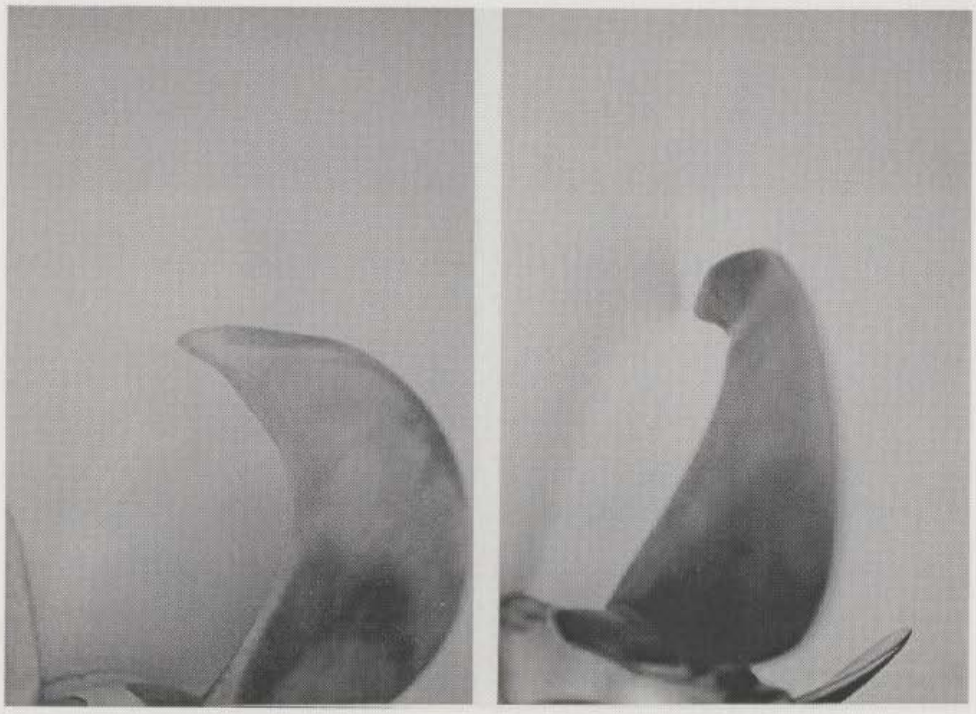

Figure 100: Photographs of Model Propeller

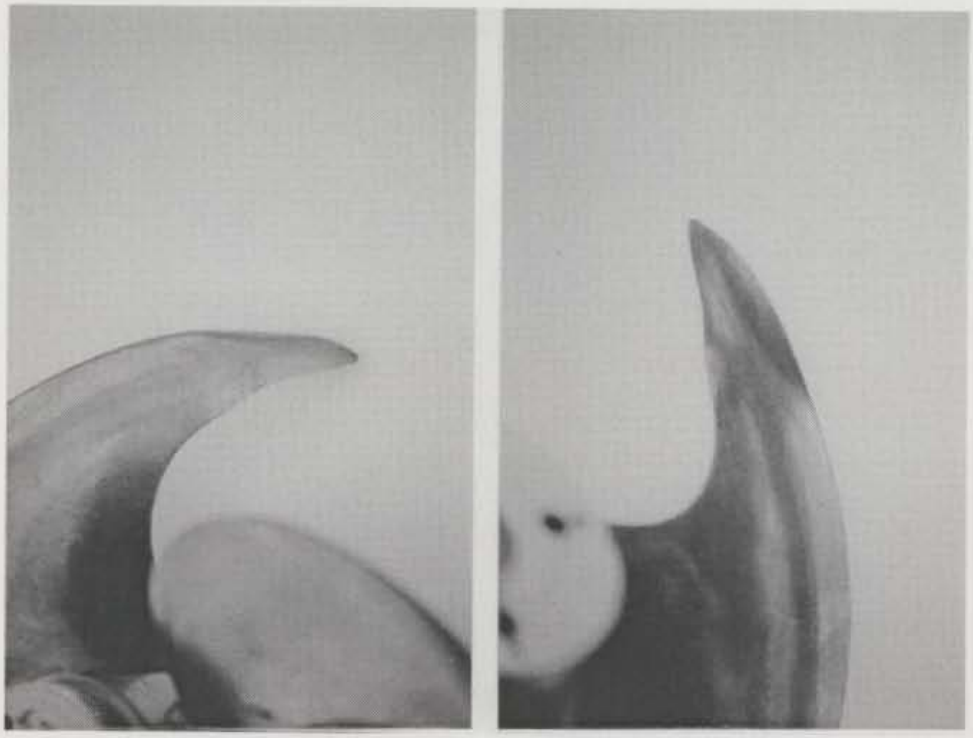

Figure 101: Photographs of Model Propeller

Appendix C

Photographs of Damage to Full Scale Propeller

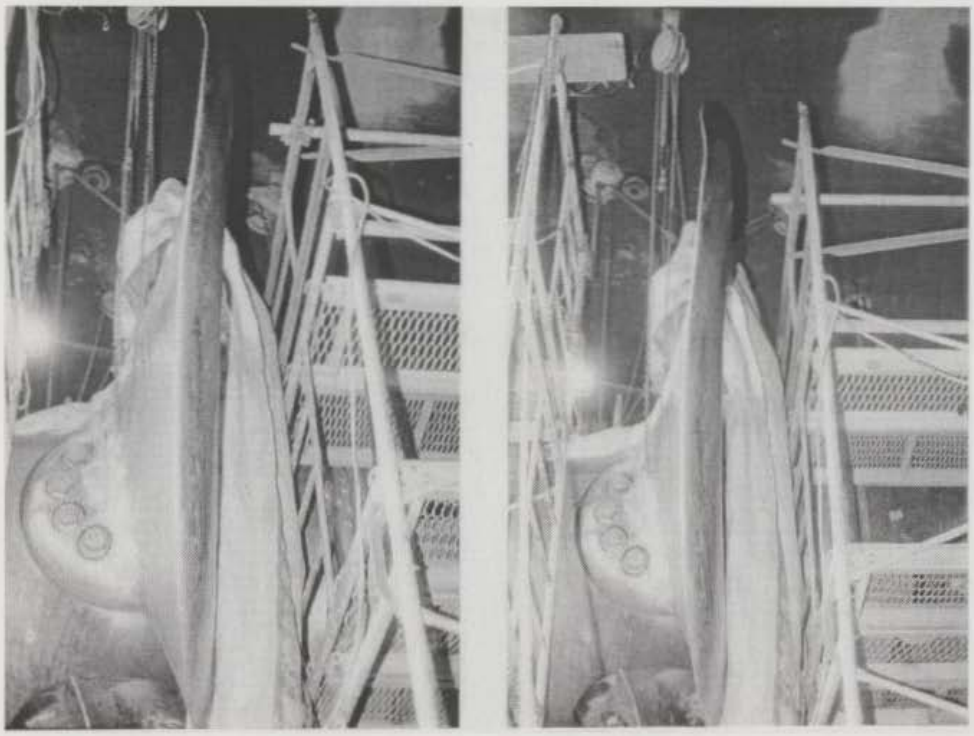

Figure 102: Photographs of Full Scale Propeller

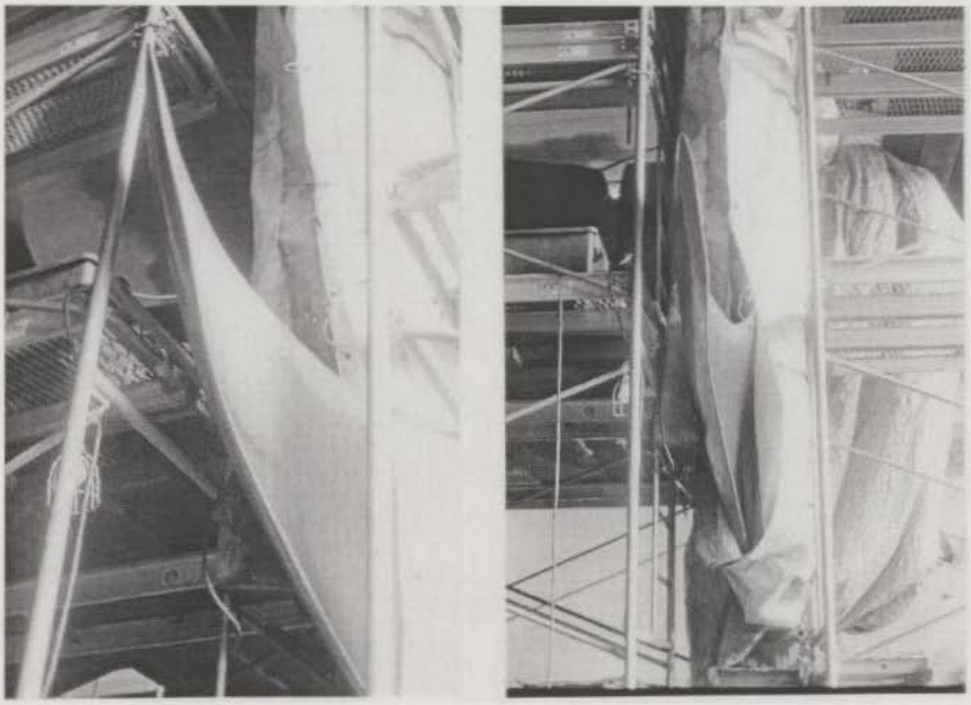

Figure 103: Photographs of Full Scale Propeller

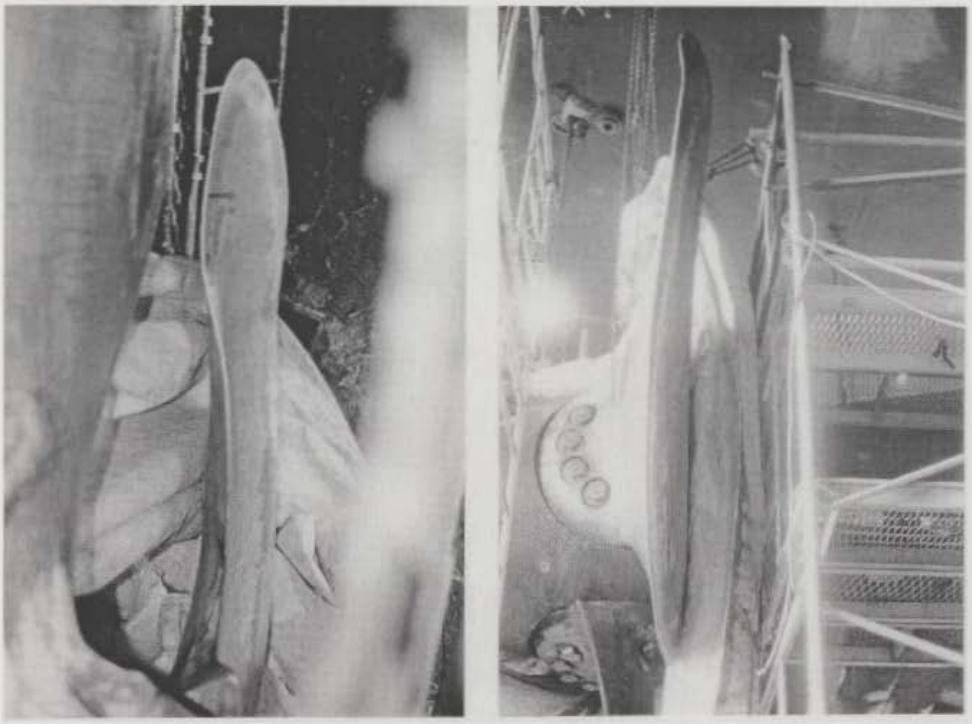

Figure 104: Photographs of Full Scale Propeller

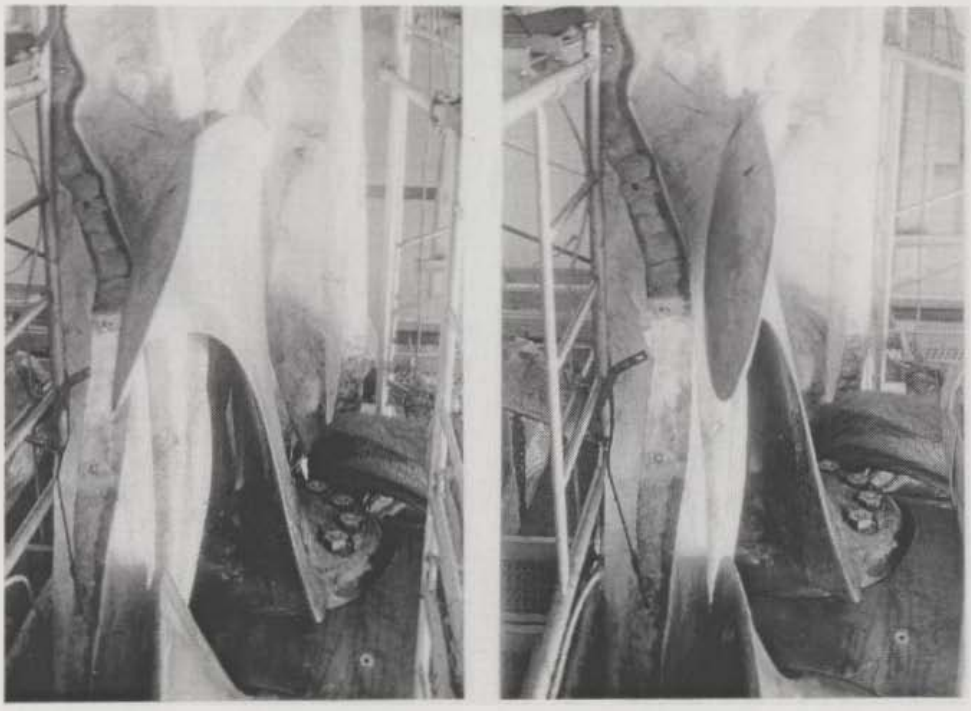

Figure 105: Photographs of Full Scale Propeller

Appendix D

Sample Time Histories and Load Density Distribution for *R-Class* Propeller Test Program

Run Name	R2_T9_T12_001
Advance Coefficient	.91
Cut Depth (mm)	25
Compressive Ice Strength (kPa)	91

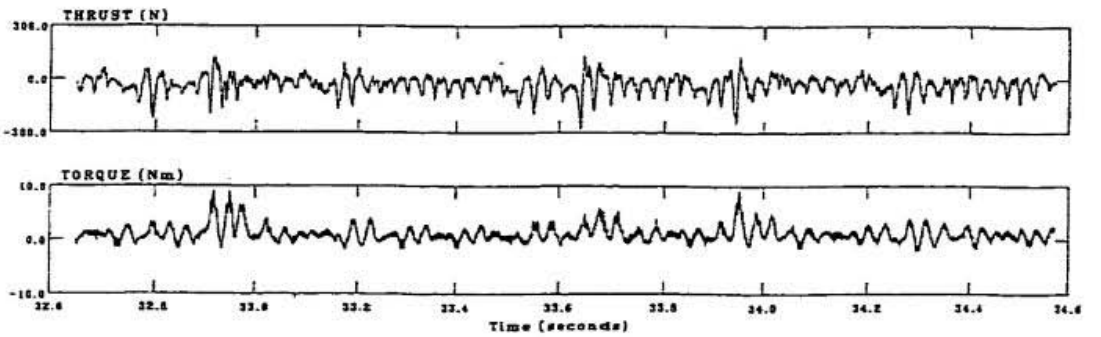

Figure 106: Time Series for Run R2_T9_T12_001

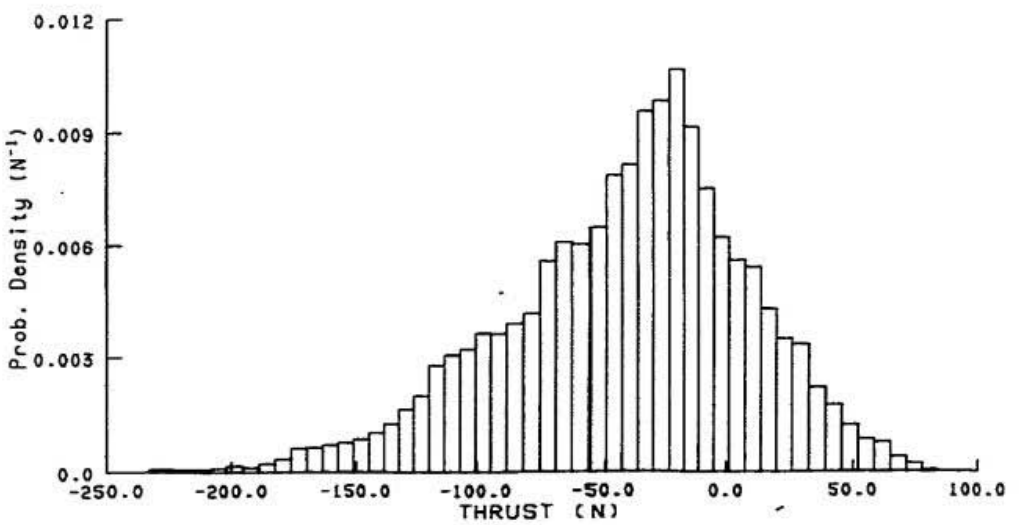

Figure 107: Thrust Distribution during run R2_T9_T12_001

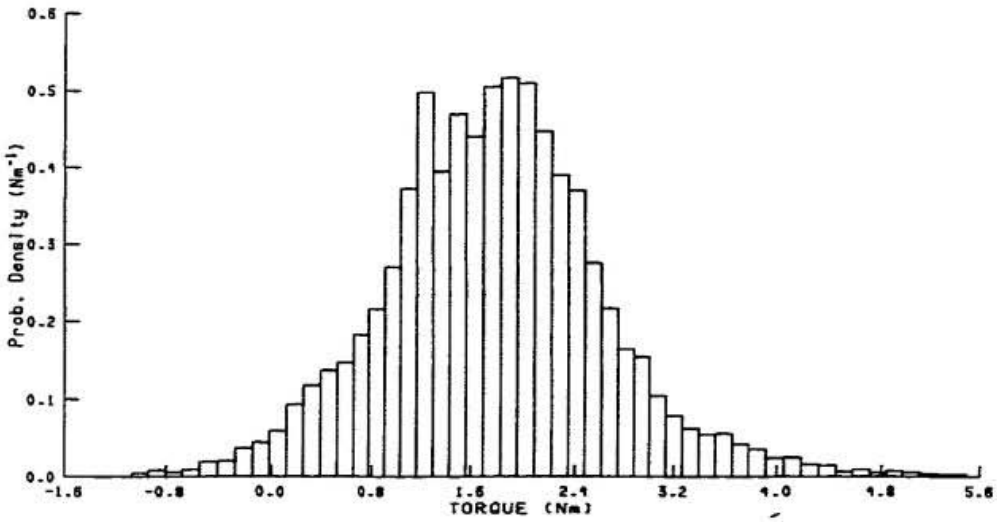

Figure 108: Torque Distribution during run R2_T9_T12_001

Run Name	R4_T21_T28_001
Advance Coefficient	-0.20
Cut Depth (mm)	25
Compressive Ice Strength (kPa)	84

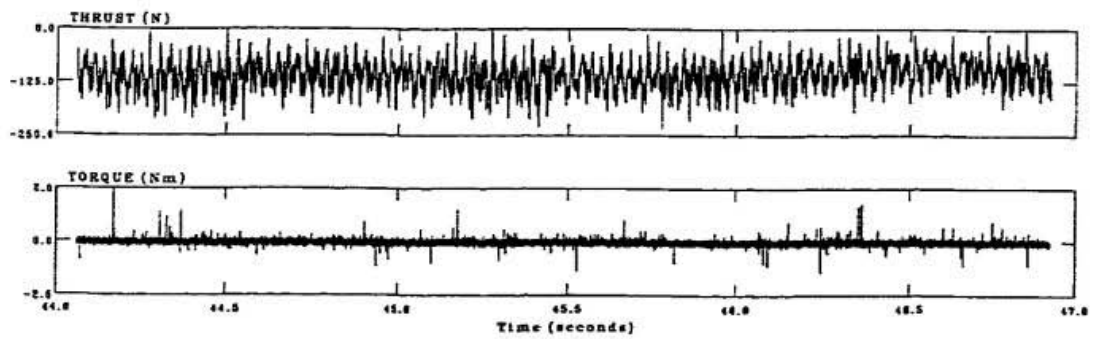

Figure 109: Time Series for Run R4_T21_T28_001

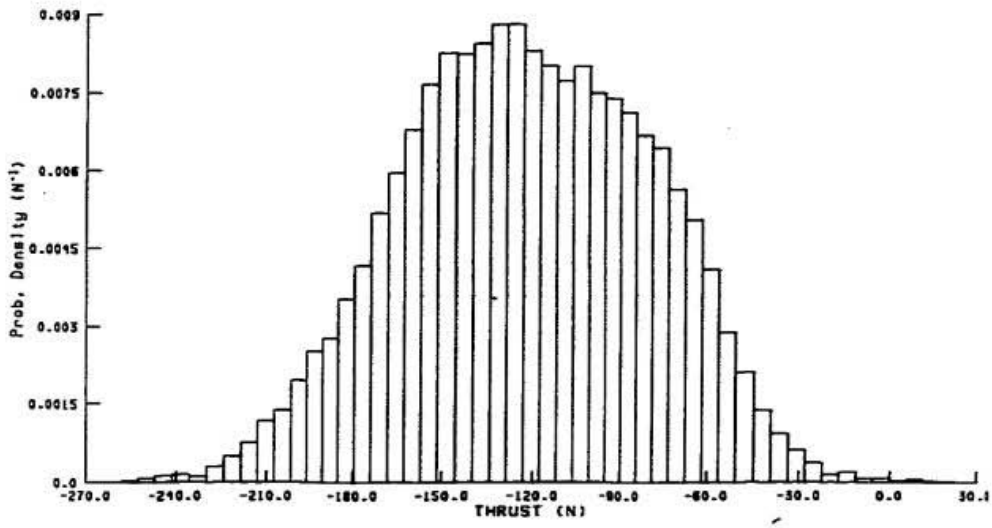

Figure 110: Thrust Distribution during run R4_T21_T28_001

Run Name	R5_T29_T36_001
Advance Coefficient	-.35
Cut Depth (mm)	25
Compressive Ice Strength (kPa)	80

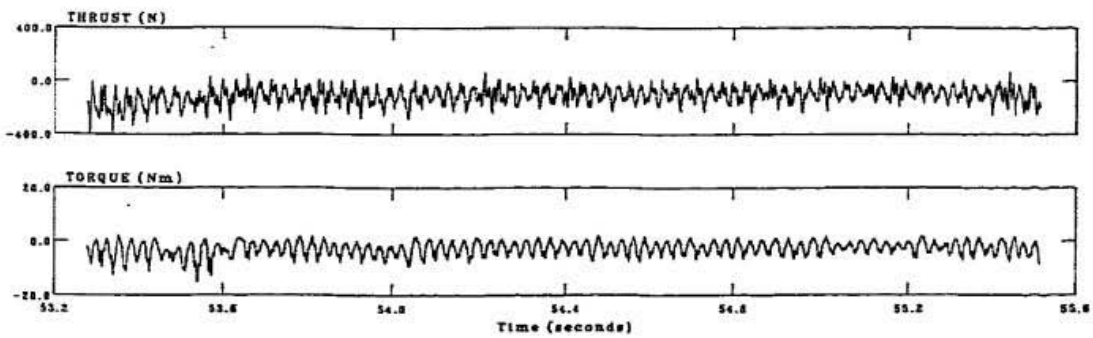

Figure 111: Time Series for Run R5_T29_T36_001

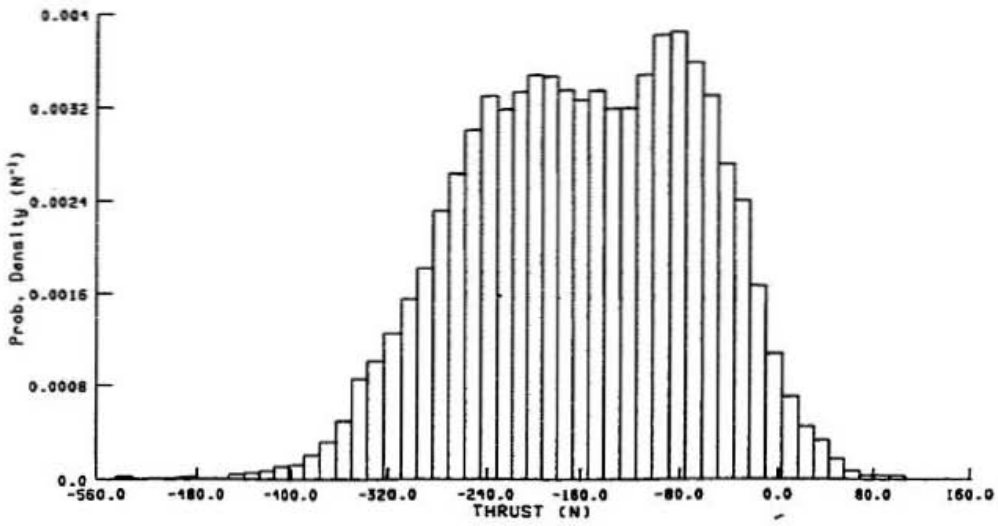

Figure 112: Thrust Distribution during run R5_T29_T36_001

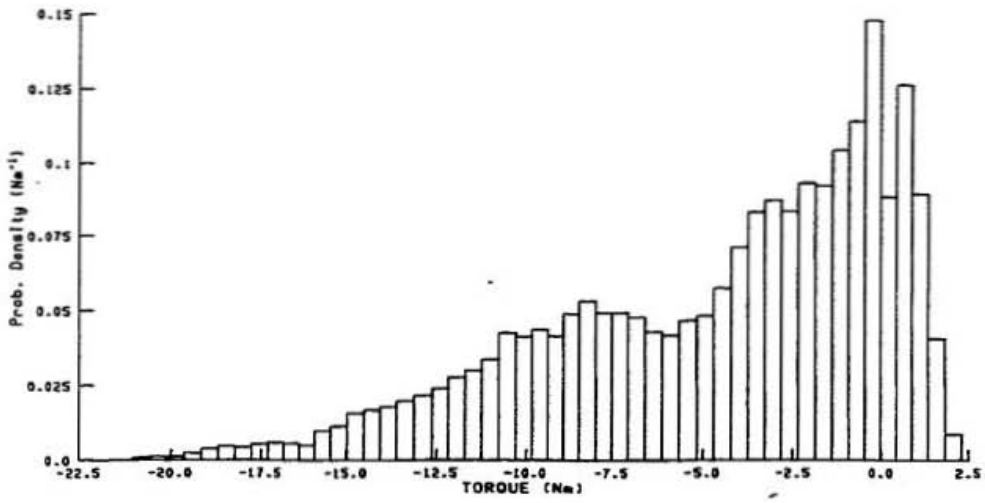

Figure 113: Torque Distribution during run R5_T29_T36_001

Run Name	R6_T37_T44_001
Advance Coefficient	0.5
Cut Depth (mm)	25
Compressive Ice Strength (kPa)	73

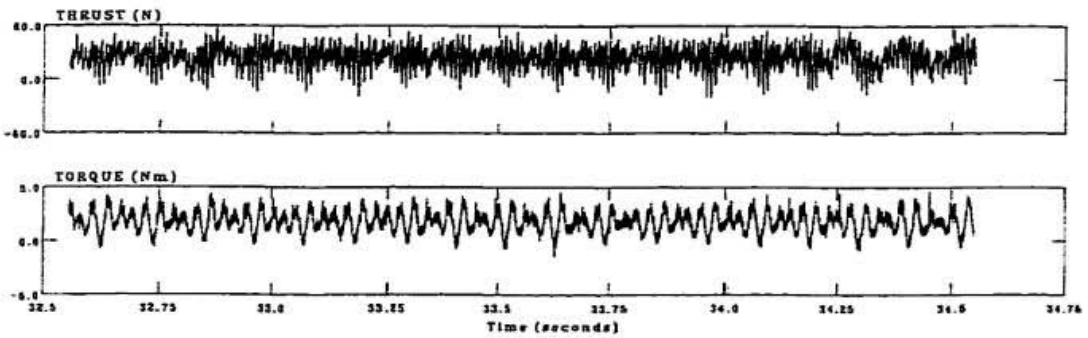

Figure 114: Time Series for Run R6_T37_T44_001

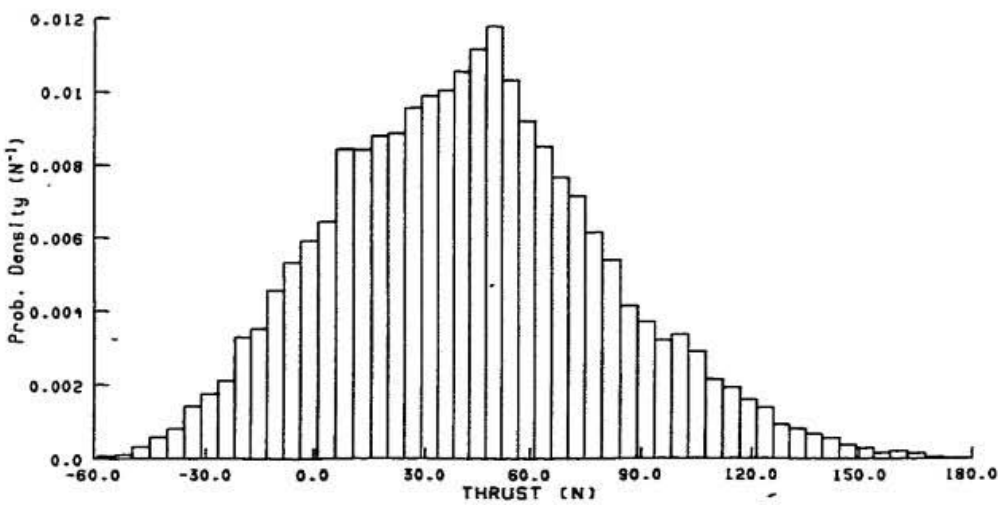

Figure 115: Thrust Distribution during run R6_T37_T44_001

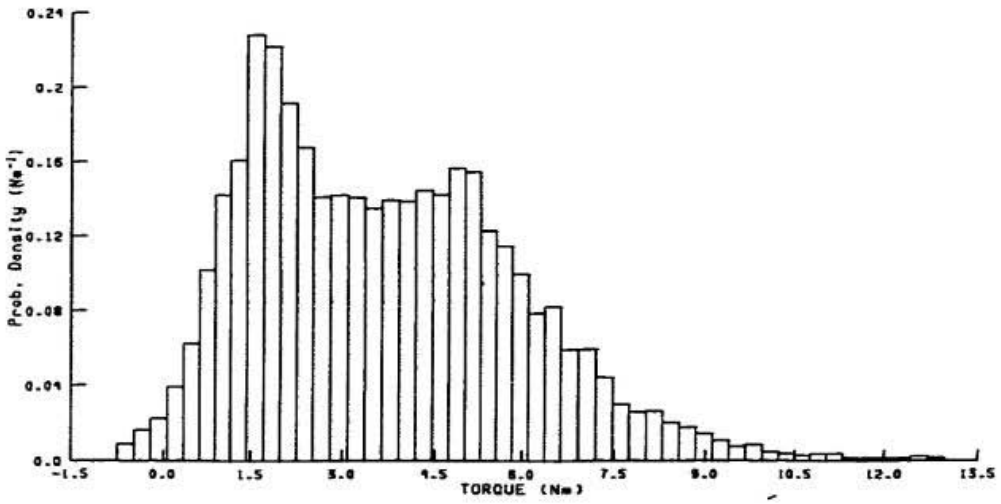

Figure 116: Torque Distribution during run R6_T37_T44_001

Run Name	R6_T45_T48_001
Advance Coefficient	0.91
Cut Depth (mm)	25
Compressive Ice Strength (kPa)	71

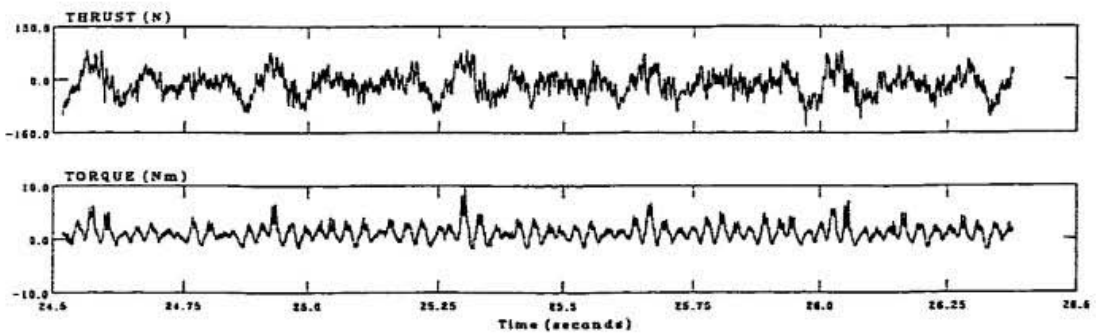

Figure 117: Time Series for Run R6_T45_T48_001

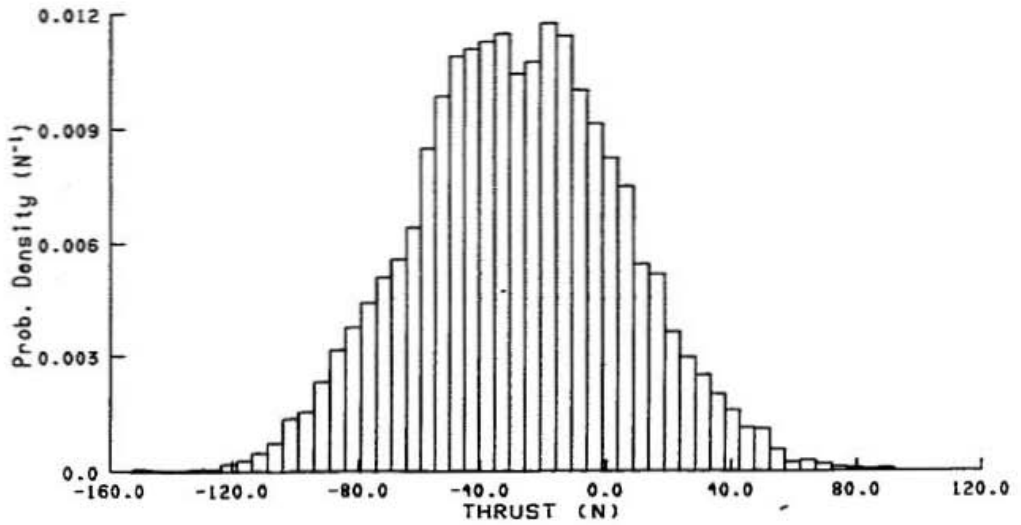

Figure 118: Thrust Distribution during run R6_T45_T48_001

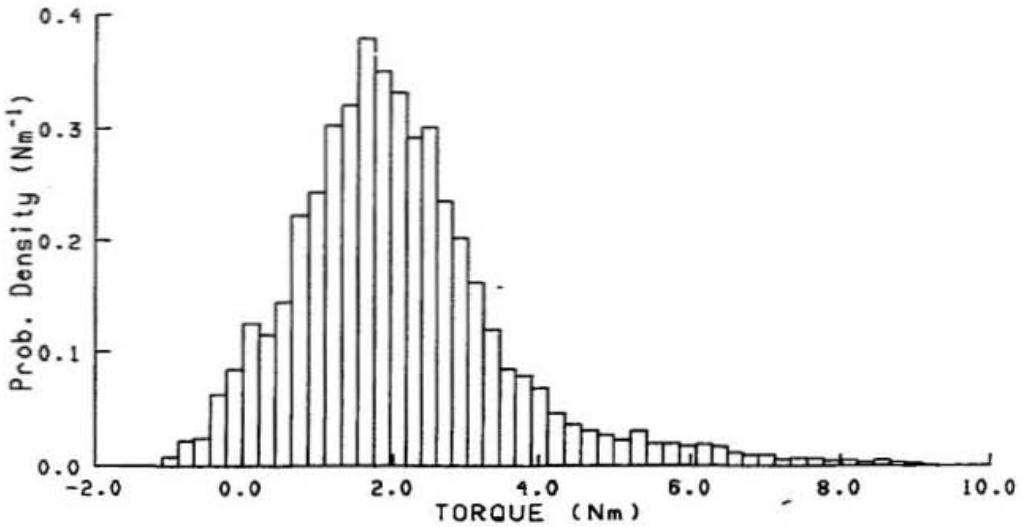

Figure 119: Torque Distribution during run R6_T45_T48_001

Run Name	R13_T81_T88_001
Advance Coefficient	-0.35
Cut Depth (mm)	25
Compressive Ice Strength (kPa)	60

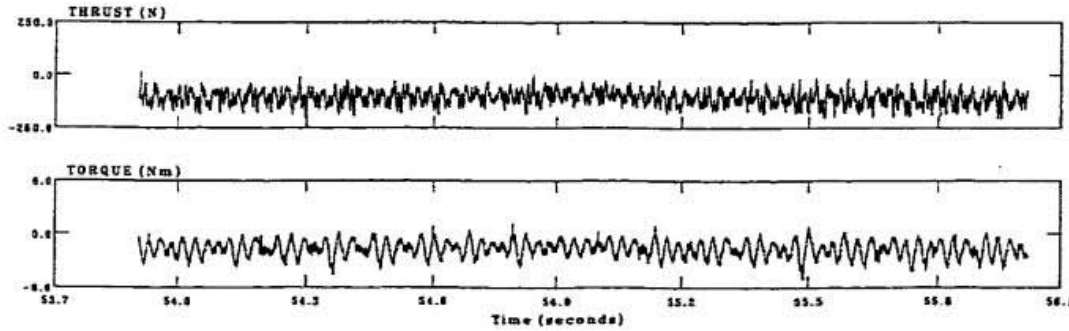

Figure 120: Time Series for Run R13_T81_T88_001

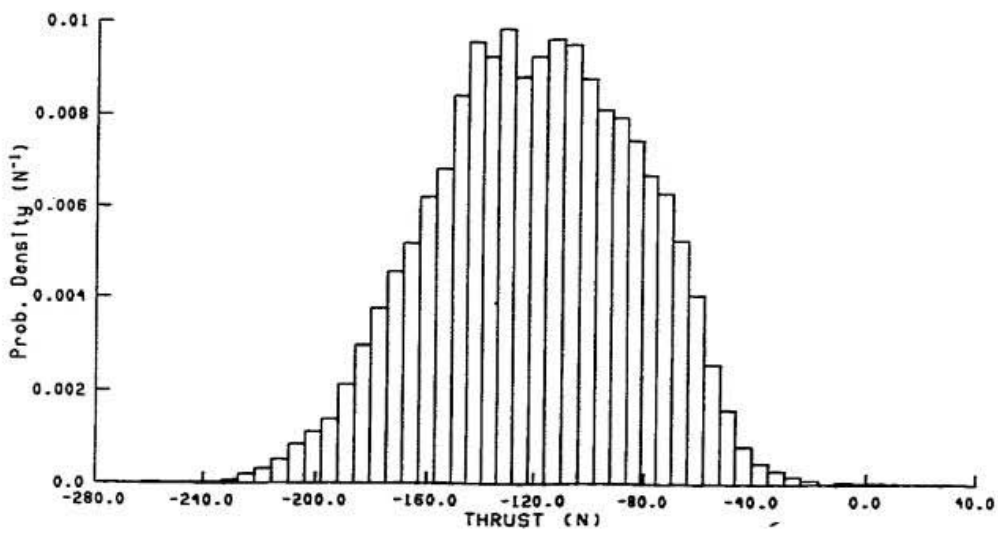

Figure 121: Thrust Distribution during run R13_T81_T88_001

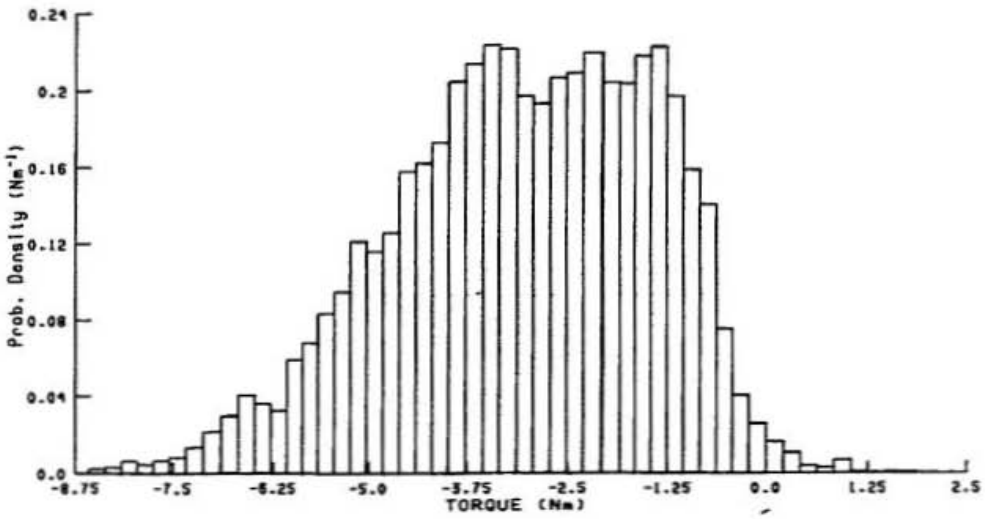

Figure 122: Torque Distribution during run R13_T81_T88_001